EXPLORING THE INTERACTION BETWEEN HISTONE H1.4 AND HP1α

A thesis presented in partial fulfillment of the requirements for the degree of
Master of Science
in Genetics
at Massey University, Palmerston North,
New Zealand.

Lauren Brebner-Fox

2024

Contents

List of Tables

List of Figures

Abstract

In eukaryotic organisms, the genome is organised into chromatin. Inside the nucleus, this chromatin is compartmentalised into regions of transcriptionally active euchromatin and transcriptionally inactive heterochromatin. The homeostasis of these two chromatin domains is essential for genomic stability and structural stability of the nucleus. Both histone H1.4 and the heterochromatin protein HP1α are enriched in heterochromatin and contribute to heterochromatin homeostasis. These two proteins have been demonstrated to interact through the C-terminal domain (CTD) of H1.4 and the hinge region (HR) of HP1α. This study investigated the H1.4-HP1α interaction *in vitro* and *in vivo* to determine how truncations or alterations to the H1.4 CTD impact its interaction with HP1α.

The rare genetic disorder, Rahman Syndrome, is caused by a frameshift mutation occurring in the CTD of H1.4. Disruptions to heterochromatin homeostasis have been observed in Rahman syndrome patient fibroblast cells highlighting the importance of histone H1.4 in heterochromatin.

It was demonstrated that the H1.4 CTD is important for the in vivo co-localisation of H1.4 to HP1α. H1.4 with a CTD altered due to a truncation or frameshift mutation showed a reduction in its co-localisation with HP1α. Expression of Rahman syndrome H1.4 was associated with alterations to HP1α mediated heterochromatin changes to nuclear morphology, indicating that it may be impacting chromatin condensation and the mechanical properties of the nucleus.

Overall, these findings demonstrate the importance of the H1.4 CTD in HP1α mediated heterochromatin homeostasis

Acknowledgements

I would like to thank my supervisor, Dr Tracy Hale, for providing all of the valuable knowledge throughout this journey and always being there when I had any questions.
I would also like to thank all my family and friends for their constant support during my studies.

Chapter 1

Introduction

1.1 Nuclear Organisation

The presence of a nucleus is a key feature of eukaryotic cells. It is the largest organelle in the eukaryotic cell and is a biochemically distinct compartment that functions to house and protect the genome of the organism (Lammerding, 2011; Martins et al., 2020). It is enclosed by the nuclear envelope, a lipid bilayer that contains nuclear pore complexes allowing for selective transport of molecules in and out of the nucleus (Lammerding, 2011; Martins et al., 2020). The nuclear envelope is composed of an outer nuclear membrane (ONM) which faces the cytoplasm as well as an inner nuclear membrane (INM) which faces the nucleoplasm (Martins et al., 2020). Lamin proteins line the inside of the nucleus strengthening the nuclear membrane structure (Lammerding, 2011). Inside the nucleus, the genome is packaged into chromatin. This packaging is key to controlling important nuclear processes in the cell such as transcription, DNA replication, and DNA repair (Parmar & Padinhateeri, 2020).

1.2 Organisation of Chromatin

The organization of chromatin inside the nucleus allows for the dynamic interplay of genomic information (Ghosh & Meyer, 2021; Sequeira-Mendes & Gutierrez, 2015). Chromatin structure is often described through its different levels of folding, with these levels important for the regulation of gene expression. Starting from the single nucleosome to the 10nm nucleosomal arrays to the 30nm chromatin fiber and resulting higher-order chromatin structures, these different layers of chromatin folding make up the overall 3D chromatin structure within the nucleus. However, as the visualization of these different chromatin structures has been mainly observed through *in vitro* electron and cryo-electron microscopy studies this has led to the debate of whether the 30nm chromatin fiber exists at all as it has never been observed *in vivo* (Maeshima et al., 2014).

Chromatin in the nucleus is comprised of regions of either transcriptionally active euchromatin or transcriptionally inactive heterochromatin. Regions of chromatin that are able to interact with each other, called a topologically associating domain (TAD) form regulatory boundaries that allow for the compartmentalisation of chromatin in the nucleus (da Costa-Nunes & Noordermeer, 2023; Rajderkar et al., 2023). This compartmentalisation is crucial for the normal function of the genome (Rajderkar et al., 2023).

1.2.1 The Nucleosome and Chromatosome

The most basic structural level of chromatin is the nucleosome. Its structure was originally defined after it was observed that micrococcal nuclease digestion of chromatin resulted in a length of DNA that was protected from digestion (Kornberg & Lorch, 1999). The nucleosome consists of 145-147 base pairs (bp) of DNA wrapped around an octamer of the four core histones, H2A H2B H3, and H4 (Figure 1.1) (Cutter & Hayes, 2015; Kornberg & Lorch, 1999). A fifth histone, H1, is bound to the DNA found at the entry and exit sites of the nucleosome and the addition of histone H1 to the nucleosome forms the chromatasome (Cutter & Hayes, 2015). Each nucleosome or chromatasome is linked by a stretch of DNA, named linker DNA that can range in length from approximately 20-90 bp (Szerlong & Hansen, 2011). Early electron microscopy studies described the structure of these nucleosomes connected by linker DNA as 'beads on a string' (Olins & Olins, 1974). The addition of histone H1 is also key to nucleosome structure and is essential for the folding of nucleosomal arrays into the more compact chromatin fiber structure (Bednar et al., 2017).

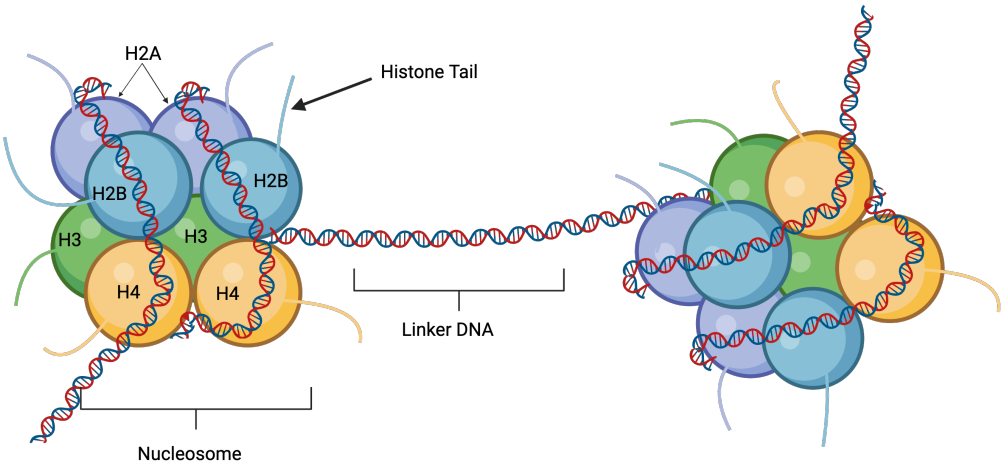

Figure 1.1: **A nucleosome core particle with approximately 147 bp of DNA wrapped around an octamer of the core histones H2A H2B H3, and H4.** The histone N-terminal and C-terminal tails can protrude out from the nucleosome structure. Each nucleosome is connected via a stretch of DNA referred to as 'linker DNA'. Image adapted from Caputi et al. (2017) and created using BioRender.

1.2.2 Core Histones

The core histone proteins are small proteins (11-15kDa) and share a similar structure, each containing an N-terminal tail, a histone fold domain, and a C-terminal tail (Cutter & Hayes, 2015). The histone fold motif comprises three α-helices connected by two loops which form a protein-protein interface directing histone H3-H4 and H2A-H2B heterodimers to form (Cutter & Hayes, 2015). When under physiological ionic conditions the H3-H4 heterodimers associate to form a tetramer mediated through

an H3-H3 interface. The remaining H2A-H2B heterodimers associate with the H4-H3-H3-H4 tetramer through an association between H4 and H2B to form a histone octamer structure (Cutter & Hayes, 2015). DNA is tightly associated with the histone octamer through a combination of hydrogen bonds and electrostatic forces. The core histones contain a high quantity of basic residues such as lysine and arginine giving them an overall positive charge. This results in favorable electrostatic interactions between the histones and the negatively charged DNA backbone.

The N-terminal and C-terminal tails are unstructured domains, however they are able to undergo post-translational modifications. These post-translational modifications support the stability of the nucleosome and allow for the control of gene expression (CITE). The histone tails interact with enzymes that carry out the post-translational modifications such as methyltransferases or acetyltransferases as they freely protrude from the nucleosome core particle structure and these modifications play an important role in the organisation of higher-order chromatin structure (Bednar et al., 2017; Cutter & Hayes, 2015). A key function of chromatin is to allow for the control of gene expression and these post-translational modifications to histone tails are a key mechanism for this function.

1.2.3 Linker Histone H1

In humans, there are eleven variants of histone H1. Histone H1.1 through to H1.5 along with H1.0 and H1.x are all somatic subtypes, while H1t, H1T2, and H1LS1 are all testis-specific subtypes and H1oo is oocyte-specific. These variants all share a structure consisting of an N-terminal domain, a globular domain, and a C-terminal domain. The globular domain is highly conserved between histone H1 variants while the N-terminal domain and C-terminal domain are more variable. The binding of histone H1 is associated with the compaction of chromatin leading to it being initially proposed to function as a repressor of transcription. However, not all of the H1 histones are associated with repression of gene expression. Instead, each of the H1 variants shows differences in areas such as their affinity for chromatin, location in the nucleus, and compaction of chromatin (Clausell et al., 2009).

Only two of the somatic histone H1 variants, H1.0 and H1.x, are replication-independent meaning that they are expressed throughout the cell cycle (Prendergast & Reinberg, 2021). The remaining somatic H1 variants are replication-dependent and instead are only expressed during S-phase (Marzluff & Koreski, 2017). It was observed that the histone mRNAs of replication-dependant histones were observed in high levels during the start of the S-phase of the cell cycle, while the end of the S-phase is associated with the degradation of the remaining histone mRNAs (Marzluff & Koreski, 2017; Prendergast & Reinberg, 2021). The mRNA of replication-dependent histones have no poly-A tail and instead contain a 3' stem-loop structure that is important as it allows for the rapid degradation of the mRNA at the end of the S-phase and the overall regulation of the histone proteins (Marzluff & Koreski, 2017).

The globular domain of the linker histone contains a winged helix motif responsible for the binding of H1 to the linker DNA located at the nucleosome dyad. The histone variants H1.1, H1.2, H1.3, H1.4, and H1.5 are the only variants with nearly identical globular domain sequences. The exact orientation of H1 at the nuclear dyad has been up for debate surrounding the two different modes of H1 binding to the nucleosome dyad, on dyad binding or off-dyad binding (Bednar et al., 2017; Perišić et al., 2010; Prendergast & Reinberg, 2021). On-dyad binding refers to the binding of the H1 globular domain directly to the linker DNA at the central dyad position, while off-dyad binding occurs when H1

is bound to the linker DNA slightly to the left or right of this central dyad position. This difference in binding orientation on the dyad appears to be dependent on the H1 variant with the histone variants H1.5 and H1.0 typically binding on-dyad while the histone variant H1.4 binds off-dyad (Bednar et al., 2017; Prendergast & Reinberg, 2021). This difference in dyad binding, despite the early identical globular domains of the different histone H1 variants, suggests that other factors contribute to the positioning of linker histones on the nucleosome.

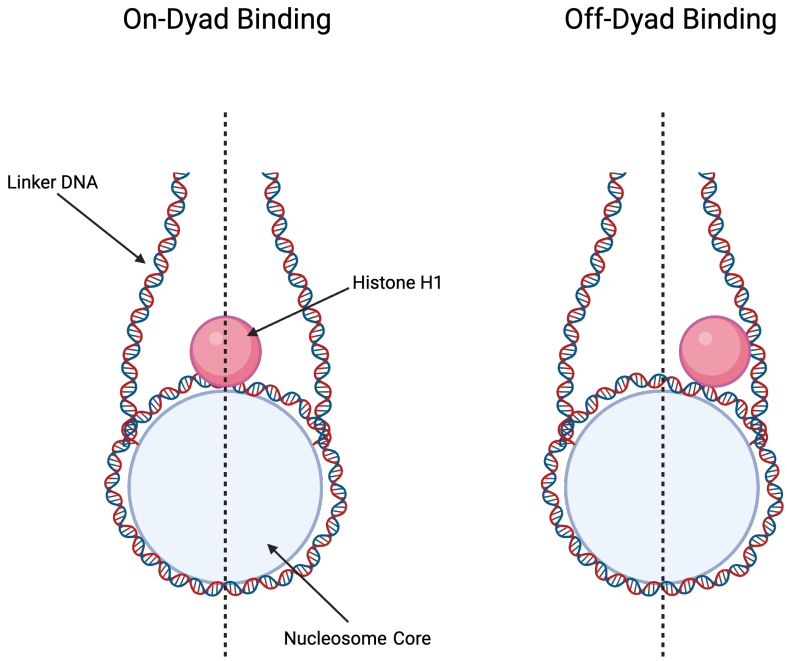

Figure 1.2: **Schematic diagram of linker histone H1 binding to nucleosome dyad.** The linker histone H1 binds to the nucleosome dyad and two models of H1-dyad binding have been demonstrated. On-dyad binding (left) refers to the binding of histone H1 on the central axis of the nucleosome dyad. Off-dyad binding (right) refers to the binding of histone H1 either slightly left or slightly right to the central axis of the nucleosome dyad. The central axis is represented by a dotted line in this diagram. Image created with BioRender.

The C-terminal domain (CTD) is a highly basic domain that makes up around half of the mass of the protein, the basic nature of the CTD is a key factor that allows for its interaction with the negatively charged linker DNA. The CTD is highly variable between the different H1 histones and this variation is suggested to be the determining factor behind the differences in chromatin affinity and condensation (Clausell et al., 2009).

It was observed that the H1 variants H1.4 and H1.5, which are associated with chromatin condensation, have a strong affinity for chromatin. The histones H1.1 and H1.2 are weak compactors of chromatin and are associated with regions of active transcription (Clausell et al., 2009). Histone H1.1 and H1.2 additionally have shorter C-terminal domains compared to H1.4 and H1.5 potentially indicating that the length of the CTD may play a role in chromatin condensation. The importance of CTD length was investigated in FRAP studies using human H1.1 CTD truncation mutants (Hendzel et al., 2004). It was determined that deletion of the amino acids 183-214 reduced the binding affinity of H1.1 to

chromatin (Hendzel et al., 2004). This loss of binding affinity continued to reduce with the removal of additional terminal amino acids (Hendzel et al., 2004).

The histone H1 variants have also been shown to have different nuclear localisations. Confocal immunofluorescence of T47D cells stained with antibodies for histone H1 variants showed that histone H1.0 H1.2, H1.3, and H1.5 were more enriched at the nuclear periphery while H1.4 and H1.X were evenly distributed throughout the nucleus (Salinas-Pena, M., Rebollo, E., & Jordan, A., 2023). The location of the H1 histones during mitosis was also observed. Histone H1.3 and H1.5 were observed to remain at the periphery of mitotic chromosomes (Salinas-Pena, M., Rebollo, E., & Jordan, A., 2023). However, during mitosis, H1.0 was observed to change its patterning from even dispersion to being located at the periphery of mitotic chromosomes (Salinas-Pena, M., Rebollo, E., & Jordan, A., 2023). The location of H1.x was observed to change during mitosis with it instead accumulating to the perichromosomal region (Salinas-Pena, M., Rebollo, E., & Jordan, A., 2023).

H1.2 depletion in T47D cells was shown to result in global chromatin decompaction (Salinas-Pena et al., 2024). However, Salinas-Pena et al. (2024) also demonstrated that the combined depletion of H1.2 and H1.4 produced more global chromatin decompaction than just H1.2 alone. Sancho et al. (2008) indicated that histone H1.4 depletion in T47D cells disrupted cell growth and survival and that depletion of H1.2 produced G1 arrest in T47D cells.

While the exact functions of histone H1 heterogeneity are not fully understood, the differences in nuclear localisation and importance in development indicate that there are variant specific functions for H1 histones.

1.2.4 30nm Chromatin Fiber Structure

10-nm nucleosomal arrays have been shown to further condense into a 30-nm chromatin fiber. The 30-nm chromatin fiber was first suggested to be the secondary chromatin fiber structure in 1976 by Finch and Klug after they observed, using electron microscopy(EM), that 10-nm nucleosomal arrays would fold into fibers with a diameter of 30-nm. Their study also showed that this folding was dependent on the presence of histone H1 as nucleosomal arrays that were depleted of H1 would not condense into 30-nm chromatin fibers (Finch & Klug, 1976). From the EM images, Finch and Klug suggested a solenoid structural model for the 30-nm fiber (Finch & Klug, 1976). The solenoid model suggested that the nucleosomal arrays were condensed into a 30-nm fiber with a one-start helix and that each nucleosome is in direct contact with the one directly neighboring it (Finch & Klug, 1976; Luger, Dechassa, & Tremethick, 2012; Perišić, Collepardo-Guevara, & Schlick, 2010). A second zig-zag model of the 30nm chromatin fiber was then proposed after observation of isolated nucleosomes (Woodcock et al., 1984). In the zig-zag model, the nucleosomal arrays were arranged in a two-start helix where instead alternate nucleosomes interact with each other (Luger et al., 2012; Woodcock et al., 1984; Worcel et al., 1981). Another difference between these two models is that in the solenoid model, there is the bending of the linker DNA however in the zig-zag model the linker DNA is straight (Luger, Dechassa, & Tremethick, 2012) However, since these discoveries, the exact structural model of 30-nm chromatin has not been resolved. Most research on 30-nm chromatin structure has been done using *in vitro* studies and this led to a debate on whether this model accurately represents the structure of chromatin *in vivo*.

Studies have suggested that the length of the linker DNA connecting each nucleosome, also known as the nucleosomal repeat length (NRL), could be contributing to the differences in the structure of the 30-nm chromatin fiber that is formed (Perišić et al., 2010; Routh et al., 2008). One study that used a modeling and simulation approach suggested that nucleosomal arrays with short NRLs were more likely to form a two-start zig-zag 30-nm chromatin fiber structure while nucleosomal arrays with longer NRLs were more likely to form a solenoid 30-nm chromatin fiber structure (Perišić, Collepardo-Guevara, & Schlick, 2010). While Routh et al. (2008) observed the compaction of nucleosomal arrays with a NRL of either 167 bp or 197 bp. The compaction of the nucleosomal array with the NRL of 167 was associated with a 30-nm fiber with the zig-zag conformation (Routh et al., 2008).

The majority of the research on the 30-nm has been done using *in vitro* due to the difficulty of observing chromatin structure *in vivo*. This led to a debate on whether this model accurately represents the structure of chromatin *in vivo*. To better understand how the 30-nm chromatin fiber functions *in vivo* cryo-EM studies were initially used as a way to visualize chromosomes in a near-native state, however, these studies failed to visualize any 30nm chromatin fibers (McDowall et al., 1986; Dubochet et al., 1986). Small-angle X-ray scattering analysis on HeLa cells was also used to try and visualise the structure of chromatin *in vivo*, however, they did not observe any 30-nm structure (Nishino et al., 2012). Additional studies suggested that 30-nm fiber structures may instead only appear as a transient structure *in vivo* (Maeshima, Imai, Tamura, & Nozaki, 2014).

1.2.5 Higher Order Chromatin Domains

Higher-order chromatin organisation is essential for the proper control of gene expression. Chromatin in the nucleus associates with itself and surrounding structures and proteins such as the nucleolus and lamina protein (Hansen, Cattoglio, et al., 2017; Rada-Iglesias et al., 2018). The spatial organisation of chromatin in the nucleus allows for increased levels of regulation and specificity of transcription throughout development and the cell cycle (Hansen, Cattoglio, et al., 2017; Rada-Iglesias et al., 2018). The levels of these higher-order chromatin structures go from the formation of chromatin loops to chromosome domains to chromosome compartments and then to chromosome territories.

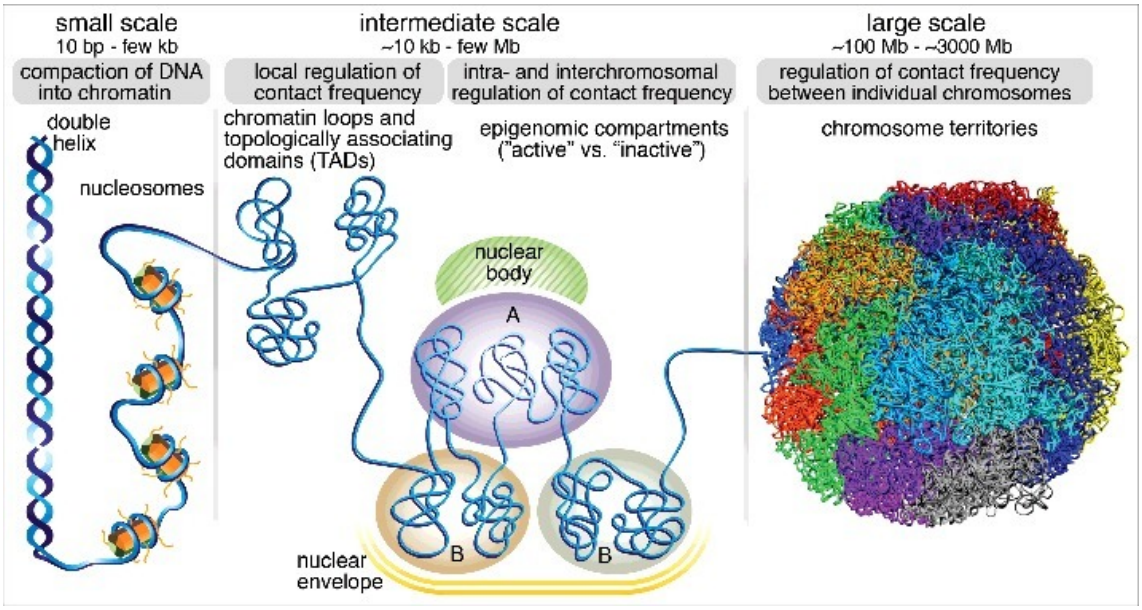

Figure 1.3: **Schematic diagram of different levels of chromatin organisation.** Small-scale chromatin organisation includes the formation of nucleosomes and nucleosomal arrays. At an intermediate scale, chromatin is spatially organised into topologically associated domains (TADs) and is also able to interact with nearby chromatin fibers to form chromatin loops. Chromatin has also been observed to be compartmentalized into regions of active chromatin called A compartments and regions of inactive chromatin called B compartments. At a large scale, chromosome territories are observed. Image from Hansen et al., (2017).

It has been observed that the regulatory elements of genes, such as enhancers, can be found at a great distance from the target genes along the linear genome (Hansen, Pustova, et al., 2017). The expression of these target genes was shown to be able to occur through the formation of a chromatin loop (Hansen, Pustova, et al., 2017). The formation of a chromatin loop would allow for this enhancer to be brought into close proximity to the target gene in 3D space (Hansen, Pustova, et al., 2017). The formation of these loops was originally studied through chromosome conformation capture (3C) however more recent work in this area uses the updated version of this method, Hi-C, which is able to detect genome-wide chromatin interactions (Hansen, Cattoglio, et al., 2017).

The formation of the chromatin loops has been shown to occur through the binding of the CCCTC-binding factor (CTCF) protein to CTCF-binding sites on the chromatin. The ring-shaped cohesin protein then holds the loop together (Hansen, Pustova, et al., 2017). The importance of the CTCF binding site was demonstrated by de Wit et al. (2015) as they showed that deletions of the CTCF binding sites resulted in a loss of chromatin loops. A reason for the need for these chromatin loops is suggested to be due to the promiscuity of promoters. Therefore, if they are separated they are unable to influence neighboring genes. It has also been shown that genes that are temporarily or permanently repressed have also been associated with specific chromatin loops

Chromosomes are spatially segregated into sub-megabase scale domains called topologically associating domains (TADs) (Hansen, Cattoglio, et al., 2017). The spatial partitioning of the genome into TADs is associated with the control of gene expression. One of the proposed functions of TADs is to ensure that enhancers and promoters only interact with those inside of their own TAD (Hansen, Cattoglio, et al., 2017). Loss of TAD boundaries is associated with abnormal gene expression (Hansen,

Cattoglio, et al., 2017). TAD boundaries have been shown to be enriched in CTCF binding sites which has led to the idea that these boundaries are made of chromatin loops (Hansen, Cattoglio, et al., 2017).

Chromatin has also been shown to interact with lamina proteins to form lamina associate domains (LADs) (Pradhan et al., 2021; Stephens et al., 2019; Stephens et al., 2018). The majority of the genes located in the lamina-associated domains are transcriptionally inactive (Pradhan et al., 2021). This association of heterochromatin at the nuclear periphery and associated with lamina proteins has also been shown to be structurally important for the nucleus (Pradhan et al., 2021; Stephens et al., 2019; Stephens et al., 2018). Disruption of just heterochromatin at the nuclear periphery alone was enough to result in changes to the mechanical properties of the nuclear membrane (Pradhan et al., 2021; Stephens et al., 2019; Stephens et al., 2018)

Chromatin is organized into two distinct forms in the nucleus, heterochromatin or euchromatin. Euchromatin is a less condensed form of chromatin that is easily accessed by transcriptional machinery and therefore is transcriptionally active (Morrison & Thakur, 2021). The condensed state of heterochromatin silences genes found in these regions (Morrison & Thakur, 2021). These two different types of chromatin are spatially separated inside of the nucleus with regions of euchromatin referred to as 'A' compartments and regions of heterochromatin referred to as 'B' compartments (Hildebrand & Dekker, 2020).

1.2.6 Euchromatin

Euchromatin is found in regions containing actively transcribed genes and regulatory elements. It has a more open structure is identified through key histone post-translational modifications such as methylation of histone H3 lysine 4 (H3K4me3) and acetylation of histone H3 lysine 27 (H3K27ac) (Morrison & Thakur, 2021). The post-translational modification H3K4me3 is found near transcription start sites of active genes (Beacon et al., 2021; Morrison & Thakur, 2021). Acetylation of histones, such as H3K27ac, reduces the affinity of DNA to the core histones inside the nucleosome, creating more relaxed and less tightly wound DNA which makes transcription easier (Sterner & Berger, 2000).

1.2.7 Heterochromatin

Heterochromatin is comprised of highly condensed chromatin allowing for the silencing of genes found in these regions as it makes it difficult for transcription to occur (Morrison & Thakur, 2021). There are two types of heterochromatin, facultative and constitutive. Facultative heterochromatin contains developmentally regulated genes and allows the genes to switch between active transcription and repression depending on developmental cues present in the cell (Morrison & Thakur, 2021). Constitutive heterochromatin contains satellite DNAs, ribosomal DNAs, and transposable elements as these types of repetitive sequences are generally constantly repressed in the cell (Morrison & Thakur, 2021). Functions of heterochromatin include protecting telomeres and the suppression of transposon activity (Janssen et al., 2018).

The presence of dimethylated or trimethylated lysine 9 on histone H3 (H3K9me2 or H3K9me2) is regarded as a key marker for constitutive heterochromatin (Morrison & Thakur, 2021; Nielsen et al., 2001; Padeken et al., 2022). In humans, the methylation of H3K9 revolves around the binding of

the SUV39H1 histone methyltransferase to H3K9 (Morrison & Thakur, 2021; Nielsen et al., 2001; Padeken et al., 2022). The structure of SUV39H1 consists of a SET domain with methyltransferase activity and a chromodomain that binds to methylated H3K9 (Morrison & Thakur, 2021; Nielsen et al., 2001). Constitutive heterochromatin is the only type of heterochromatin that has been shown to persist throughout the cell cycle (Azzaz, A. M., 2014). The chromosome centromere is surrounded by pericentric heterochromatin, a form of constitutive heterochromatin that is important for the timing of chromosome segregation and for the assembly of the nuclear envelope (Morrison & Thakur, 2021; Nielsen et al., 2001). The pericentric heterochromatin supports the binding of the sister chromatids at the centromere preventing premature segregation of the chromosome during mitosis. Pericentric heterochromatin is also suggested to be involved in the formation of the nuclear envelope during cell division (Ghosh & Meyer, 2021)

A distinctive feature of facultative heterochromatin is trimethylated lysine 27 residues on histone H3 (H3K27me3) (Janssen, Colmenares, & Karpen, 2018; Morrison & Thakur, 2021). Facultative heterochromatin is regulated by polycomb group (PcG) proteins through the trimethylation of H3K27 (Ghosh & Meyer, 2021). Facultative heterochromatin is observed both over an entire chromosome, such as X-chromosome inactivation as well as in smaller domains in the nucleus (Ghosh & Meyer, 2021). Facultative heterochromatin is important for the inactivation of one of the X-chromosomes in female mammals and this is done in early embryonic development (Ghosh & Meyer, 2021).

Heterochromatin localised to the nuclear periphery has been shown to play a role in supporting the structural integrity of the nuclear envelope alongside the lamina proteins (Stephens et al., 2019; Stephens et al., 2018). Loss of heterochromatin at this region was associated with a weaker nuclear membrane despite no alterations to the lamin proteins. (Stephens et al., 2019; Stephens et al., 2018).

Overall this indicates that heterochromatin has a key functional role that is beyond just the silencing of genes. It plays a key role in the progression of the cell cycle and in the structural support of the nuclear lamina alongside protecting the overall genomic stability within the nucleus. Therefore the homeostasis of heterochromatin is important to ensure normal cellular function.

1.3 Heterochromatin Homeostasis

1.3.1 Heterochromatin Protein 1 (HP1)

Architectural proteins, such as Heterochromatin Protein 1 (HP1), are important for maintaining and forming constitutive heterochromatin. Homologs of heterochromatin proteins are found to be evolutionarily conserved in most eukaryotes highlighting their importance in chromatin (Kumar & Kono, 2020). In humans, there are three paralogs of HP1, HP1α, HP1β, and HP1γ. They each share the same overall structure with a disordered N-terminal extension (NTE), hinge region (HR), and C-terminal extension (CTE) as well as two folded domains; the chromodomain (CD) and the chromoshadow domain (CSD) (Kumar & Kono, 2020; Machida et al., 2018). The sequence similarity of each of these regions differs slightly between each of the three paralogs with the CD and the CSD sharing the highest sequence identity (Kumar & Kono, 2020). Each of the HP1 variants has specific functions with HP1α mainly associated with constitutive heterochromatic regions while HP1β and

HP1γ are associated with both gene activation and gene silencing and are found in both heterochromatin and euchromatin (Kumar & Kono, 2020).

HP1 is recruited to chromatin through the interaction between the CD of HP1 with H3K9me3, once recruited to the heterochromatin it is able to promote the spreading of H3K9me3 to other nucleosomes (Maeda & Tachibana, 2022). Homodimerisation of the HP1 proteins is mediated through the CSD which creates a hydrophobic binding site where proteins containing the PXVXL motif can bind and interact with HP1, including methyltransferases that are important for the spread of H3K9me3 (Maison & Almouzni, 2004., Maeda & Tachibana, 2022). The hinge domain links the chromodomain and chromoshadow domains together (Schoelz& Riddle, 2022). Without the presence of HP1, it was observed in mouse embryonic stem cells that the levels of methyltransferases were reduced along with a reduction in H3K9me2/3 (Maeda & Tachibana, 2022) indicating the importance of its role in the maintenance and stability of heterochromatin. Changes to the expression of HP1 have also been observed in a range of different cancers (Kumar & Kono, 2020)

1.3.2 HP1α

The HP1 paralog, HP1α is found primarily in constitutive heterochromatin(Kumar & Kono, 2020; Pradhan et al., 2021). It interacts with both dimethylated and trimethylated H3K9 through its chromodomain, a key marker for constitutive heterochromatin, where it contributes to the propagation and maintenance of heterochromatin(Kumar & Kono, 2020; Pradhan et al., 2021).
A key finding showing the importance of HP1α in heterochromatin homeostasis is that the knockdown of HP1α in MCF7 cells was associated with disruptions to the mechanical properties of the nucleus(Pradhan et al., 2021). Atomic force microscopy (ATM) and optical tweezers (OT) were used in this study to investigate the impact HP1α knockdown had on the nuclear membrane(Pradhan et al., 2021). It was determined that the HP1α knockdown had softer and weaker nuclear membranes than the control MCF7 cells(Pradhan et al., 2021). Changes to the lamin were also observed in these MCF7 cells indicating that the loss of HP1α mediated heterochromatin homeostasis was disrupting the lamina at the nuclear periphery (Pradhan et al., 2021). These findings demonstrate the importance of HP1α to chromatin organisation. HP1α has also been demonstrated to interact with the histone protein H1.4 with this interaction likely playing a role in the maintenance of heterochromatin homeostasis (Hale et al., 2006).

Figure 1.4: **Schematic diagram of the HP1α structure**. HP1α has a disordered N-terminal extension (NTE), hinge region (HR), and C-terminal extension (CTE) as well as two folded domains; the chromodomain (CD) and the chromoshadow domain (CSD). Image created using BioRender.

1.4 Rahman Syndrome

Rahman syndrome is an autosomal-dominant neurodevelopmental syndrome that was first described in 2014 and is caused by a frameshift mutation to the histone H1 variant, H1.4 (Burkardt & Tatton-Brown, 2020). Histone H1.4 is a ubiquitously expressed somatic H1 variant that is enriched in heterochromatin. It has a strong affinity to chromatin as well as a strong ability to condense chromatin (Clausell et al., 2009).

Varying frameshift mutations associated with Rahman Syndrome have been observed to occur in the HIST1H1E (H1.4) gene (Burkardt & Tatton-Brown, 2020; Flex et al., 2019). The commonality of these variants is that all mutations occur in the C-terminal domain (CTD) of the H1.4 protein resulting in an early stop codon as shown in figure 1.5 (Burkardt & Tatton-Brown, 2020; Flex et al., 2019). Overall there have been 20 reported H1.4 frameshift variants that all result in similarly truncated C-terminal domains (Burkardt & Tatton-Brown, 2020; Flex et al., 2019). The mutation to the HIST1HIE (H1.4) gene typically occurs de novo and follows an autosomal dominant pattern of expression (Burkardt & Tatton-Brown, 2020; Flex et al., 2019).

Figure 1.5: **Schematic diagram of histone H1.4 showing the N-terminal domain, globular domain, and C-terminal domain.** The different HIST1H1E frameshift variants and the region of the CTD that they affect have been labeled. Image from Flex et al., 2019

Rahman syndrome is characterized by intellectual disability, overgrowth, and distinctive facial features with many individuals also presenting with additional symptoms such as skeletal and cardiac anomalies, hypotonia, or abnormal brain MRI findings (Burkardt & Tatton-Brown, 2020; Flex et al., 2019). Recently it has been shown that some individuals with Rahman syndrome display an accelerated aging phenotype, this observed phenotype has been further corroborated by Flex et al who looked at fibroblasts from these individuals which had had a reduced proliferation rate and increased SA-*beta*-gal activity when compared to fibroblasts from healthy individuals indicating that aging was occurring at an increased rate in these cells (Flex et al., 2019). In order to determine factors behind the accelerated aging Flex et al used the same fibroblasts from individuals with Rahman syndrome to look at heterochromatin markers and also investigated how the frameshift affects chromatin binding and protein stability. They showed that there were alterations to the levels of heterochromatin markers such as H3K9me3 and H3K27me compared to fibroblasts from healthy control subjects, indicating that heterochromatin homeostasis is impaired in these cells (Flex et al., 2019). As the frameshift H1.4 truncated proteins have been shown to be associated with chromatin it has been suggested that the frameshift H1.4 protein in Rahman syndrome has a dominant negative effect (Flex et al., 2019).

Due to the rarity of this condition, there is little research focused on Rahman Syndrome, with a

lot of the research focused on cataloging the different Rahman Syndrome frameshift variants and the associated symptoms in patients. This leaves a gap in the current research to further explore how the frameshift H1.4 affects heterochromatin homeostasis and its interaction with other key heterochromatin proteins such as HP1α.

1.5 Interaction between H1.4 and HP1α

Both histone H1.4 and HP1α are enriched in heterochromatic regions and have roles in heterochromatin homeostasis. Histone H1.4 binding to the nucleosome results in chromatin compaction and is also thought to have an additional role of targeting HP1α to the chromatin. The presence of HP1α ensures the maintenance and propagation of heterochromatin, highlighting its importance for heterochromatin homeostasis. Previous studies have established that these two proteins interact.

Daujat et al. (2005) investigated the H1.4-HP1α through *in vitro* binding assays using purified H1.4 and HP1α peptides. They were specifically investigating the importance of H1.4 lysine 26 methylation (H1.4K26me) on its interaction with HP1α (Daujat et al., 2005). The findings from Daujat et al. (2005), demonstrated that H1.4K26me was necessary for the H1.4-HP1α interaction to occur *in vitro*. Loss of H1.4K26me resulted in the loss of H1.4s association with HP1α(Daujat et al., 2005). The binding of H1.4K26me with various HP1α domain deletion mutants determined that this interaction was occurring through the chromodomain of HP1α.

However, Hale et al. (2006) demonstrated that the methylation of H1.4K26 was not required for the binding of H1.4 to HP1α as H1.4 proteins that were not specifically methylated at H1.4K26 were able to sustain the H1.4-HP1α interaction *in vitro* . The study used *in vitro* pulldown assays using GST-HP1α which concluded that only full-length HP1α and HP1α that contained the hinge region was able to pulldown H1.4. Further *in vitro* pulldown assays also determined that H1.4 with the CTD removed was no longer able to interact with HP1α. Overall, the findings from this study determined that the interaction between H1.4 and HP1α occurred through the CTD of H1.4 and the hinge region of HP1α.

Contrary to these findings, a study by Ryan and Tremethick (2018) demonstrated that H1.4 binding to nucleosomal arrays instead prevented the binding of HP1α. However, FRET analysis has also been used to confirm the H1.4-HP1α interaction *in vivo*. The differences in these findings regarding the H1.4-HP1α interaction may suggest that there is a need for an additional component to contribute to mediating the interaction. Unpublished preliminary data has suggested that RNA may be involved in mediating the H1.4-HP1α interaction. Both the CTD of H1.4 and the hinge region of HP1α are basic domains that have an affinity toward negatively charged nucleic acids such as RNA.

The frameshift mutation in H1.4 associated with Rahman syndrome occurs in the CTD. As there is strong evidence for the H1.4-HP1α interaction to occur through the CTD of H1.4 and HR of HP1α, this raises the question of whether the mutant H1.4 can still interact with HP1α. Loss of the H1.4-HP1α interaction in Rahman syndrome may explain some of the changes to heterochromatin markers observed in patient fibroblast (Flex et al., 2019).The exact regions of the H1.4 CTD required for this interaction have also not been established.

Overall there is little research looking specifically at the interaction between HP1α and H1.4 and this leaves a gap in the research as more understanding is needed about the specific conditions that allow for the interaction between HP1α and H1.4 to occur.

1.6 Objectives

The aims of this study are to:
1. Investigate what regions of the C-terminal domain of H1.4 are important for its interaction with HP1α *in vitro*.

Objectives:
- Express H1.4 proteins with differing C-terminal domain truncations as well as the H1.4 frameshift variant p.Lys148Glnfs48.
- Develop and perform an *in vitro* pulldown assay with HP1α and the H1.4 CTD deletion mutants to determine what region of the CTD of H1.4 is necessary for binding to HP1α.

2. Investigate how different H1.4 C-terminal domain truncation mutants affect heterochromatin in a cell and the co-localisation of H1.4 with HP1α.

Objectives:
-Transiently transfect NIH3T3 cells with the H1.4 frameshift variant p.Lys148Glnfs48 along with additional H1.4 CTD truncation mutants.
-Examine any resulting changes in heterochromatin markers, cellular morphology, and co-localisation of H1.4 with HP1α.

Chapter 2

Materials and Methods

2.1 Cloning of H1.4 Mutants into pET24a and pcDNA3.1Neo Plasmids

2.1.1 Inverse PCR

To generate pET24a-H1.4-HA plasmids and pcDNA3.1Neo-FLAG plasmids with various C-terminal domain deletions inverse PCR was used. PCR reactions contained 20 ng of either the pET24a-H1.4-HA expression vector or the pcDNA3.1-H1.4-FLAG expression vector, 0.3 μM of the forward and reverse primers, 1x KAPA HiFi buffer, 0.3 mM KAPA dNTP mix and 1 unit of KAPA HiFi Hotstart polymerase in 50 μL. The primers used for generating the CTD mutations in the pET24a-H1.4-HA expression vector are listed in Table 2.1. The primers used for generating the CTD mutations in the pcDNA3.1Neo-FLAG expression vector are listed in Table 2.2. The annealing temperatures 62°C, 64°C, 66°C, 68°C and 70°C were tested initially and it was confirmed that 70°C was the optimal annealing temperature. Therefore the cycling parameters of 3 minutes at 95°C, 25 cycles at 98°C for 20 seconds, 70°C for 15 seconds, and 72°C for 6 minutes. The final extension was at 72°C for 6 minutes.

Primer Name	Primer Sequence	Length
pET24a Start	GGC GGA GGC TAT CCA TAT GAT GTT CCA GAT TAT GCT TAG AAG	42
Δ189	CGC TGG GCT CTT GGG CGC	18
Δ160	CTT CTT CGC CTT CTT TGG GGT CTT CTT GGC GCT	33
Δ147	GGG GGT GGC CGC CCC CG	17
Δ145	GGC CGC CCC CGT CGC CTT C	19
ΔCTD	CTT GGT CTG CAC CAG GGT GCC CTT G	25

Table 2.1: **Inverse PCR primer sequences to generate H1.4 CTD deletion mutants in the pET24a expression vector.** Primers were sourced from Integrated DNA Technologies (IDT).

Primer Name	Primer Sequence	Length
pcDNA3.1 Start	TCG ACG GAT CCG GTA CCA GAT TAC AAG GAC GAC G	34
Δ147	GGG GGT GGC CGC CCC CG	17
ΔCTD	CTT GGT CTG CAC CAG GGT GCC CTT G	25

Table 2.2: **Inverse PCR primer sequences to generate H1.4 CTD deletion mutants in the pcDNA3.1Neo expression vector.** Primers were sourced from Integrated DNA Technologies (IDT).

The PCR was confirmed via electrophoresis of 5 μL of PCR product combined with 1μL of 6x DNA loading dye (see Section 2.5.1). Following this, PCR reactions were purified with the QIAquick PCR purification kit (Qiagen) and eluted by the addition of 30 μL of distilled H_20 (dH_20). The purified PCR product was combined with 10x BlueJuice (Invitrogen) to get a 1x concentration and then electrophoresed using a 1x agarose gel (see Section 2.5.1). The resulting gel was viewed under UV light and the bands of the correct size were excised from the gel using a scalpel. These excised bands were then purified using the QIAquick gel purification kit (Qiagen) and eluted into 30 μL dH_20.

A kinase reaction was then performed on the gel-purified PCR products using 10 mM adenosine triphosphate (ATP, Thermo Fisher), 20 Units of T4 Polynucleotide Kinase (Thermo Fisher), and 1x of the accompanying reaction buffer A. The reaction was made up to a final volume of 40 μL using dH_20. The reaction was incubated at 37°C for 20 minutes and then placed at 75°C for 10 minutes to heat inactivate the reaction. The completed kinase reaction was then purified using the QIAquick PCR Purification kit (Qiagen) and eluted with 30 μL dH_20.

Blunt-end ligation reactions of the phosphorylated vector were then set up containing 100 ng of the vector, 1 μL of T4 DNA Ligase (NEB), a 1x concentration of the associated ligase buffer (NEB), and dH_20 to bring to total reaction volume to 10 μL. This reaction was incubated at 16°C overnight (16-18 hours) and then heat-inactivated at 65°C for 10 minutes.

2.1.2 Blunt End Cloning to generate pcDNA3.1Neo plasmid with H1.4 p.Lys148Glnfs*48

The H1.4 Rahman syndrome frameshift variant p.Lys148Glnfs*48, hereafter referred to as H1.4-FS, supplied by GeneScript had been previously cloned into the pET24a-HA expression vector. As the H1.4 H1.4-FS protein sequence is the same as the wild-type H1.4 up until amino acid 147 the frameshift region was extracted from the pET24a H1.4 H1.4-FS-HA plasmid using PCR and then blunt-end cloned into a pcDNA3.1Neo plasmid that contained an H1.4 sequence that was truncated at amino acid 147 (H1.4 Δ147).

PCR reactions that contained 10ng of the pET24a-H1.4 H1.4-FS-HA expression vector, 0.3 μM of the forward and reverse primers (Table 2.3), 1x KAPA HiFi buffer, 0.3 mM KAPA dNTP mix and 1 unit of KAPA HiFi Hotstart polymerase were set up with a total reaction volume of 50μL. The cycling parameters used for the PCR were 3 minutes at 95°C, 25 cycles at 98°C for 20 seconds, 66°C for 15 seconds, and 72°C for 15 seconds. The final extension was at 72°C for 1 minute. The PCR was confirmed to be correct via electrophoresis of 5 μL of PCR product combined with 1 μL of 6x DNA loading dye to get a 1x concentration (see Section 2.5.1).

Primer Name	Primer Sequence	Length	Tm
H1.4 Frameshift Forward	CAA GAA GAG CGC CAA GAA GAC CCC AAA G	28	63.0
H1.4 Frameshift Reverse	ACT GCT TTG GCC TTC GCT GGG C	22	65.2

Table 2.3: **Forward and reverse primers to extract H1.4 p.Lys148Glnfs*48 frameshift region**. Primers were sourced from Integrated DNA Technologies (IDT)

Following this, PCR reactions were purified with the QIAquick PCR purification kit (Qiagen) and eluted by the addition of 30 μL of distilled H_20 (dH_20). The purified PCR product was combined with 10x BlueJuice (Invitrogen) to get a 1x concentration and then electrophoresed using a 1x agarose gel (see Section 2.5.1). The resulting gel was viewed under UV light and the band of the correct size was excised from the gel using a scalpel. The excised band was then purified using the QIAquick gel purification kit (Qiagen) and eluted into 30 μL dH_20. A kinase reaction was then performed on the gel-purified PCR product using 10 mM adenosine triphosphate (ATP, Thermo Fisher), 20 Units of T4 Polynucleotide Kinase (Thermo Fisher), and 1x of the accompanying reaction buffer A. The reaction was made up to a final volume of 40 μL using dH_20. The reaction was incubated at 37°C for 20 minutes and then placed at 75°C for 10 minutes to heat inactivate the reaction. The completed kinase reaction was then purified using the QIAquick PCR Purification kit (Qiagen) and eluted with 30 μL dH_20.

Inverse PCR was performed on the pcDNA3.1Neo-H1.4-FLAG vector to generate a 72 amino acid deletion from the CTD resulting in a 147 amino acid long H1.4 sequence in the pcDNA3.1Neo vector. This was referred to as pcDNA3.1Neo-H1.4-Δ147-FLAG. The inverse PCR reaction was carried out as described in Section 2.1.1 except that the gel purified vector was not phosphorylated or blunt end ligated.

The H1.4-FS frameshift region extracted using PCR was then blunt-end cloned into the pcDNA3.1Neo-H1.4-Δ147-FLAG vector generated through inverse PCR. As the pcDNA3.1Neo-H1.4-Δ147-FLAG plasmid was linear after the inverse PCR process it did not require cutting with restriction enzymes. Blunt end ligation reactions were set up with a 1:1 and 1:3 molar ratio of insert to vector. In each reaction, 50 ng of the linear pcDNA3.1Neo-H1.4-Δ147-FLAG plasmid was added with the frameshift PCR product added at either a 1:1 and 1:3 molar ratio along with 1 μL of T4 DNA Ligase (NEB), a 1x concentration of the associated ligase buffer (NEB) and dH_20 to bring to total reaction volume to 20 μL. This reaction was incubated at 16°C overnight (16-18 hours) and then heat-inactivated at 65°C for 10 minutes.

2.1.3 Plasmid transformation and purification

Plasmids generated via inverse PCR (see Section 2.1.1) and blunt-end cloning (see Section 2.1.2) were transformed into DH5α competent cells. 5 μL of the ligation reaction was added to a 50 μL aliquot of DH5α cells and then left to incubate on ice for 30 minutes. The reaction was then heat shocked at 42°C for 45 seconds and then incubated on ice for a further 2 minutes. Super Optimal broth with Catabolite repression (S.O.C, Thermo Fisher) was added to the reaction and then it was incubated at 37°C for 1 hour. 100 μL of the reaction was then plated on a Luria Broth (LB) agar plate that contained the appropriate antibiotic (Kanamycin for the pET24a plasmids and Ampicillin for the pcDNA3.1Neo plasmids)

Single transformed colonies were then selected and were used to innoculate 5 mL of LB that contained the appropriate antibiotic for the plasmid. Cultures were incubated overnight at 37°C shaking at 200 rpm. Cultures were then purified using the QIAprep spin Miniprep kit (Qiagen) and eluted into 30 ul of dH_20.

The purified plasmid DNA was assessed using a DeNovix DS-11 spectrophotometer. Once the quality and quantity of the DNA were checked the plasmids containing the correct products were confirmed via sequencing. Sequencing was performed at the Massey Genome Service using T7 promoter and terminal primers.

2.1.4 Midi-Prep of pcDNA3.1Neo Plasmids

Mini-prepped pcDNA3.1Neo plasmids containing the desired H1.4 wild-type or mutant sequences were transformed into DH5α competent cells as described in Section 2.1.3. Single transformed colonies were then selected and were used to innoculate 10 mL of LB + Ampicillin. The culture was then left at 37°C shaking at 200 rpm for 6 hours.

200 μL of this culture was transferred to a flask containing 500 mL of LB media and Ampicillin. The culture was left to grow at 37°C shaking at 200 rpm for 16 hours. The culture was then prepped according to the Qiagen Plasmid Midi-Prep protocol.

2.1.5 Diagnostic Restriction Digest

Diagnostic restriction digest of the miniprepped pET24a-H1.4-δCTD-HA plasmid was performed using 1 μg of the pET24a-H1.4-δCTD-HA plasmid, 10 units of each restriction enzyme HindIII (NEB) and Nde1 (NEB) Cutsmart 2.1 buffer (NEB) at a 1x concentration. The reaction was incubated at 37°C for 1 hour. The results from the diagnostic restriction digest were observed on a 1% agarose gel/1%TAE EtBr (see Section 2.5.1).

2.2 Protein Expression and Purification

2.2.1 Expression and partial purification of H1.4-HA constructs

Mini-prepped pET24a-H1.4-HA plasmids containing the desired H1.4 wild-type or mutant sequences were transformed into BL21 (DE3) cells. 1 μL of the plasmid was added to 50 μL of BL21 (DE3) cells and then left to incubate on ice for 30 minutes. The reaction was then heat shocked at 42°C for 45 seconds and then incubated on ice for a further 2 minutes. S.O.C media (Thermo Fisher) was added to the reaction and then incubated at 37°C for 1 hour. 20 μL of the transformation reaction was then plated on LB+ agar plates containing Kanamycin (30 mg/mL).

Single transformed colonies were selected and used to innoculate 50 mL of LB + Kanamycin (30 mg/mL). The culture was grown at 37°C shaking at 200 rpm until it reached an absorbance reading of A600 0.6. The culture was then transferred to a flask containing 500 mL of LB + Kanamycin (30 mg/mL). The culture was once again grown at 37°C shaking at 200 rpm until it reached an absorbance

reading of A600 0.6. Isopropyl βD-1-thiogalactopyranoside (IPTG) was then added to the culture at a concentration of 2.5 mM and was then transferred to 30°C shaking at 200 rpm for 2 hours to induce the expression of the H1.4 proteins. 50 μL samples of the culture before and after the addition of IPTG were taken and referred to as before and after induction samples. The remaining culture in the flasks was then transferred (poured) into a centrifuge bottle. The cells were then pelleted at 5000 xg 5min at 4°C.

The cell pellets were resuspended with 4 mL of ELB buffer(400 mM NaCl, 50 mM Hepes pH7.5, 5 mM EDTA pH8, and 0.1% NP-40) + Complete tablet (Roche). The resuspended cell pellets were then lysed using sonication (6x 10sec 20% AMP, 20sec pause). Lysate was frozen using liquid nitrogen before being immediately thawed, this was repeated three times. Perchloric acid extraction was performed on the cell lysate to partially purify the lysate. To do this 364 μL of 60% perchloric acid was added to the lysate which was then incubated on ice for 10 minutes. The lysate was centrifuged at 3700 rpm at 4°C for 15 minutes and the supernatant was removed and transferred to a separate tube each containing 1 mL. To each of these 1 mL tubes, 220 μL of 100% trichloroacetic acid (TCA) was added and then incubated on ice for 30 minutes. The supernatant was then centrifuged at 13300 rpm for 40 minutes at 4°C. The supernatant was once again removed and the pellet was washed with 750 μL acidified acetone (100 mL acetone/0.5 mL conc HCl) and centrifuged for 2 minutes at max speed (13300 rpm) at 4°C. Additional wash steps were performed with 1 mL acetone at 13300 rpm for 2 minutes at 4°C. The pellet was then left to dry before being resuspended in 250 μL Tris-buffered saline (TBS). To get to a final pH of 7, 1M Tris HCL pH8.0 was added until the desired pH was achieved.

2.2.2 Expression of GST-HP1α and GST

PGEX2T-HP1α and PGEX2T-GST plasmids were transformed into BL21 (DE3) cells. 1 μL of the plasmid was added to 50 μL of BL21 (DE3) cells and then left to incubate on ice for 30 minutes. The reaction was then heat shocked at 42°C for 45 seconds and then incubated on ice for a further 2 minutes. S.O.C media (Thermo Fisher) was added to the reaction and then it was incubated at 37°C for 1 hour. 20 μL of the transformation reaction was then plated on LB agar plates containing Ampicillin (100 mg/mL).

Single transformed colonies were then used to inoculate 10 mL of LB media containing Carbenicillin at 50 mg/mL. The culture was left shaking at 37°C overnight (16-18 hours). 1 mL of the overnight culture was transferred to a 1 L flask containing 500 mL of LB media containing Carbenicillin at 50 mg/mL. The culture was once again grown at 37°C shaking at 200 rpm until it reached an absorbance reading of A600 0.6. Isopropyl βD-1-thiogalactopyranoside (IPTG) was then added to the culture at a concentration of 1 mM and the flask was then transferred to 30°C shaking at 200 rpm for 2 hours to induce the expression of the GST-HP1α and GST proteins in the culture. 50 μL samples of the culture before and after the addition of IPTG were taken and referred to as before and after induction samples. The remaining culture in the flasks was then transferred (poured) into a centrifuge bottle. The cells were then pelleted at 5000 xg for 5 min at 4°C.

Cell pellets were resuspended in CSB buffer (1x Phosphate Buffered Saline (PBS) and 100 mM 0.5 M EDTA pH8.0). An EDTA-free complete protease inhibitor tablet (Roche) was added to the CSB buffer. Resuspended cell pellets were sonicated (6x 10 sec, 20% AMP, 20 sec pause) to lyse the cells

and then 10% triton X-100 was added to the lysate. Lysate was centrifuged at 8000rpm for 10 minutes at 4°C. After centrifugation, the supernatant was removed and the lysate was stored at -80°C.

2.3 Quantification of Protein Concentration

2.3.1 BCA Assay

The H1.4-HA proteins that were bacterially expressed and partially purified using perchloric acid extraction were quantified using the Pierce™ BCA Protein Assay Kit (Thermo Scientific). The BSA standards provided in the BCA Protein Assay Kit were replaced with Calf Thymus Histone protein standards. The resulting protein quantifications from the BCA assay were analysed using SDS-PAGE (see Section 2.5.2) to confirm the concentrations.

2.4 Total RNA extraction

In order to obtain total RNA, MCF7 cells were grown to 80% confluency. The growth media (DMEM + 10%FBS + pen/strep) was removed from the cells and the cells were washed with 1x PBS. Cells were removed from the flask via trypsinization. The trypsin reaction was halted by the addition of growth media to the cells. Cells were centrifuged at 800 rpm for 5 minutes and then the growth media was removed and cells were resuspended with 1x PBS. The RNA was then extracted from the MCF7 cells according to the Qiagen RNeasy kit protocol. The resulting RNA was quantified using the DeNovix DS-11 spectrophotometer.

2.5 Gel Electrophoresis

2.5.1 Agarose Gel Electrophoresis

A 1% Agarose gel was made in 1x TAE (40 mM Tris, 20 mM Acetic Acid, 1 mM EDTA) with 0.5 μg/mL ethidium bromide (EtBr). After the addition of the samples to the 1% Agarose gel, the gel was electrophoresed at 100 volts.

2.5.2 SDS-PAGE

To perform sodium dodecyl sulfate (SDS) poly-acrylamide gel electrophoresis (PAGE) a 12% 29:1 acrylamide/bisacrylamide resolving gel made up of 375 mM of Tris-HCl (pH 8.8), 0.1% ammonium persulfate (APS), 0.1% SDS and 0.1% tetramethylethylenediamine (TEMED) was initially made. A 5% 29:1 acrylamide/bisacrylamide stacking gel was then made using 125 mM Tris HCl (pH 6.8), 0.1% SDS, 0.1% APS, and 0.1% TEMED to go atop the resolving gel. Samples loaded into the SDS-PAGE gel were mixed with 6x SDS-loading dye to get a final 1x SDS-loading dye concentration (62.2 mM Tris-HCl (pH 6.8), 1.67% SDS, 7.5% glycerol, 0.01% bromophenol blue, 37.75 mM β-mercaptoethanol). 5 μL of Precision Plus Protein Dual Color Standards (Bio-Rad, 1610374) was loaded to determine protein sizes. Samples were heated at 95°C for 5 minutes before being loaded into the gel. Electrophoresis was performed in 1x TGS buffer (25 mM Tris, 192 mM glycine, 0.1% SDS) at a constant 30 mA until the dye front reached the bottom of the gel.

Gels were stained with 0.1% Coomassie brilliant blue R250 in 10% acetic acid and 50% methanol

overnight (16-18 hours). Gels were de-stained overnight (16-18 hours) using a de-staining solution comprised of 50% methanol, and 10% acetic acid. Gels were imaged using a Bio-Rad ChemiDoc.

2.6 Western Blot

Western blots were performed by transferring proteins resolved on an SDS-PAGE gel (see Section 2.5.1) to a 0.2 μm nitrocellulose membrane using AMPSO transfer buffer (25 mM AMPSO [pH 9.5], 20% methanol). The proteins were transferred at 70 volts for 2 hours at 4°C. After transfer the membrane was stained with Ponceau S staining solution until visible bands were observed. The Ponceau S staining solution was washed off the membrane using dH_20 and then the membrane was blocked in 5% non-fat milk powder in 1xTBS with Tween-20 (5% Nonfat milk (NFM) in 1xTBS/0.05% Tween-20) for 1 hour. Primary antibody (Table 2.4) was added at the appropriate dilution to the 5% Nonfat milk (NFM) in TBS/0.05% Tween-20 solution and incubated at 4°C overnight on a rocker.

The membrane was then rinsed and washed with 1xTBS/0.05% Tween-20 four times before being incubated with the secondary antibody (Table 2.5). The secondary antibody was diluted in 5% Non-fat milk (NFM) in 1xTBS/0.05% Tween-20 at the appropriate dilution and left to incubate for 1 hour on the rocker at room temperature. Following the secondary antibody incubation the membrane was rinsed and washed with 1xTBS/0.05% Tween-20 for a further four times.

The blot was developed using the ECL Prime western blotting detection reagent (Amersham) for 5 minutes as per the protocol instructions. The blot was then imaged using chemiluminescence.

Antibody	Manufacturer	Host Species	Dilution
Anti-HA	Invitrogen 2-2.2.14	Mouse	1:1000

Table 2.4: **Table of primary antibodies and their associated dilutions used in western blot experiments.**

Antibody	Manufacturer	Host Species	Dilution
Anti-mouse HRP	Cytiva (NA931)	Sheep	1:10,000

Table 2.5: **Table of secondary antibodies and their associated dilutions used in western blot experiments.**

2.7 *In Vitro* Binding Assay

2.7.1 Preparation of Pierce™ Glutathione Agarose beads

Pierce™ Glutathione Agarose beads were prepared for the *in vitro* binding assay by centrifuging 500 μL of the 50% bead slurry at 1000 rpm for 2 minutes at 4°C. The storage buffer was then removed and the Glutathione Agarose beads were washed twice using cold CSB buffer(1xPBS, 100 mM 0.5M EDTA pH8.0 plus 1 complete tablet (Roche)). The beads were then centrifuged again at 1000 rpm for 2 minutes at 4°C. The supernatant was then removed and 250 μL of CSB buffer(1xPBS, 100 mM 0.5M EDTA pH8.0 plus 1 complete tablet (Roche)) was added to the beads to maintain the 50% slurry.

2.7.2 GST-pulldown with RNA

180 μL of the GST-HP1α lysate and 120 μL of the GST lysate (see Section 2.2.2) were added to 200 μL of the prepared 50% GST slurry. The beads and lysates were left to rotate for 2 hours at 4°C. The tubes were then centrifuged for 3 minutes at 500g and at 4°C. The supernatant was removed and the binding reaction was washed 3 times using cold NEB buffer (250 mM NaCl, 2.5 mM Tris pH 8.0, 0.1 M EDTA pH 8.0, 5% Glycerol, 0.2% NP-40). After the wash steps the supernatant was removed and 600 μL of cold NEB buffer was then added to the beads to give a 14% slurry. 3.5μg of total mRNA (see Section 2.4) was added to both the GST-HP1α and GST reactions. The binding reaction was then left rotating for 30 minutes at 4°C.

The tubes were then centrifuged for 3 minutes at 500 g and at 4°C. The supernatant was removed and the binding reaction was washed 3 times using cold NEB buffer (250 mM NaCl, 2.5 mM Tris pH 8.0, 0.1 M EDTA pH 8.0, 5% Glycerol, 0.2% NP-40). After the wash steps the supernatant was removed and 200 μL of NEB buffer (275 mM NaCl, 2.5 mM Tris pH 8.0, 0.1 M EDTA pH 8.0, 5% Glycerol, 0.2% NP-40) was then added to the beads to give a 33% slurry.

Eight pulldown reactions were set up. Two different amounts of H1.4 protein were added to the reaction, either 1.3 mg of H1.4-HA or H1.4-FS-HA or 2.6 mg of H1.4-HA or H1.4-FS-HA. Along with 30 μL of the 33% slurry 522 μL NEB buffer (275 mM NaCl) and 6 μL acetylated-BSA at 5 μg/μL. These reactions were incubated overnight rotating at 4°C.

The binding reactions were then centrifuged for 5 minutes at 500 g at 4°C and the supernatant was removed. The beads and protein complex are washed 4 times with 750 μL of NEB buffer (275 mM NaCl). The supernatant was then removed and 30 μL of 1.5x SDS loading dye was added to the reaction. The results from the in vitro binding assay were visualised using a western blot (see Section 2.6)

2.7.3 GST-pulldown without RNA

140 μL of the GST-HP1α lysate and 35 μL of the GST lysate (see Section 2.2.2) were added to 200 μL of the prepared 50% GST slurry. The beads and lysates were left to rotate for 2 hours at 4°C. The tubes were then centrifuged for 3 minutes at 500 g and 4°C. The supernatant was removed and the binding reaction was washed 3 times using cold NEB buffer (275 mM NaCl, 2.5 mM Tris pH 8.0, 0.1 M EDTA pH 8.0, 5% Glycerol, 0.2% NP-40). After the wash steps the supernatant was removed and replaced with 200 μL of NEB (275 mM NaCl). The pulldown reactions were set up the same as in section 2.7.2 however only 2 μg of the H1.4-HA proteins was added to each binding reaction. These reactions were incubated overnight rotating at 4°C.

The binding reactions were then centrifuged for 5 minutes at 500 g at 4°C and the supernatant was removed. The beads and protein complex are washed 4 times with 750 μL of NEB buffer(275 mM NaCl). The supernatant was then removed and 30 μL of 1.5x SDS loading dye was added to the reaction. The results from the in vitro binding assay were visualised using a western blot (see Section 2.6)

2.8 Tissue Culture Methods

2.8.1 NIH3T3 Cell Lines Maintenance

NIH3T3 cells were used in this study and were grown in Dulbecco's Modified Eagle Medium (DMEM) supplemented with 10% v/v Calf Serum (CS) and 1% penicillin-streptomycin. The NIH3T3 cells were maintained at 37°C in 5% CO_2 and passaged every three days in 75 cm^5 flasks. To passage the cells the media was removed and the cells were washed twice with 10 mL Gibcos 1x Phosphate Buffered Saline (PBS), then 1.5 mL Gibcos Trypsin-EDTA was added to the flask to detach the cells from the flask. After 5 minutes 8.5 mL of media (1x DMEM, 10% CS, 1% Penicillian-Streptomycin) was added to the flask to stop the trypsinization reaction. The suspended cells were then passaged into a new flask at a 1:15 dilution factor.

2.9 Microscopy Techniques

2.9.1 Fibronectin Coverslip Coating

Coverslips were incubated with 20 μg/mL of Fibronectin for 2 hours at 37°C with 5% CO_2. Coverslips were then washed 2x with 1x PBS

2.9.2 Immunofluorescence

Fibronectin-coated glass coverslips (see Section 2.9.1) were placed in 6 well plates. NIH3T3 cells were seeded at a density of 0.4 x10^5 cells/mL and then incubated at 37°C with 5% CO_2 overnight. 250 ng of pcDNA3.1 H1.4-FLAG or H1.4 CTD mutant and 750 ng of carrier DNA (puc19) was added to 100 μL of Gibco Opti-MEM Reduced Serum Media. 3 μL of X-tremeGENE Transfection Reagent(Roche) was then added to each reaction tube and incubated for 15 minutes. Each transfection mixture was then added to the cells in the associated well and left to incubate at 37°C with 5% CO_2 for 48 hours. Coverslips were then washed with PBS (+MgCl) and then fixed with 4% paraformaldehyde for 15 minutes. After fixation coverslips were washed, then permeabilised using 1x PBS with 0.5% Triton-X for 5 minutes and then washed again. Coverslips were then transferred to a 24-well plate and incubated for 30 minutes with 300 μL of blocking buffer(10% Bovine Serum Albumin (BSA), 0.5% Tween-20, 1x PBS+MgCl). Coverslips were washed in 1x PBS+MgCl and then incubated overnight at 4°C with the primary antibodies as indicated in Table 2.6. Antibodies were diluted in blocking buffer.
Following the overnight incubation, the coverslips were washed with 1x PBS+MgCl and then incubated with the appropriate secondary antibody(Table 2.7) diluted in blocking buffer for 1 hour. The coverslips were washed again with 1x PBS+MgCl and then fixed with 2% paraformaldehyde for 15 minutes. Additional wash steps were then performed with 1x PBS+MgCl before the coverslips were mounted onto a slide using SlowFade Diamond Antifade Mountant with DAPI.

Antibody	Manufacturer	Host Species	Dilution
Anti-FLAG	Sigma, F1804	Mouse	1:1000
Anti-HP1α	Cell Signalling, 2616	Rabbit	1:200
Anti-H3K9me3	Abcam, ab8898	Rabbit	1:700
Anti-H1.4K26me	Sigma, H8289	Rabbit	1:1000
Anti-PIN1	Abcam, ab1220	Rabbit	1:1000
Anti-Lamin A/C	Invitrogen, MA5-35284	Rabbit	1:200

Table 2.6: **Table of primary antibodies and their associated dilutions used in immunofluorescence experiments.**

Antibody	Manufacturer	Host Species	Dilution
Anti-mouse Alexa 647	Abcam	Mouse	1:500
Anti-Rabbit Alexa 555	Abcam	Rabbit	1:500

Table 2.7: **Table of secondary antibodies and their associated dilutions used in immunofluorescence experiments.**

Chapter 3

Investigating the Histone H1.4 and HP1α Interaction *In Vitro*

3.1 Introduction

The interaction between histone H1.4 and the heterochromatin protein HP1α has been previously shown, with a proposed function of this interaction being to target HP1α to heterochromatin (Daujat et al., 2005; Hale et al., 2006). Previous *in vitro* binding assays have proposed two potential mechanisms for the H1.4-HP1α interaction. Daujat et al. (2005) demonstrated that only H1.4 methylated on lysine 26 interacted with the chromodomain of HP1α. However, according to Hale et al. (2006), the H1.4-HP1α interaction was instead demonstrated to occur through the CTD of H1.4 and the hinge region (HR) of HP1α. While it was previously demonstrated that H1.4 missing its CTD was unable to bind to HP1α *in vitro*, the exact regions of the H1.4 CTD required for binding to HP1α were not determined (Hale et al., 2006). Fluorescence resonance energy transfer (FRET), was also used to demonstrate that the H1.4-HP1α interaction also occurred *in vivo* (Hale et al., 2006). As previously discussed, the differences in the mechanisms behind the H1.4-HP1α interaction in the literature may suggest that an additional component is required to mediate the interaction. Unpublished preliminary findings have suggested that RNA is required to mediate the interaction between the H1.4 CTD and HP1α HR.

In patients with Rahman syndrome, a frameshift mutation in the CTD of H1.4 causes a change in the reading frame, with the new amino acid sequence coding for an early stop codon. The H1.4-FS mutation focused on in this study occurs at the amino acid position 148 of H1.4, resulting in an early stop codon at the amino acid position 194. Between amino acid 148 and the end of the CTD is a stretch of 46 amino acids with a completely different composition to the original H1.4 CTD. This change to not only the length of the CTD but also the differing amino acid composition could potentially impact the ability of HP1α to bind to H1.4 through the CTD. A loss of the H1.4-HP1α interaction may result in changes to heterochromatin homeostasis and as changes to heterochromatin markers have been previously observed in Rahman syndrome patient fibroblasts this may be a mechanism behind these changes (Flex et al., 2019).

This research aims to further investigate the H1.4-HP1α interaction using *in vitro* binding assays,

specifically focusing on the role of the H1.4 CTD. To investigate the regions of the H1.4 CTD required for the H1.4-HP1α interaction, five HA-tagged histone H1.4 constructs were generated that have progressive deletions of the CTD. Multiple phosphorylation sites are found across the H1.4 CTD and progressive deletions of the CTD therefore remove some of these phosphorylation sites. Phosphorylation of histone H1.4 is associated with a loss of the H1.4-HP1α and a reduction in its ability to condense chromatin (Hale et al., 2006). Therefore, this may also provide further information surrounding the importance of these phosphorylation sites in the H1.4-HP1α interaction.

A HA-tagged histone H1.4 H1.4-FS construct was also obtained to investigate if the pathogenic H1.4 frameshift mutant can bind to HP1α. To investigate if the alteration to the CTD resulting from the frameshift mutation that occurs at amino acid 148 in the H1.4 H1.4-FS Rahman syndrome variant (shown in red in Figure 3.1) disrupts the interaction with HP1α the H1.4 CTD deletion mutant Δ147 was designed. The H1.4 Δ147 mutant contains the same first 147 amino acids as H1.4 H1.4-FS however does not contain the frameshift region (Figure 3.1).

These constructs were used to bacterially express the various H1.4 proteins for use in *in vitro* GST pull-down assay to investigate the interaction between HP1α and the H1.4 CTD deletion mutants or H1.4 frameshift mutant.

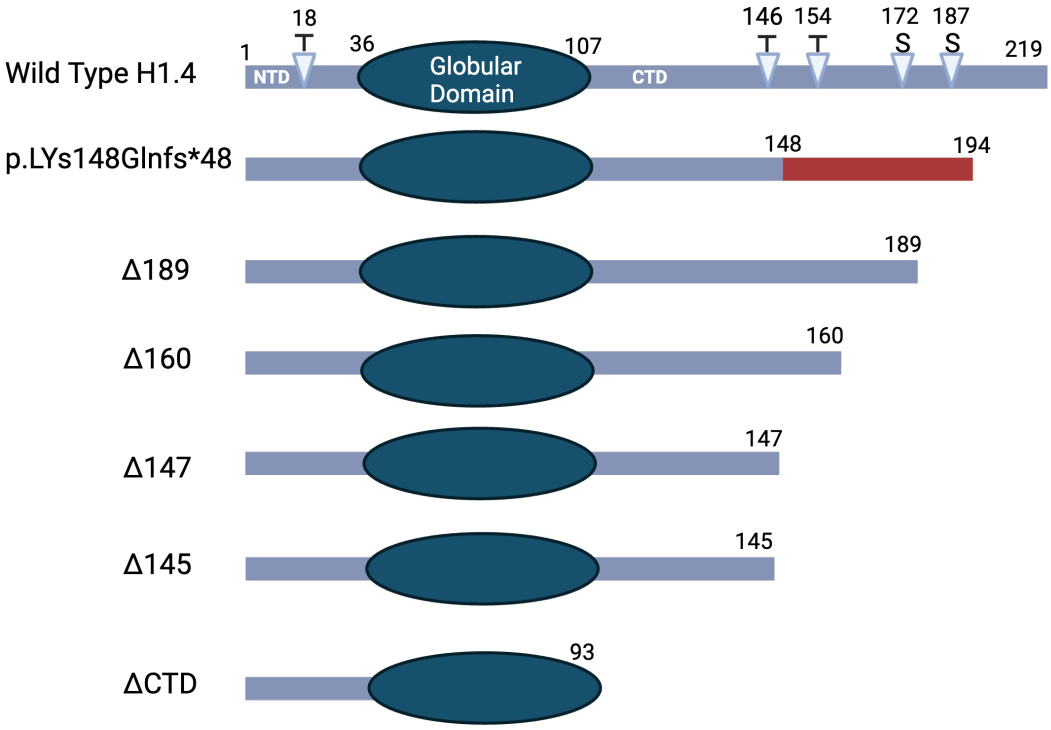

Figure 3.1: **Schematic diagram of histone H1.4, Rahman syndrome variant p.Lys148Glnfs*48 and H1.4 CTD deletion mutants.** Wild-type histone H1.4 is 219 amino acids in length and has a tripartite structure with an N-terminal domain (NTD) a central globular domain and a C-terminal domain (CTD). p.Lys148Glnfs*48 is a pathogenic frameshift mutation in histone H1.4 that is found in individuals with Rahman Syndrome. The p.Lys148Glnfs*48 Frameshift mutation is found at amino acid 148 and results in a change to the reading frame and a truncated CTD which is shown in red, however, the NTD and globular domain remains the same as wild-type H1.4. The CTD deletion mutants Δ189, Δ160, Δ147, and Δ145 all contain the same NTD and globular domain sequence as wild-type H1.4 however they each have progressively shorter C-terminal domains and each H1.4 CTD mutant is referred to by their overall length (e.g H1.4 Δ189 is 189 amino acids in length). ΔCTD refers to the H1.4 construct with no C-terminal domain and this construct was selected to act as a negative control as it has been previously shown to not interact with HP1α. Phosphorylation sites across the H1.4 protein have also been labeled. Image created with BioRender.

3.2 Development of Histone H1.4 Proteins for Pulldown Assay

3.2.1 Cloning of H1.4 Constructs into the pET24a expression vector

To obtain the H1.4 CTD deletion proteins required for the *in vitro* pulldown assays, inverse PCR was performed on a pET24a H1.4-HA plasmid (see Section 2.1.1). Inverse PCR primers were designed to generate the H1.4 CTD deletion mutants Δ189, Δ160, Δ147, Δ145 and ΔCTD (Table 2.1). Primers were designed to bind to the region of the H1.4 gene where the CTD deletion would start and the region of the pET24a plasmid at the terminal end of the H1.4 gene as shown in Figure 3.2.A. The placement of the primers results in a PCR product with the selected CTD deletion as shown in Figure 3.1. The ends of the PCR product created through inverse PCR were ligated together in order to re-form the pET24a plasmid that now contains the H1.4-HA gene with the CTD deletion (Figure 3.2.C). Inverse PCR was used to generate the H1.4 CTD deletion mutants Δ189, Δ160, Δ147, and Δ145. The H1.4 frameshift variant H1.4-FS had been previously cloned into a pET24a bacterial expression

vector using a sequence generated by Genescript.

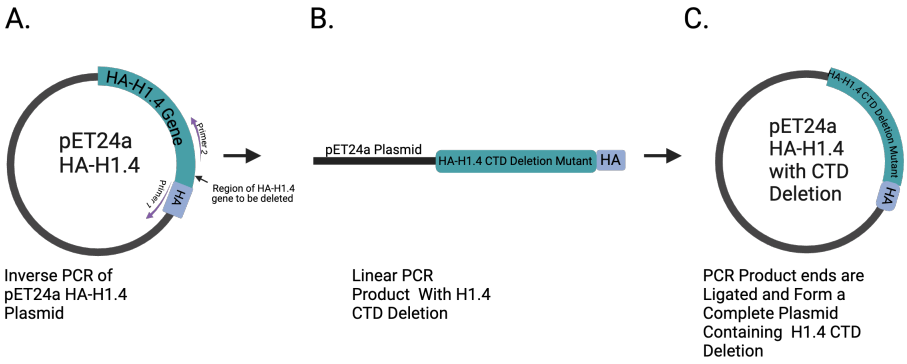

Figure 3.2: **Inverse PCR as a method to create H1.4-HA CTD deletion mutants.** Inverse PCR of the pET24a H1.4-HA plasmid was performed in order to create the H1.4-HA CTD deletion mutants Δ189, Δ160, Δ147, Δ145 and ΔCTD. **A)** A primer was designed to bind to the region of the pET24a plasmid that directly followed the CTD of the H1.4 gene. A second primer was designed to bind within the H1.4 gene in order to result in part of the terminal end of the CTD being removed during the amplification process. **B)** PCR amplification resulted in linear products that contained the pET24a plasmid sequence and the H1.4 gene with the selected region of the CTD removed. **C)** The ends of the PCR product were ligated to form a pET24a plasmid containing the HA-H1.4 CTD deletion mutant. Image created using BioRender.

Various annealing temperatures were tested in order to optimise the inverse PCR conditions for generating the H1.4 deletion constructs. Four annealing temperatures, ranging from 62°C to 70°C were used during the PCR of Δ145 and ΔCTD (Figure 3.3). All four annealing temperatures resulted in the amplification of the H1.4 CTD deletion constructs Δ145 and ΔCTD as shown by bands at the expected size, 5.6Kb for ΔCTD and 5.7Kb for Δ145 (Figure 3.3). Figure 3.3 also showed that PCR of H1.4-Δ145 resulted in non-specific PCR products, however, the amount of this non-specific PCR product decreased with higher annealing temperatures.

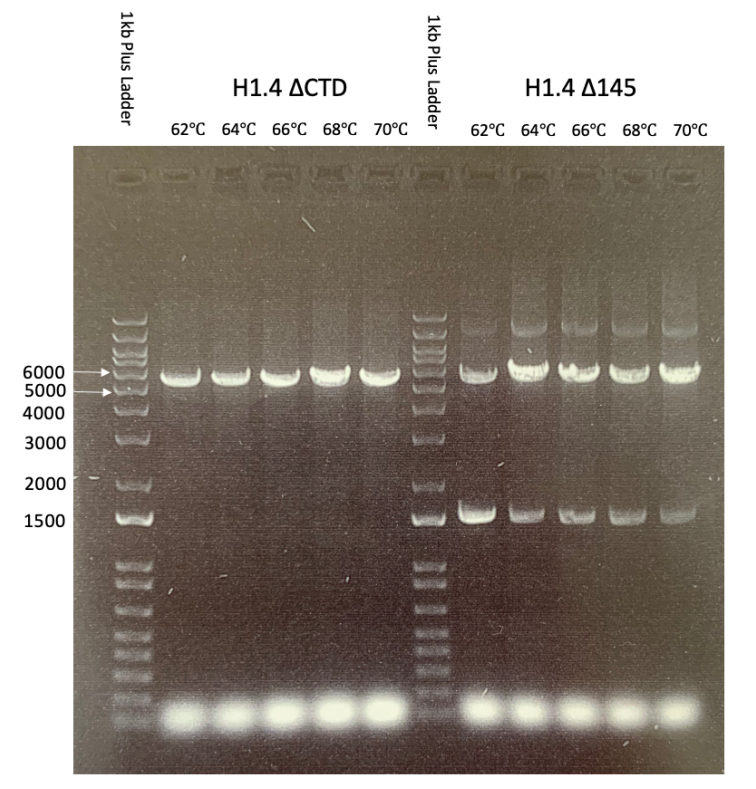

Figure 3.3: **Titration of annealing temperatures during inverse PCR.** 5μL of PCR product from each annealing temperature (62°C, 64°C, 66°C, 68°C, and, 70°C) was loaded onto a 1% agarose gel and analysed using DNA gel electrophoresis. The gel was stained with EtBr to visualise the PCR products.

For the other H1.4 CTD deletion constructs, PCR was performed using annealing temperatures of 62°C, 66°C, and 70°C. Although all annealing temperatures produced PCR products of the correct size, nonspecific PCR products were also observed. For H1.4δ189, the annealing temperature of 70°C resulted in the least amount of nonspecific PCR products. Similar sized nonspecific bands were still present for H1.4δ147 at all annealing temperatures as well as faint nonspecific bands for H1.4δ160.

Overall, the annealing temperature of 70°C resulted in reduced nonspecific bands for the H1.4δ145 (Figure 3.3) and H1.4δ189 (Figure 3.4) constructs while also producing a well defined PCR product band for all of the H1.4 CTD deletion constructs. Therefore 70°C was the annealing temperature selected to produce all of the H1.4 CTD deletion constructs used in this investigation.

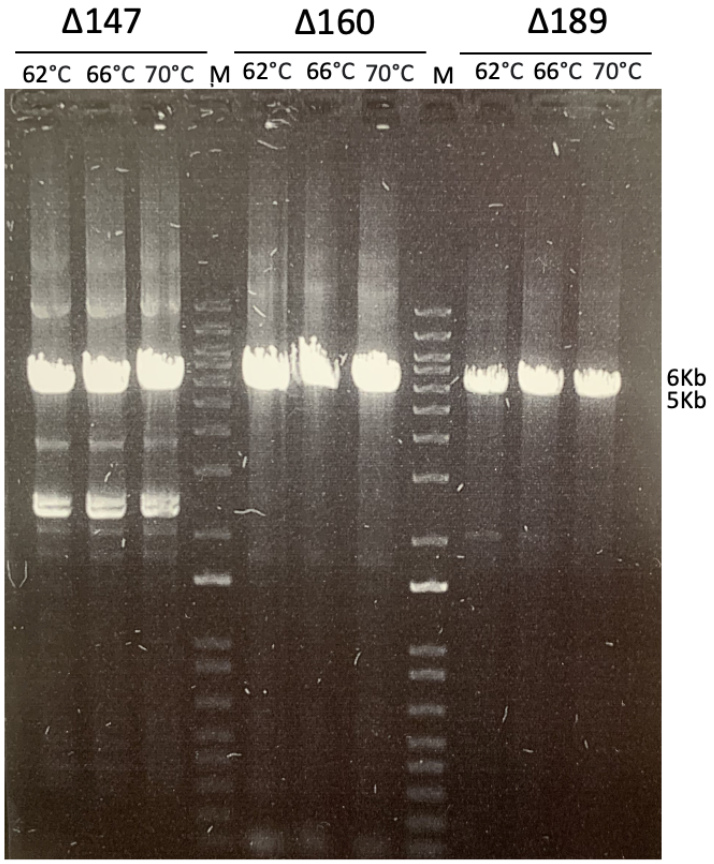

Figure 3.4: **Titration of annealing temperatures during inverse PCR to produce Δ147, Δ160 and Δ189 H1.4 CTD deletion constructs.** 5μL of PCR product from each annealing temperature (62°C, 66°C, and 70°C) was loaded onto a 1% agarose gel and analysed using DNA gel electrophoresis. The gel was stained with EtBr to visualise the PCR products.

3.2.2 Expression and Partial Purification of Histone H1.4 Proteins

To express the histone H1.4 proteins BL21 DE3 *Escherichia coli* (*E. coli*) cells were transformed with the pET24a H1.4-HA plasmid and each of the pET24a H1.4-HA CTD mutant plasmids as shown in Figure 3.1. Expression of each of the H1.4-HA proteins was induced through the addition of IPTG to the culture (see Section 2.2.1). After induction, the cultures were lysed and the soluble fractions were obtained and enriched for H1.4 by perchloric acid extraction (see Section 2.2.1). As H1.4 is a highly basic protein, this resulted in a solution containing predominantly the expressed histone H1.4 proteins as it removed the majority of the bacterial proteins. The acid-extracted H1.4-HA proteins were then resolved by SDS-PAGE shown in Figure 3.5. Single pronounced bands were observed for all of the H1.4 proteins apart from H1.4-ΔCTD. Lower bands were also visible that may represent shorter versions of the H1.4 protein or residual bacterial proteins. As no pronounced band was observed for the H1.4-ΔCTD protein, this indicated that the complete loss of the basic C-terminal domain may have prevented the acid extraction from being successful or that the protein was either insoluble or not expressed.

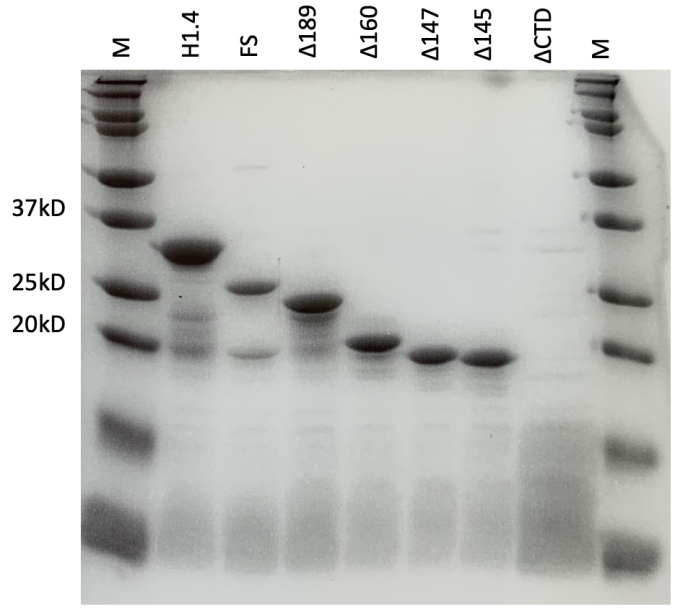

Figure 3.5: **Perchloric acid extracted H1.4-HA and H1.4-HA CTD mutants.** 5μL of perchloric acid extracted H1.4-HA, H1.4p.Lys148Glnfs*48-HA (FS), H1.4Δ189-HA, H1.4Δ160-HA, H1.4Δ147-HA, H1.4Δ145-HA and H1.4ΔCTD-HA was resolved on a 12% SDS-PAGE gel stained with Coomassie Blue blue.

To determine why there was no H1.4-ΔCTD protein present after acid extraction a diagnostic double digest was performed on the pET24a H1.4-ΔCTD-HA plasmid to determine if it still contained an insert. The diagnostic double digest was performed using the restriction enzymes HindIII and Nde1 as these were the original restriction enzymes used to clone the H1.4-HA gene into the pET24a bacterial expression vector. Two separate clones of the pET24a H1.4-ΔCTD-HA plasmids were initially purified, with the pET24a H1.4-ΔCTD-HA plasmid 2 used for the previous bacterial protein expression. A diagnostic double digest was performed on both H1.4-ΔCTD-HA plasmid 1 and H1.4-ΔCTD-HA plasmid 2 to ensure that they both contained the insert. Figure 3.6 demonstrates a band at approximately 300 base pairs (bp) for both plasmids indicating the insert is present. The H1.4ΔCTD-HA plasmids were then re-sequenced and confirmed to be correct.

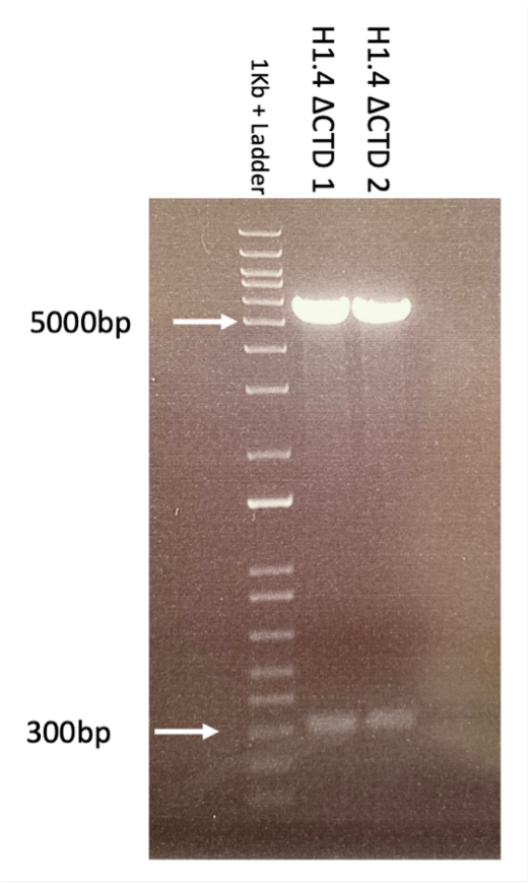

Figure 3.6: **Diagnostic double digest of HA-H1.4ΔCTD plasmids using HindIII and Nde1.** HA-H1.4ΔCTD plasmid 1 and HA-H1.4ΔCTD plasmid 2 were digested with the restriction enzymes HindIII and Nde1 to check they contained the insert with the H1.4ΔCTD gene. The double restriction digest samples were run on a 1% agarose/1%TAE EtBr gel with a band at approximately 300bp indicating the presence of the plasmid insert with the H1.4ΔCTD gene.

As the pET24a H1.4ΔCTD-HA plasmid was confirmed to be correct, a western blot of the H1.4-ΔCTD before and after-induction samples was performed along with the acid-extracted H1.4 and H1.4 CTD mutant proteins (Figure 3.7). The proteins were resolved on a 12% SDS-PAGE gel which was then transferred onto a 0.2 μm nitrocellulose membrane (see Section 2.6). This was done to determine if there was any expression of the H1.4ΔCTD protein after induction and to confirm that the bands in Figure 3.5 were the true HA-tagged H1.4 proteins. However, due to issues with the western blot in Figure 3.7, it is not possible to determine anything from this blot. Therefore it is unknown if the H1.4-ΔCTD was expressed. Due to time constraints, optimisation of the expression of H1.4-ΔCTD was not pursued. Therefore, it was not used in any of the in vitro binding assays. The purpose of the HA-H1.4ΔCTD protein was to function as a negative control as it has been shown to not interact with HP1α (Hale et al., 2006).

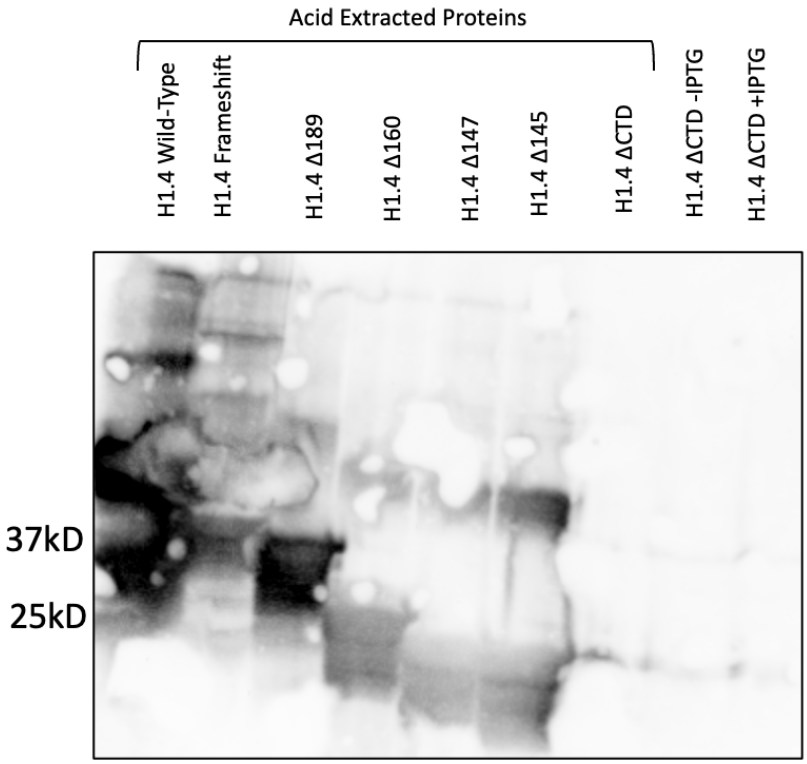

Figure 3.7: **Western blot to determine if H1.4ΔCTD-HA is present after induction culture sample.** Perchloric acid extracted H1.4-HA and H1.4-HA CTD mutants along with before and after induction samples of H1.4ΔCTD-HA were resolved on a 12% SDS-PAGE gel before being transferred onto a 0.2μm nitrocellulose membrane and proteins were detected using anti-HA antibody.

3.2.3 Quantification of Acid Extracted H1.4 Proteins

The acid-extracted HA-H1.4, HA-H1.4 Frameshift (HA-H1.4-FS), and H1.4-HA CTD deletion mutants were quantified using a bicinchoninic acid (BCA) assay (see Section 2.3.1). Calf thymus H1 was used as the standard for the BCA assay to increase the accuracy of the protein concentration. The accuracy of the protein concentrations determined by the BCA assay was then checked by resolving the samples on a 12% SDS-PAGE gel (see Section 2.5.2). The bands for the acid-extracted H1.4-HA and H1.4-HA CTD deletion mutants were approximately the same intensity, however, there was less H1.4-FS-HA protein shown by the less intense band indicating that the BCA assay concentration may not be accurate(Figure 3.8). Additional increasing amounts of H1.4-FS-HA protein were also resolved to determine if a ratio between the concentration of H1.4-FS-HA to one of the other H1.4 proteins could be observed. The band that resulted from resolving 10 μg of HA-H1.4-FS was approximately equivalent to the bands that represented 5 μg of the other proteins resolved on the same 12% SDS-PAGE gel and therefore it was decided to use twice as much of the HA-H1.4-FS in the pulldown assays (Figure 3.8).

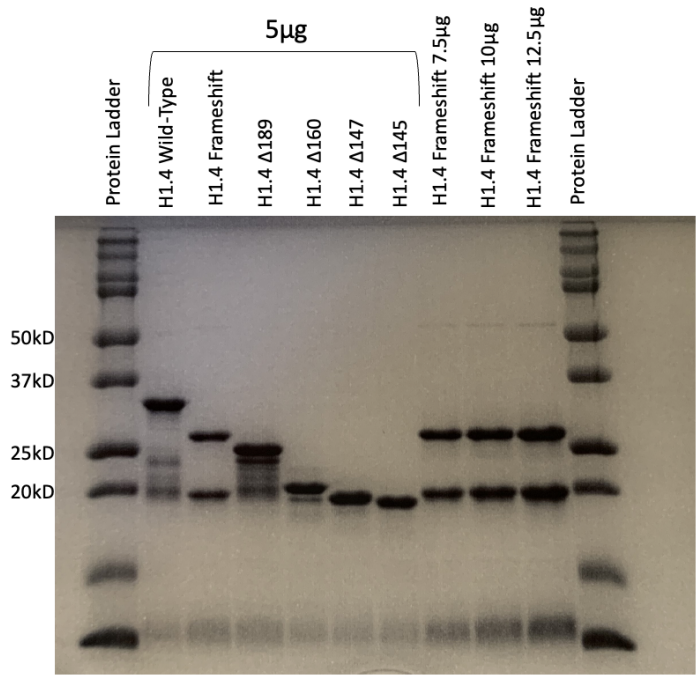

Figure 3.8: **Perchloric acid extracted H1.4-HA and H1.4-HA CTD mutant quantification.** 5μg of perchloric acid extracted H1.4-HA, H1.4 p.LYs148Glnfs*4-HA (H1.4-FS), H1.4Δ189-HA, H1.4Δ160-HA, H1.4Δ147-HA, H1.4Δ145-HA and H1.4ΔCTD-HA was resolved on a 12% SDS-PAGE gel stained with Coomassie blue.

To better determine the concentration of the H1.4-FS-HA protein for use in the GST-HP1α pulldown assay a titration of different amounts of the HA-H1.4 and H1.4-FS-HA proteins was resolved on a 12% SDS-PAGE gel and then a Western blot was performed using an anti-HA antibody (Figure 3.9). The bands detected in this Western blot represent the amount of HA-tag in the sample and as each H1.4-HA or H1.4-FS-HA has exactly one HA tag per protein this allows for a better representation of how true the protein concentrations determined by the BCA assay are. The protein concentrations from the BCA assay had been previously checked through the resolving of an exact amount of the proteins on a 12% SDS-PAGE gel which was then stained with Coomassie blue (Figure 3.8). The bands that appear on the SDS-PAGE result from the interaction of the Coomassie blue dye with basic amino acids that are found in the proteins resolved on the SDS-PAGE. Differences in the percentages of these basic amino acids in the protein samples may result in the appearance of bands that do not truly reflect their actual concentration. The H1.4-FS-HA protein has a reduced percentage of basic amino acids due to the frameshift mutation in the CTD which may be the reason for the difference in the band size for the H1.4-FS-HA protein on the SDS-PAGE (Figure 3.8). Figure 3.9 shows that H1.4-FS-HA protein appears to be less concentrated than what was determined by the BCA assay. The band on the Western blot that represents 0.25 μg of the H1.4-FS-HA protein appears to be more equivalent to the band that represents 0.75 μg of the H1.4-HA protein indicating that there was three times as much of the H1.4-FS-HA protein than the H1.4-HA protein (Figure 3.9).

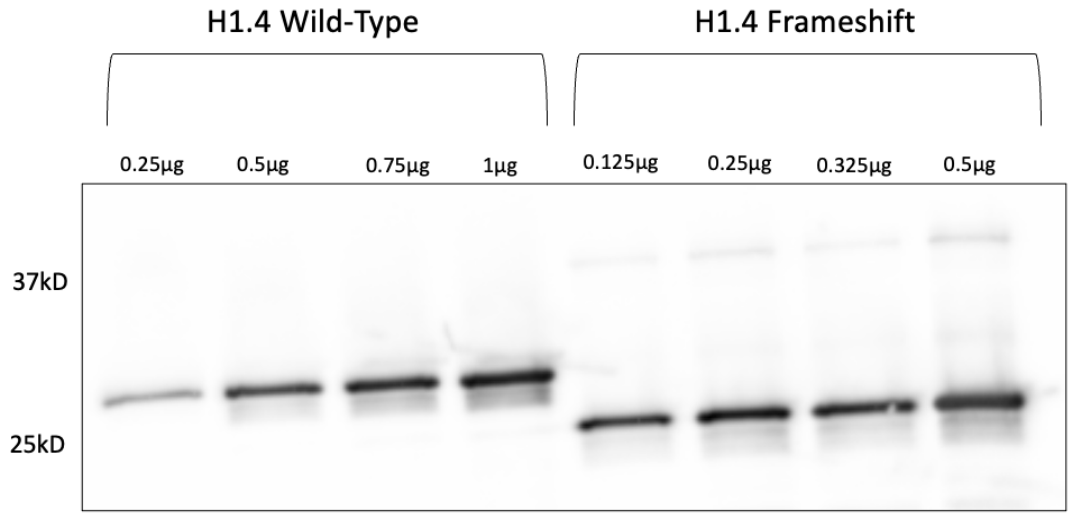

Figure 3.9: **Western blot of H1.4-HA and H1.4-FS-HA protein concentration titration.** Titrating amounts of H1.4-HA(H1.4 Wild-Type) and H1.4 p.Lys148Glnfs*48-HA (H1.4-FS) were resolved on a 12% SDS-PAGE gel and then a Western blot using an anti-HA antibody was performed.

3.3 Expression of GST Tagged HP1α Proteins for Pulldown Assay

To perform the GST-HP1α pulldown assays, GST tagged HP1α along with GST was expressed. The PGEX2T-GST-HP1α and PGEX2T-GST plasmid constructs (see Section 2.1.2) were transformed into *E.coli* BL21 DE3 competent cells and expression of the GST-HP1α and GST proteins was induced by the addition of IPTG to the culture. Before and after induction samples of the whole cell culture for GST and GST-HP1α were resolved on a 12% SDS-PAGE gel which indicated that both GST-HP1α and GST were expressed (3.10). A band at approximately 50 kD in the after-induction sample that was not present in the before-induction sample indicated the presence of GST-HP1α, while a band at approximately 26 kD in the after-induction sample indicated the presence of GST (Figure 3.10).

After induction, the supernatant containing the soluble protein was collected and resolved on an SDS-PAGE gel to determine if GST-HP1α and GST were still present in the soluble fraction of the lysate(Figure 3.11). Both GST-HP1α and GST were determined to be present in the soluble fraction as indicated by bands at 50kD in the GST-HP1α samples and bands at 25kD in the GST samples (Figure 3.11). Additional bands were also observed in figure 3.10 and 3.11 due to bacterial proteins that remained present in the lysate.

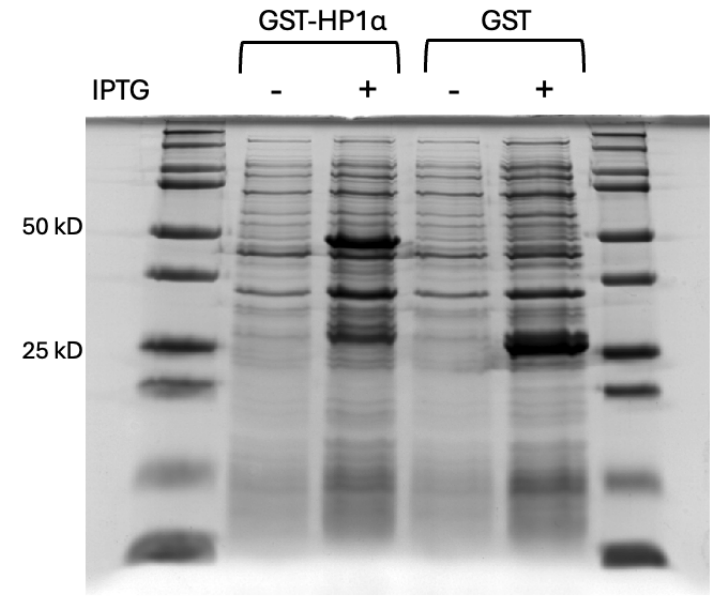

Figure 3.10: **GST-HP1α and GST before and after induction samples on 12% SDS PAGE** GST-HP1α and GST culture samples were taken before and after the addition of IPTG. 50μL of the before-induction (- IPTG) and after-induction (+ IPTG) samples were resolved on a 12% SDS-PAGE gel which was stained with Coomassie Brilliant Blue R to visualise the proteins.

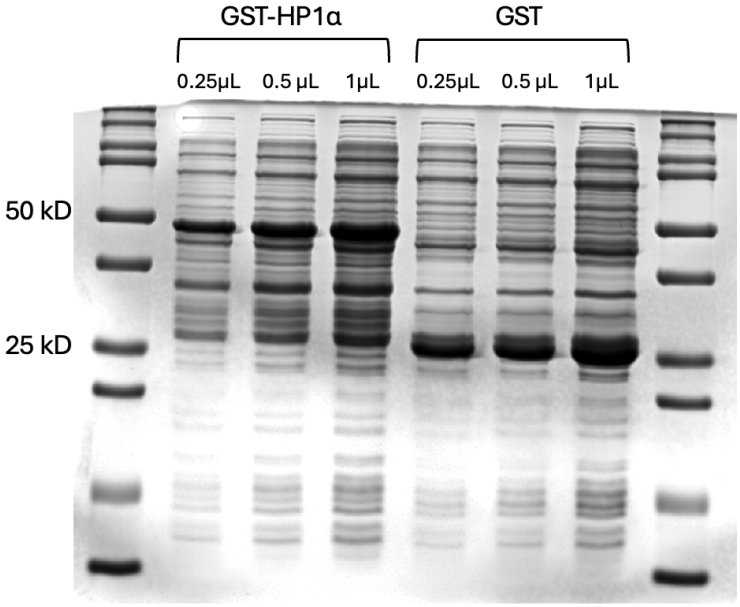

Figure 3.11: **Titration of GST-HP1α and GST lysate on 12% SDS-PAGE.** 0.25μL, 0.5μL and 1μL of the cleared soluble GST-HP1α and GST lysates were resolved on a 12% SDS-PAGE gel which was stained with Coomassie Brilliant Blue R.

3.4 GST-HP1α and HA-H1.4 Pulldown Assays

To investigate the role of the H1.4 CTD in the H1.4-HP1α interaction *in vitro* binding assays using GST tagged HP1α were set up (see Section 2.7). The cleared GST-HP1α lysate was incubated with Glutathione Agarose beads for 2 hours after which it underwent subsequent wash steps in order to remove any remaining bacterial protein from the reaction (see Section 2.7). GST has a high affinity to glutathione agarose beads and therefore this allows for the beads to be used for both the purification of the GST and GST-HP1α lysate as well as for the *in vitro* binding assay. Preliminary unpublished research has indicated that the H1.4-HP1α interaction may be possibly mediated by RNA. Therefore, 3.5μg of total RNA from MCF7 cells was then added to the GST-HP1α and Glutathione Agarose bead complex and left to incubate for a further 30 minutes. The RNA should bind to the hinge region of HP1α due to its affinity for nucleic acids. Any unbound RNA was removed through wash steps. An additional reaction was set up in the same way with GST instead of GST-HP1α to use as a control to determine if there was any non-specific binding of the H1.4 proteins to the GST protein.

The H1.4-HA and H1.4-FS-HA proteins were added to the GST-HP1α-Glutathione Agarose bead complex and the control GST-Glutathione Agarose bead complex with 2 different concentrations of H1.4-HA and H1.4-FS-HA protein used (1.3μg and 2.6μg). This was done to determine the appropriate conditions for the *in vitro* GST pulldown assay. The resulting complexes were resolved on a 12% SDS-PAGE gel followed by a Western blot using an anti-HA antibody to detect if the H1.4-HA or H1.4-FS-HA proteins were pulled down with the GST-HP1α or GST control (Figure 3.12). Figure 3.12 shows that both H1.4-HA and H1.4-FS-HA were pulled down in both the GST-HP1α reaction and the GST control reaction, indicating that the H1.4 proteins were binding non-specifically to the GST protein or to the Glutathione Agarose beads. Therefore further optimisation of the *in vitro* GST pulldown was performed to address the non-specific binding.

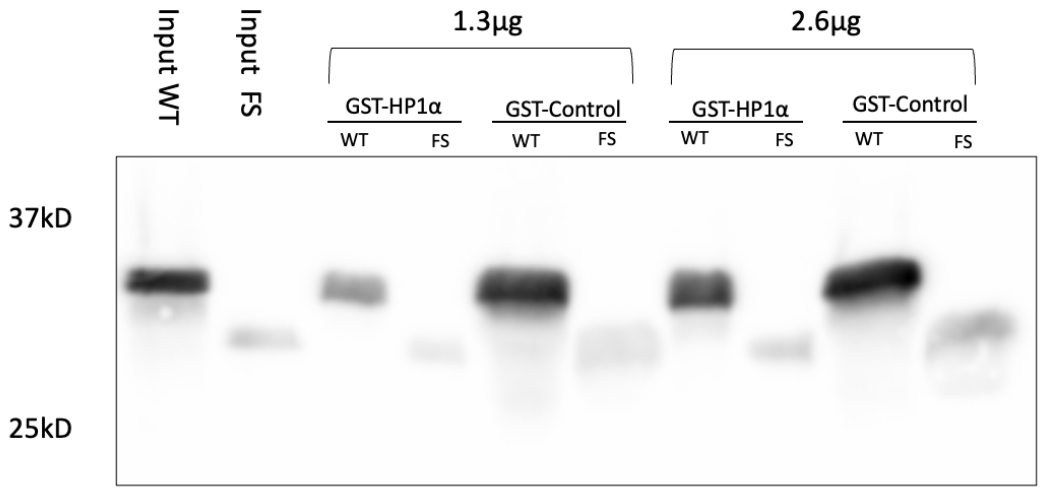

Figure 3.12: **GST-HP1α *in vitro* pulldown to investigate interaction with H1.4 p.Lys148Glnfs*48-HA (H1.4-FS).** Western blot of GST-HP1α *in vitro* pulldown. GST-HP1α and GST were bound to Pierce™ Glutathione Agarose beads, along with 3.5μg of total RNA from MCF7 cells, and then incubated with either 1.3μg or 2.6μg of H1.4-HA (WT) or H1.4 p.Lys148Glnfs*4-HA (H1.4-FS).

As pulldown reactions using GST-HP1α and H1.4 have been previously performed with no binding of H1.4 to GST alone, the GST-HP1α pulldown was repeated with optimisations in order to prevent the non-specific binding of the H1.4-HA and H1.4-FS-HA proteins to GST (Hale et al., 2006). This subsequent pulldown assay was performed with the same GST-HP1α and Glutathione Agarose beads, however the volume of both GST-HP1α and GST added to the Glutathione Agarose beads was reduced (see Section 2.7.3). A high concentration of GST-HP1α and GST in the interaction may increase the likelihood of non-specific interactions occurring. Another optimisation was to not add any additional total RNA to the reaction and to increase the number of wash steps after the 2-hour incubation step. Due to the GST-HP1α and GST proteins not being purified before use in the pulldown assay, there may be bacterial RNA from the GST-HP1α and GST protein lysate still present and binding to the GST-HP1α and GST protein during the 2-hour incubation with the Glutathione Agarose beads. If this is the case then excessive RNA in the reaction may have facilitated non-specific interactions with the H1.4-HA and H1.4-FS-HA proteins to GST. It was also observed in Figure 3.14 that the input bands were not of similar intensity, indicating that the concentrations determined in Figure 3.9 were not accurate. It was decided to continue with the original protein concentration for H1.4-FS-HA determined by the BCA assay for future GST-pulldown reactions. The thickness of the bands in Figure 3.12 also indicated that the proteins were not resolved correctly during SDS-PAGE. Potentially due to an incorrect ratio of stacking gel to resolving gel. It was therefore also ensured that the SDS-PAGE gel had an increased stacking layer to ensure that the proteins were correctly entering the resolving gel.

Figure 3.13 shows the Western blot result of the GST-HP1α pulldown assay with the above changes implemented (see Section 2.7.3) that also tested the interaction of two H1.4 CTD deletion mutants, H1.4Δ145-HA and H1.4Δ160-HA with GST-HP1α. In Figure 3.13 2μg of the H1.4-HA, H1.4-FS-HA, H1.4Δ145-HA, and H1.4Δ160-HA proteins were added to the complex of either GST-HP1α and Glutathione Agarose beads or GST and Glutathione Agarose beads and left to incubate overnight. The resulting complexes that formed were then resolved on a 12% SDS-PAGE gel and a Western blot probed with an anti-HA antibody was performed to detect the HA-tagged proteins pulled down with GST-HP1α and GST (see Section 2.6). H1.4-HA, H1.4-FS-HA, and H1.4Δ160-HA were pulled down with GST-HP1α due to the presence of a band in the HP1α lane in Figure 3.13. However, H1.4-HA and H1.4-FS-HA were also pulled down with GST indicating that it is still non-specifically binding to GST despite the optimisations to the protocol (Figure 3.13). Neither H1.4Δ160-HA nor H1.4Δ145-HA bound to GST indicating that this non-specific binding issue was specifically with the H1.4-HA and H1.4-FS-HA proteins and there was also no binding of H1.4Δ145-HA to GST-HP1α (Figure 3.13).

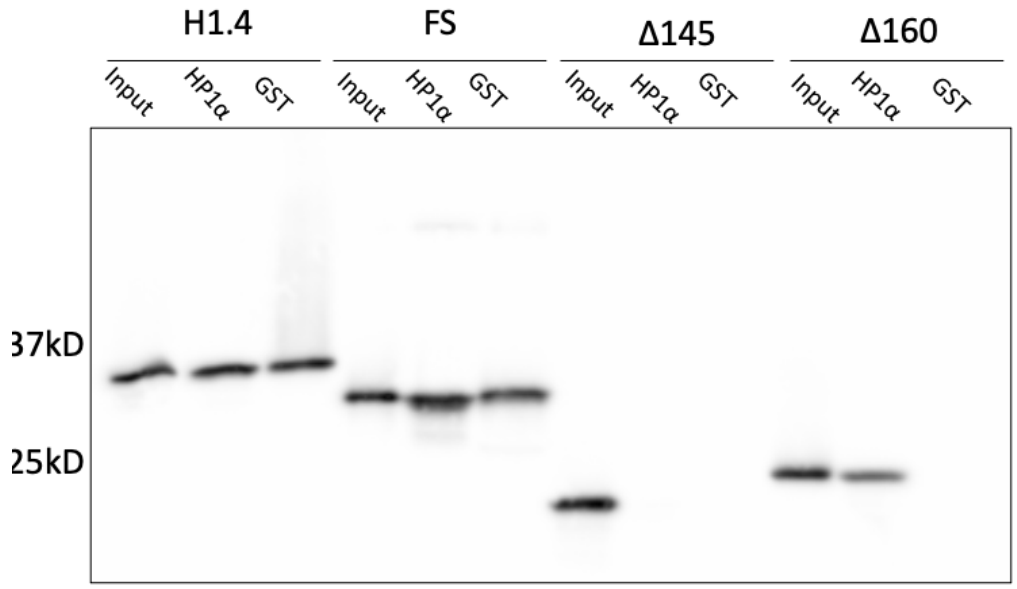

Figure 3.13: **Western blot of GST-HP1α *in vitro* pulldown.** GST-HP1α and GST were bound to Pierce™ Glutathione Agarose beads and then incubated with 2μg of either HA-H1.4 (WT), HA-H1.4 p.LYs148Glnfs*4 (FS), HA-H1.4.Δ145 (Δ145) or HA-H1.4.Δ160 (Δ160)

3.5 Summary

Due to the presence of non-specific binding of H1.4-HA and H1.4-FS-HA to GST, it is not possible to make any conclusions from this western blot surrounding how the changes to the CTD of H1.4 impact the binding to HP1α and further optimisations of the GST-HP1α pulldown assay are required (Figure 3.13). Due to time constraints, the in vitro binding assay was unable to be optimised and has not been able to be used to answer any questions about the H1.4-HP1α interaction. Future GST-pulldown assays will be performed with additional optimisations such as using bovine serum albumin (BSA) to block the Glutathione Agarose beads before use. This would be done to prevent any unspecific interactions from occurring.

Chapter 4

Investigating the Importance of the Histone H1.4 CTD *In Vivo*

4.1 Introduction

Heterochromatin homeostasis is essential for genomic stability and both histone H1.4 and HP1α are involved. FRET has been previously used to show that H1.4 was co-localising with HP1α in NIH3T3 cells (Hale et al., 2006). However, it has not been demonstrated how changes to the CTD of H1.4 affect its co-localisation with HP1α. The H1.4-HP1α interaction has been shown to involve the CTD of H1.4, which is affected by a frameshift mutation in Rahman Syndrome. The change to the H1.4 CTD combined with the findings of reduced heterochromatin markers observed in Rahman syndrome patient fibroblasts, suggests that expression of the H1.4 frameshift mutant may interfere with HP1α function (Flex et al., 2019)

While Flex et al. (2019) demonstrated that the H1.4 frameshift mutant disrupts heterochromatin, whether this is due to just the truncation of the CTD or to loss of part of the CTD or due to a change in the composition of the tail is unknown. Therefore, both the frameshift variant H1.4 H1.4-FS and the H1.4 CTD deletion mutant H1.4-Δ147 will be investigated to determine how they impact heterochromatin homeostasis and nuclear morphology. The frameshift mutation that results in the change in the reading frame starts at amino acid 148 in H1.4-FS, therefore the expression of H1.4-Δ147 will be used to determine if the new sequence in the CTD results in a different function.

Immunofluorescence studies, looking at how the expression of the H1.4 frameshift mutant and the H1.4 CTD deletion mutants affects markers involved in heterochromatin and nuclear morphology will be used in this study. This will be done to better understand the H1.4-HP1α interaction *in vivo* and its role in heterochromatin homeostasis.

4.2 Creation of Histone H1.4 Constructs in the pcDNA3.1 Vector

To investigate the role of the H1.4 CTD in HP1α mediated heterochromatin homeostasis *in vivo*, the H1.4 CTD mutants H1.4-Δ147 and H1.4-ΔCTD used along with wild type H1.4 and the Rahman syndrome H1.4 variant H1.4-FS were used. Since a pcDNA3.1Neo vector that expressed H1.4 with a c-terminal FLAG tag was already available, this vector was used to generate the H1.4 CTD mutants

H1.4-Δ147-FLAG, H1.4-ΔCTD-FLAG and H1.4-FS-FLAG. This allows for the H1.4-FLAG constructs to be transiently transfected into the selected cell line and be expressed by the cell.

The H1.4 CTD deletion mutants H1.4-Δ147-FLAG, and H1.4-ΔCTD-FLAG were generated using inverse PCR (see Section 2.1.1). Primers were designed to bind to the region of the H1.4 gene where the CTD deletion would start and also the terminal end of the pcDNA3.1 plasmid as shown in Figure 4.1.

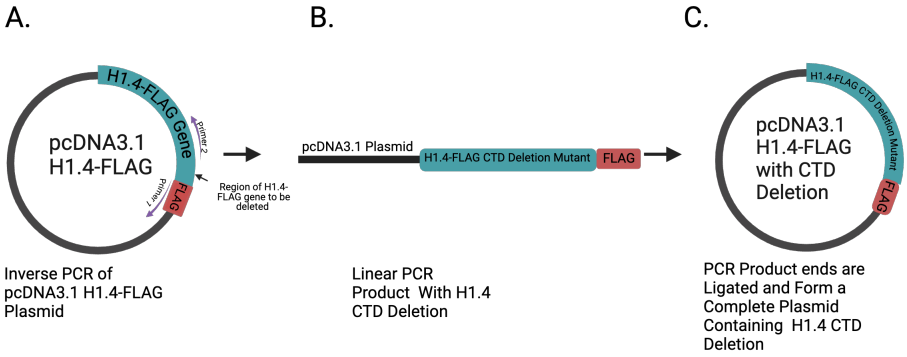

Figure 4.1: **Inverse PCR to generate H1.4 CTD mutants into the pcDNA3.1Neo vector** Inverse PCR of the pcDNA3.1Neo H1.4-FLAG plasmid was performed in order to create the H1.4-FLAG CTD deletion mutants Δ147 and ΔCTD. **A)** A primer was designed to bind to the FLAG tag and a region of the pcDNA3.1Neo plasmid that directly followed the CTD of the H1.4 gene. A second primer was designed to bind within the H1.4 gene in order to result in part of the terminal end of the CTD being removed during the amplification process. **B)** PCR amplification resulted in linear products that contained the pcDNA3.1Neo plasmid sequence and the H1.4 gene with the selected region of the CTD removed. **C)** The ends of the PCR product were ligated to form a pcDNA3.1Neo plasmid containing the H1.4-FLAG CTD deletion mutant. Image created using BioRender.

The Rahman Syndrome frameshift variant p.Lys148Glnfs*48 (H1.4-FS) was also cloned into a pcDNA3.1 expression vector through a combination of inverse PCR and blunt-end cloning(see Section 2.1).

The change in reading frame caused by the frameshift mutation starts at amino acid 148 and results in an early stop codon at amino acid 194. PCR primers were designed to extract only this frameshift region (amino acid 148 to 194) from the pET24a H1.4-FS-HA plasmid. The frameshift sequence was then blunt-end cloned into a pcDNA3.1H1.4Δ147-FLAG fragment produced using inverse PCR (see Section 2.1.2).

4.3 H1.4 CTD is important for co-localisation with HP1α *In Vivo*

The co-localisation between H1.4 and HP1α has also been shown to occur in *in vivo* with FRET studies showing that transiently transfected H1.4 will co-localise with HP1α (Hale et al., 2006). While it has been determined that the deletion of the H1.4 CTD prevents binding with HP1α *in vitro* it has not been determined what regions of the H1.4 CTD are required for co-localisation of H1.4 with HP1α *in vivo*. The Rahman syndrome frameshift variant p.Lys148Glnfs*48 (H1.4-FS-FLAG), was also tested to see if it can co-localise with HP1α *in vivo*. NIH3T3 mouse fibroblast cells were transiently transfected with constructs expressing H1.4-FLAG, H1.4-FS-FLAG, and two of the H1.4-FLAG CTD

deletion constructs, H1.4-Δ147-FLAG and H1.4-ΔCTD-FLAG.

After 48 hours the transfected NIH3T3 cells were processed for immunofluorescence using antibodies directed against the FLAG tag on the H1.4 constructs as well as endogenous HP1α (see Section 2.9.2).

Figure 4.2 shows that co-localisation of H1.4-FLAG and HP1α occurred in the NIH3T3 cells transfected with H1.4-FLAG. HP1α foci refer to the various discrete dots that occur due to the high density of HP1α at that location resulting in an increase in signal intensity. Co-localisation refers to the direct localisation of one of these HP1α foci with an H1.4 foci. However, there was some H1.4-FLAG not co-localised with HP1α and this may be due to the exogenous H1.4-FLAG resulting in excessive amounts of H1.4, with not all bound to the endogenous HP1α. Due to this increased expression of H1.4-FLAG in the NIH3T3 cells, the HP1α patterning of un-transfected cells was also observed (Figure 4.6). As the patterning of the endogenous HP1α in the NIH3T3 appeared similar to that of NIH3T3 cell expressing H1.4-FLAG, it was determined that the expression of H1.4-FLAG did not cause any changes in patterning and localisation of endogenous HP1α (Figure 4.6).

However, there was a reduction in the co-localisation between HP1α foci and H1.4-FS-FLAG (Figure 4.3), H1.4-Δ147-FLAG (Figure 4.4), and H1.4-ΔCTD-FLAG (Figure 4.5) indicating that the CTD is important for co-localisation with HP1α. Instead, the H1.4 CTD mutant foci were often found adjacent to the HP1α foci (Figure 4.3, Figure 4.4, and Figure 4.5).

These findings indicate that the change to the CTD of H1.4 results in a reduction in co-localisation of H1.4 to HP1α. Both H1.4-FS-FLAG and H1.4-Δ147-FLAG had a reduction in co-localisation with HP1α indicating that the H1.4-FS-FLAG behaves similarly to H1.4-Δ147-FLAG in regard to co-localisation with HP1α. This also suggests that the region of the CTD necessary for the co-localisation with HP1α *in vivo* is between amino acids 147 and 219.

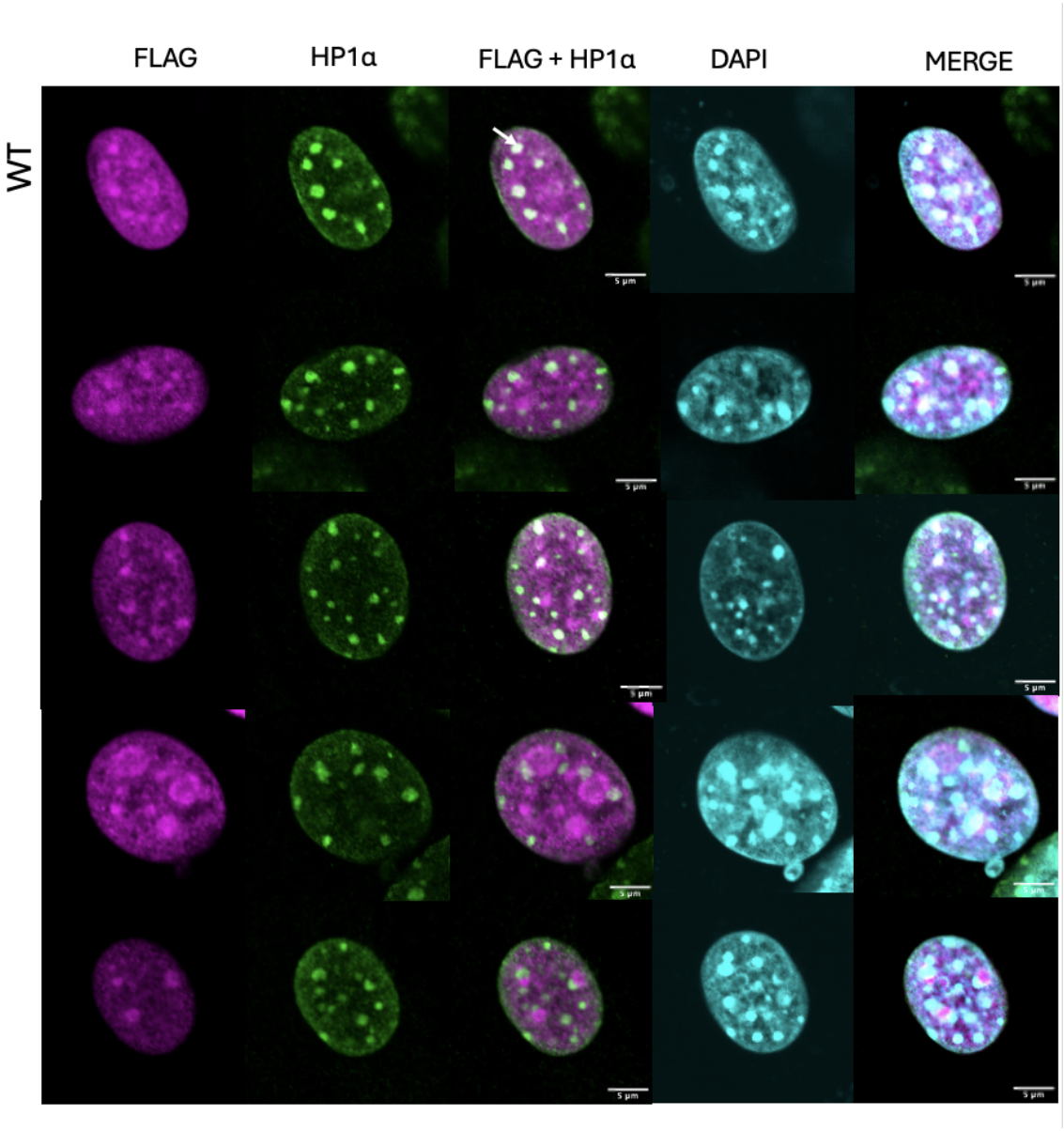

Figure 4.2: **Wild-type H1.4-FLAG and HP1α localisation in NIH3T3 cells**. Confocal microscope immunofluorescence images of NIH3T3 nuclei transiently transfected with a pcDNA3.1 plasmid expressing H1.4 with a c-terminal FLAG tag. Antibodies directed against the FLAG tag and endogenous HP1α were used as well as DAPI to stain the DNA. H1.4-FLAG wild-type (WT) is shown in magenta, HP1α green, and DAPI cyan. The scale bar is 5 μm. The white arrow indicates an example of co-localisation of FLAG and HP1α.

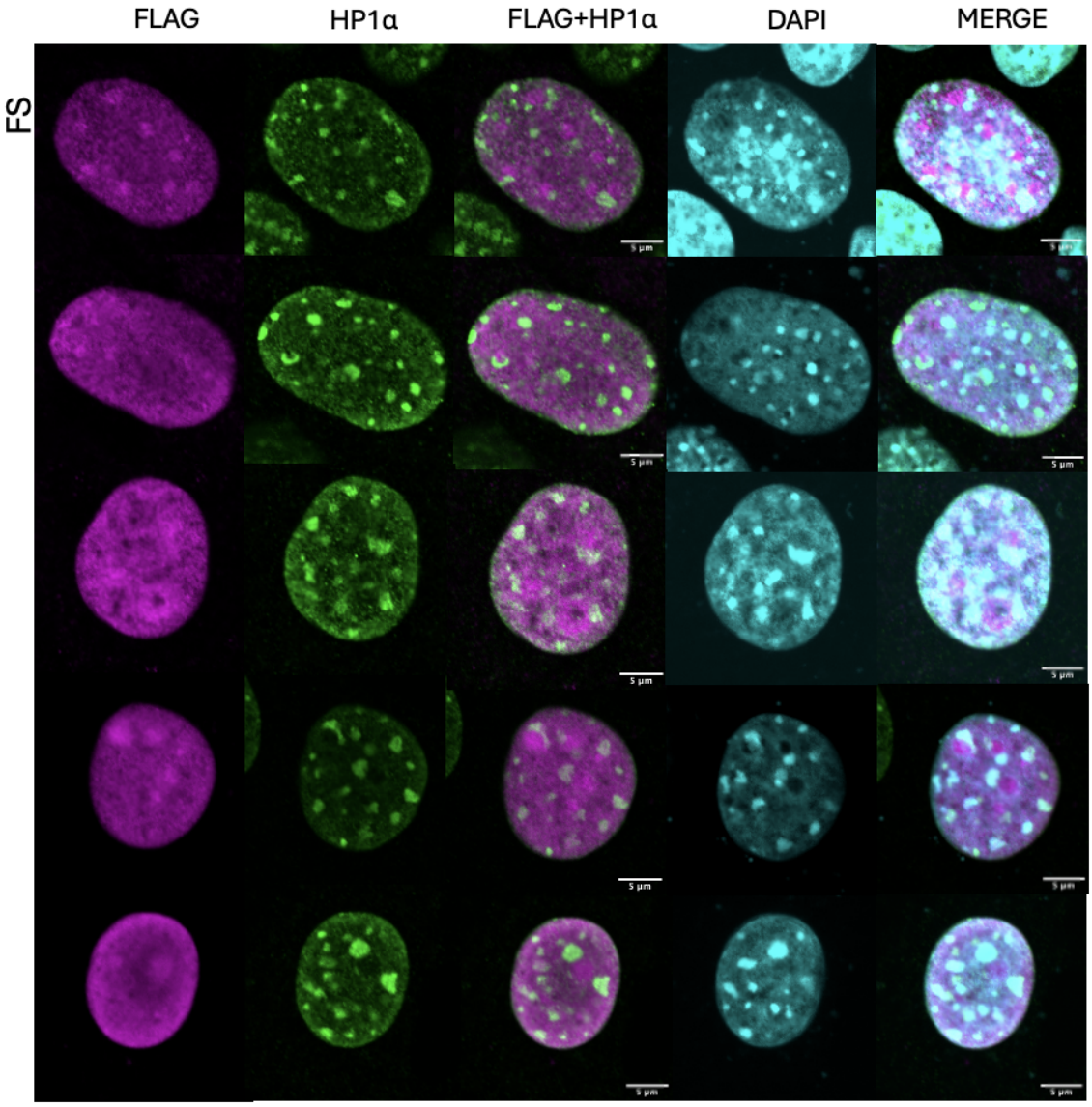

Figure 4.3: **H1.4 p.Lys148Glnfs*48-FLAG (H1.4-FS-FLAG) and HP1α localisation in NIH3T3 nuclei.** Confocal microscope immunofluorescence images of NIH3T3 nuclei transiently transfected with a pcDNA3.1 plasmid expressing H1.4-FS-FLAG (FS) with a c-terminal FLAG tag. Antibodies directed against the FLAG tag and endogenous HP1α were used as well as DAPI to stain the DNA. H1.4-FS-FLAG (FS) is shown in magenta, HP1α green, and DAPI cyan. The scale bar is 5 μm.

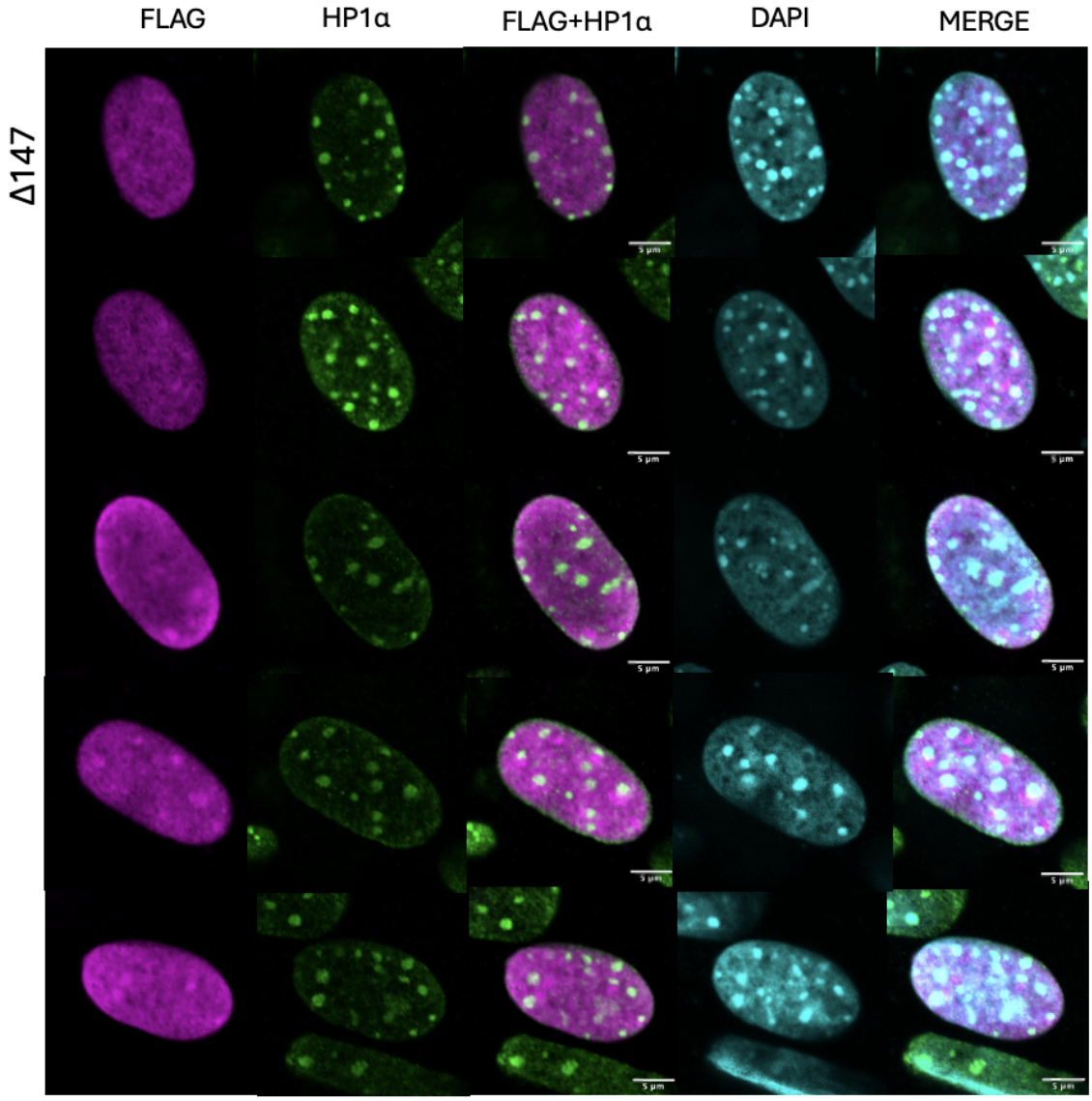

Figure 4.4: **H1.4-Δ147-FLAG and HP1α localisation in NIH3T3 nuclei.** Confocal microscope immunofluorescence images of NIH3T3 nuclei transiently transfected with a pcDNA3.1 plasmid expressing H1.4-Δ147-FLAG (Δ147) with a c-terminal FLAG tag. Antibodies directed against the FLAG tag and endogenous HP1α were used as well as DAPI to stain the DNA. H1.4-Δ147-FLAG (Δ147) is shown in magenta, HP1α green, and DAPI cyan. The scale bar is 5 μm.

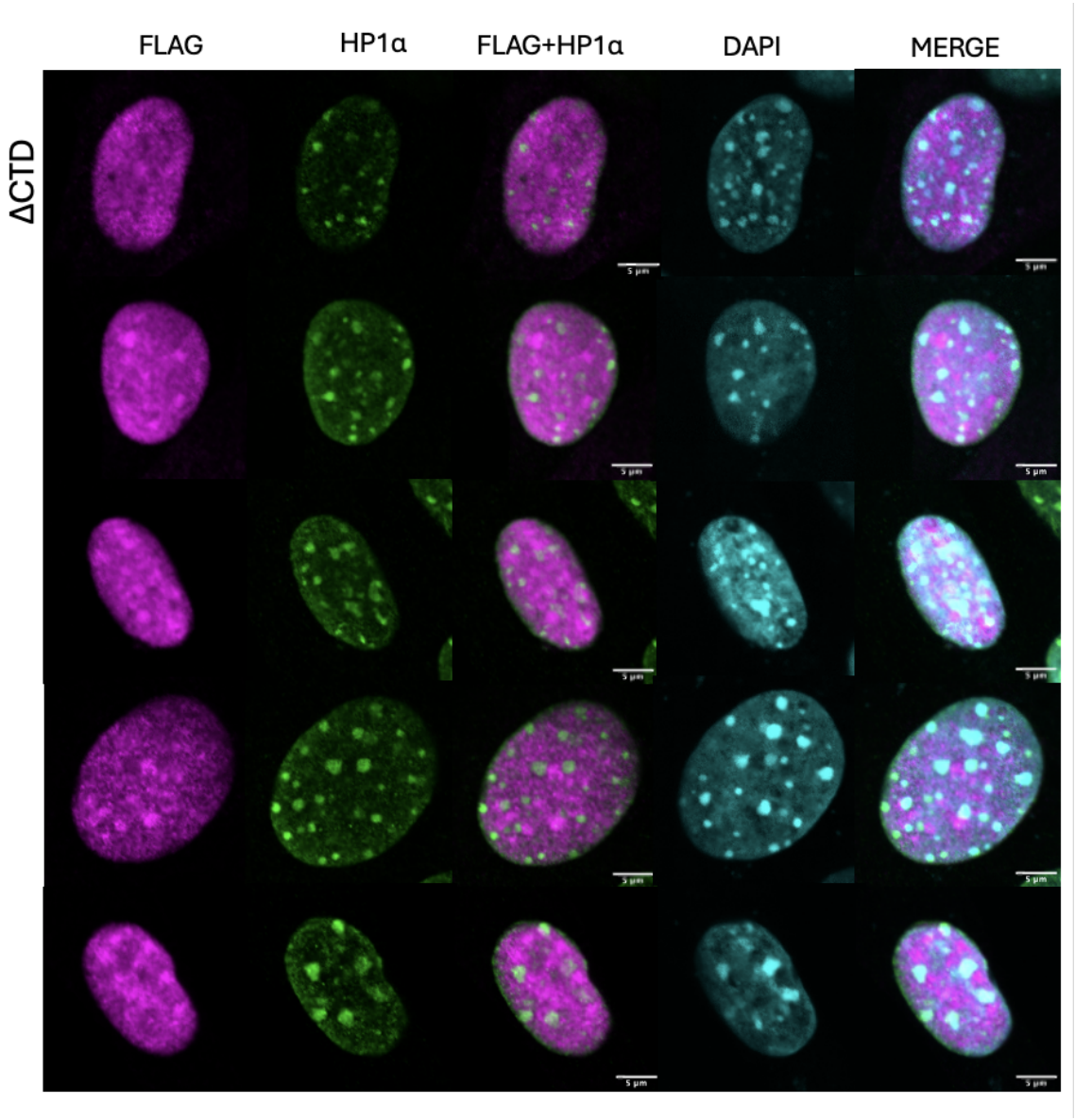

Figure 4.5: **H1.4-ΔCTD-FLAG localisation in NIH3T3 nuclei.** Confocal microscope immunofluorescence images of NIH3T3 nuclei transiently transfected with a pcDNA3.1 plasmid expressing H1.4-ΔCTD-FLAG (ΔCTD) with a c-terminal FLAG tag. Antibodies directed against the FLAG tag and endogenous HP1α were used as well as DAPI to stain the DNA. H1.4-ΔCTD-FLAG (ΔCTD) is shown in magenta, HP1α green, and DAPI cyan. The scale bar is 5 μm.

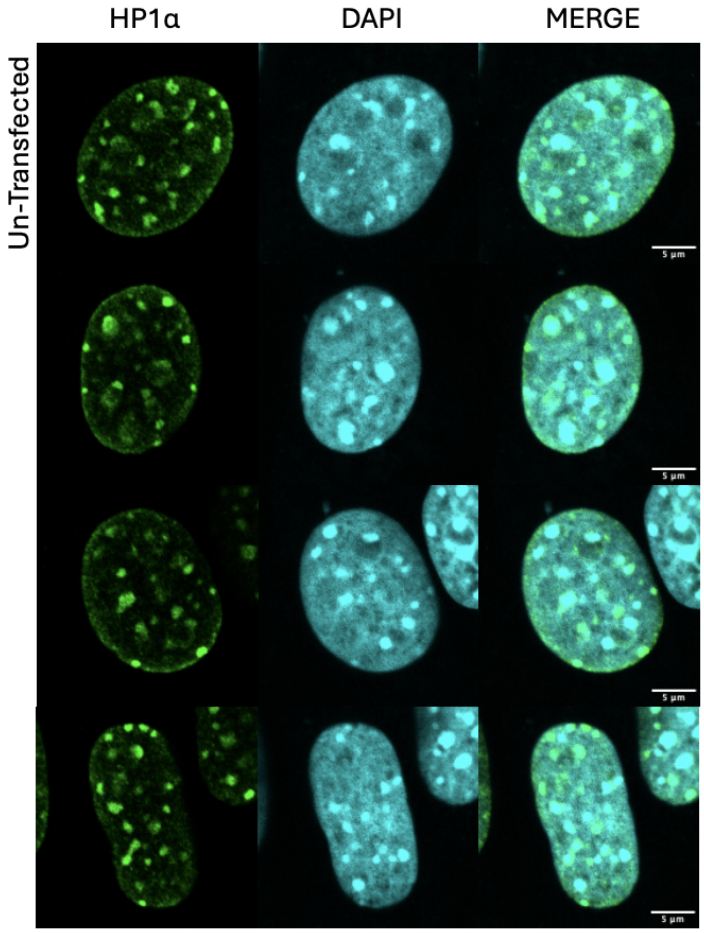

Figure 4.6: **HP1α localisation in NIH3T3 nuclei.** Confocal microscope immunofluorescence images of un-transfected NIH3T3 nuclei. Antibodies directed against endogenous HP1α were used as well as DAPI to stain the DNA. HP1α is shown in green, and DAPI is shown in cyan. The scale bar is 5 μm.

4.4 Changes to H1.4 CTD Alter Heterochromatin Patterning

To determine if the H1.4 CTD alters H3K9me3 mediated heterochromatin patterning NIH3T3 mouse fibroblast cells were transiently transfected with H1.4-FLAG, H1.4-FS-FLAG, H1.4 Δ147-FLAG and H1.4 ΔCTD-FLAG. After 48 hours the transfected NIH3T3 cells were processed for immunofluorescence with the use of an anti-FLAG antibody, an anti-H3K9me3 antibody, and DAPI to stain the DNA (see Section 2.9.2).

The NIH3T3 cells expressing H1.4-FLAG showed discrete H3K9me3 foci (Figure 4.8) however, these H3K9me3 domains did not show complete co-localisation with DAPI foci (Figure 4.12). Heterochromatic domains in the nucleus are comprised of highly condensed DNA and therefore appear as bright discrete foci after staining with DAPI. Therefore H3K9me3 foci are expected to co-localise with DAPI foci in the nucleus. As over-expression of exogenous chromatin proteins, such as histone H1.4, can impact chromatin arrangement, the H3K9me3 patterning in un-transfected NIH3T3 cells was compared to NIH3T3 cells expressing H1.4-FLAG. In untransfected NIH3T3 cells, almost complete co-localisation of H4K9me3 with DAPI was observed. This finding indicated that over-expression of functional H1.4 alters co-localisation of H4K9me3 with DAPI (Figure 4.11)

The expression of H1.4-FS-FLAG in NIH3T3 cells also did not result in high amounts of co-localisation of H3K9me3 foci and DAPI foci, however, larger and more diffuse H3K9me3 foci were observed (Figure 4.8 & Figure 4.12). Expression of the H1.4 CTD deletion mutant H1.4 Δ147-FLAG resulted in some abnormal H3K9 foci although some co-localisation was observed (Figure 4.9 & Figure 4.12). Disruption to H3K9me3 foci appeared more prevalent in NIH3T3 cells expressing H1.4 ΔCTD-FLAG (Figure 4.10 & Figure 4.12). Abnormal DAPI patterning was also more frequently observed in NIH3T3 cells expressing H1.4-FS-FLAG and H1.4-ΔCTD-FLAG indicating that their expression may be impacting heterochromatin (Figure A1).

These findings suggest that the expression of the H1.4 CTD mutants, particularly H1.4-FS and H1.4-ΔCTD results in disruptions to H3K9me3 heterochromatin as well as to DNA organisation. However, these changes were not observed in all cells which may be due to differences in the expression level of the exogenous H1.4 proteins. As co-localisation between H3K9me3 and DAPI was also shown to be disrupted with the expression of exogenous H1.4, it is also unable to be determined if the observed changes are due to the expression of the H1.4 CTD mutants or due to the cells being transiently transfected.

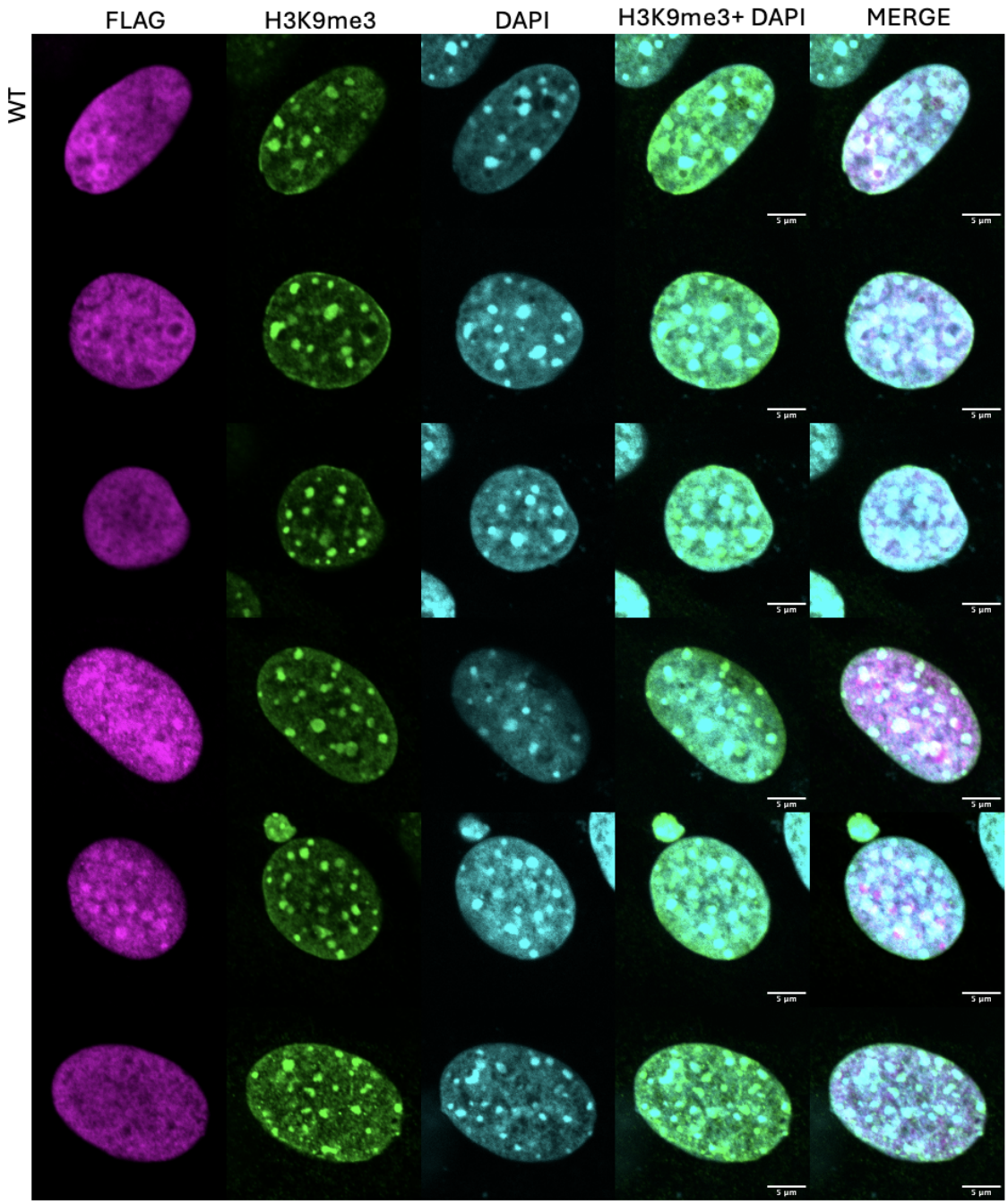

Figure 4.7: **H1.4-FLAG (WT) and H3K9me localisation in NIH3T3 nuclei.** Confocal microscope immunofluorescence images of NIH3T3 nuclei transiently transfected with a pcDNA3.1 plasmid expressing H1.4 with a c-terminal FLAG tag. Antibodies directed against the FLAG tag and H3K9me3 were used as well as DAPI to stain the DNA. H1.4-FLAG wild-type (WT) is shown in magenta, H3K9me3 green, and DAPI cyan. The scale bar is 5 μm.

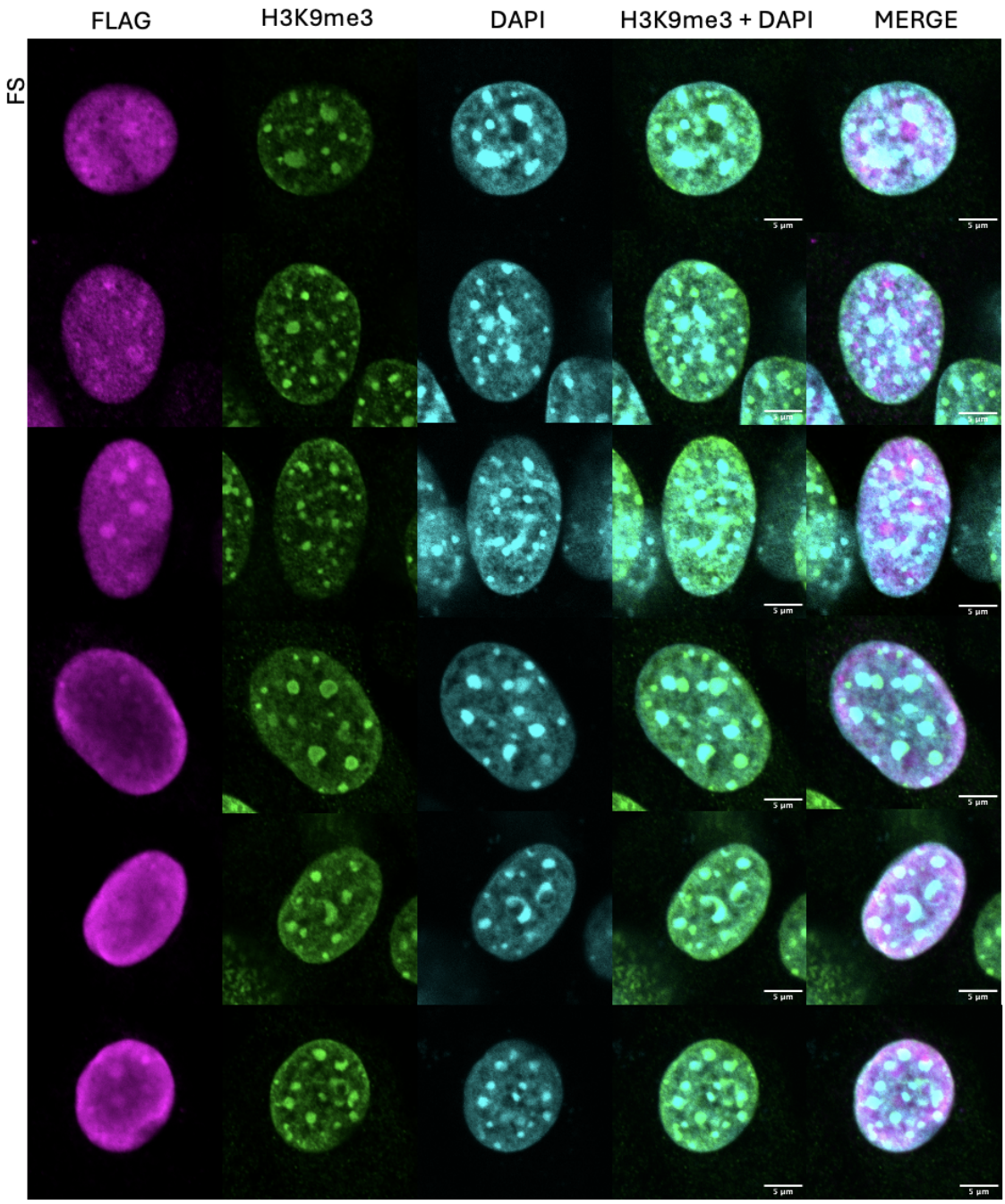

Figure 4.8: **H1.4 p.Lys148Glnfs*48-FLAG (H1.4-FS-FLAG) localisation and H3K9me3 patterning in NIH3T3 nuclei.** Confocal microscope immunofluorescence images of NIH3T3 nuclei transiently transfected with a pcDNA3.1 plasmid expressing H1.4-FS with a c-terminal FLAG tag. Antibodies directed against the FLAG tag and H3K9me3 were used as well as DAPI to stain the DNA. H1.4-FS-FLAG (FS) is shown in magenta, H3K9me3 green, and DAPI cyan. The scale bar is 5 μm.

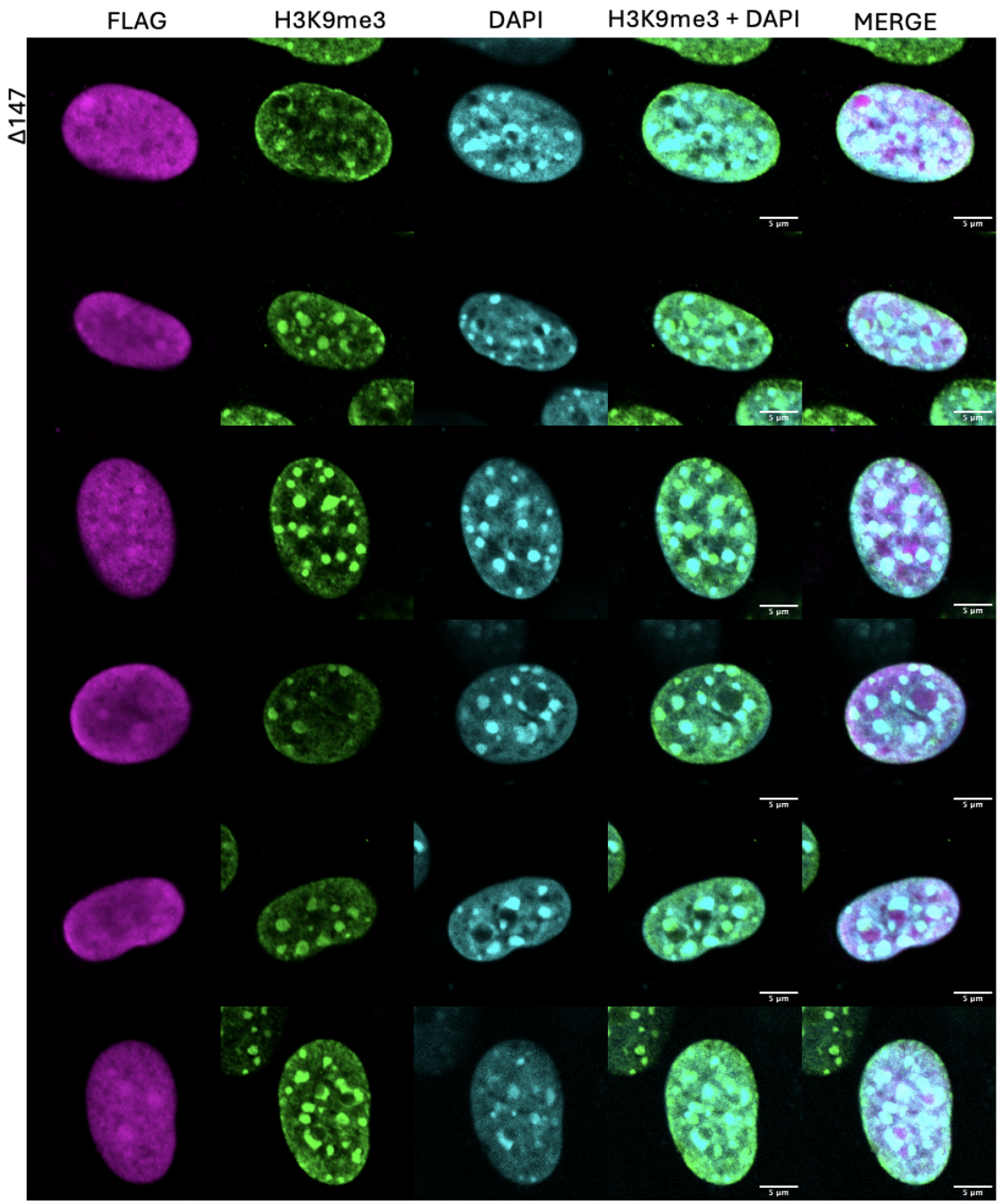

Figure 4.9: **H1.4-Δ147-FLAG (Δ147) localisation and H3K9me3 patterning in NIH3T3 nuclei.** Confocal microscope immunofluorescence images of NIH3T3 nuclei transiently transfected with a pcDNA3.1 plasmid expressing H1.4-Δ147-FLAG with a c-terminal FLAG tag. Antibodies directed against the FLAG tag and H3K9me3 were used as well as DAPI to stain the DNA. H1.4-Δ147-FLAG (Δ147) is shown in magenta, H3K9me3 green, and DAPI cyan. The scale bar is 5 μm.

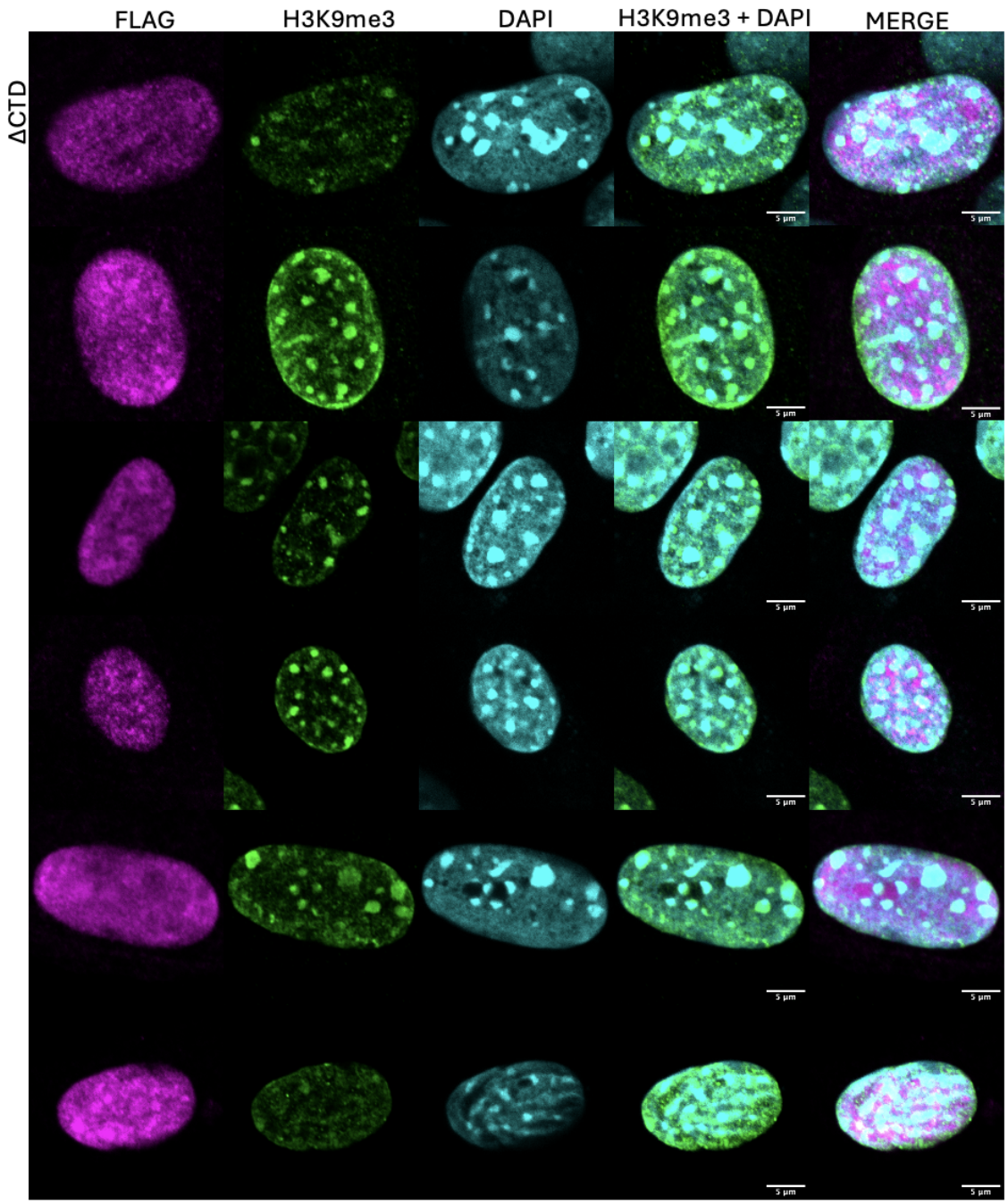

Figure 4.10: **H1.4-ΔCTD-FLAG (ΔCTD) localisation and H3K9me3 patterning in NIH3T3 nuclei.** Confocal microscope immunofluorescence images of NIH3T3 nuclei transiently transfected with a pcDNA3.1 plasmid expressing H1.4-ΔCTD with a c-terminal FLAG tag. Antibodies directed against the FLAG tag and H3K9me3 were used as well as DAPI to stain the DNA. H1.4-ΔCTD-FLAG (ΔCTD) is shown in magenta, H3K9me3 green, and DAPI cyan. The scale bar is 5 μm.

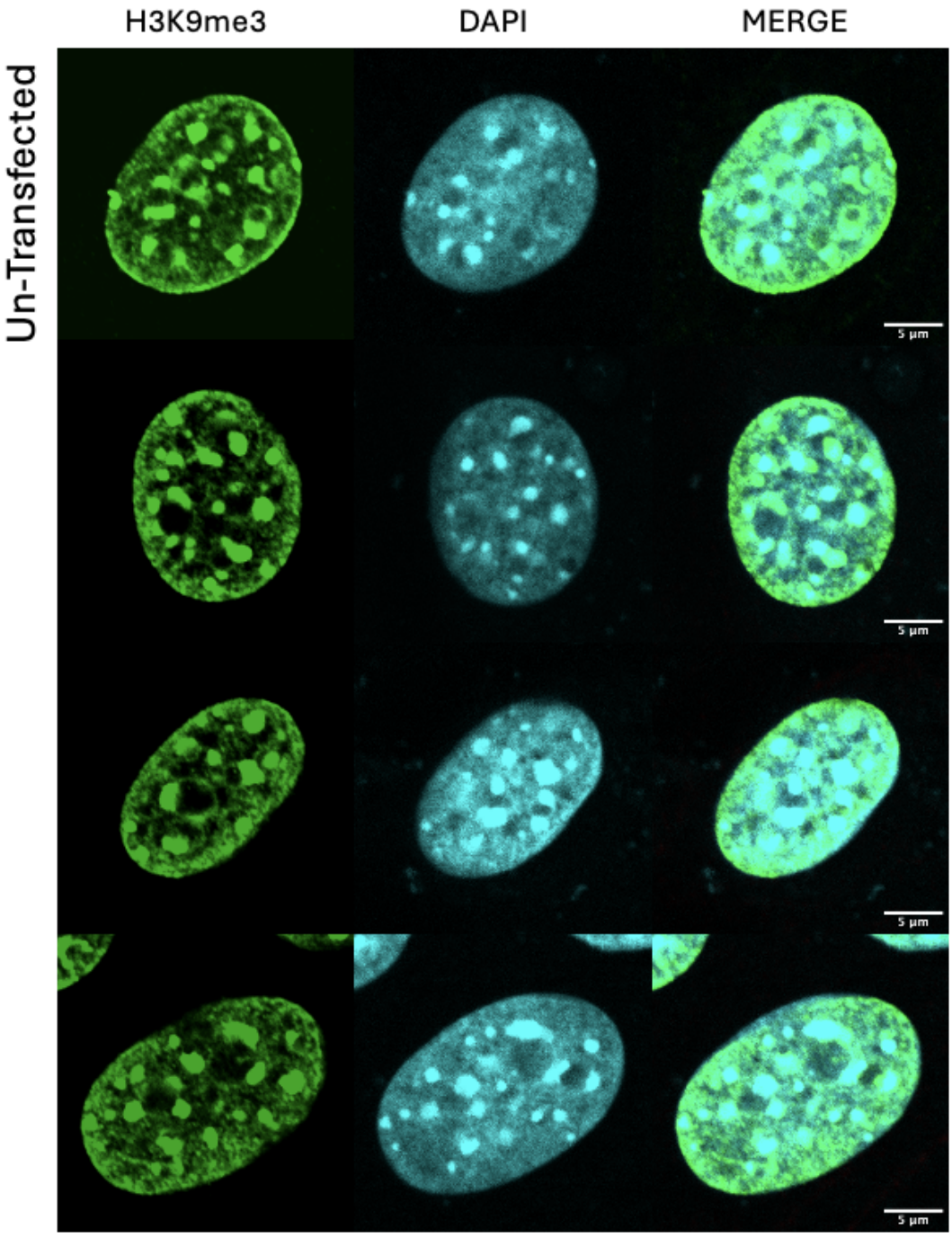

Figure 4.11: **H3K9me3 patterning in un-transfected NIH3T3 nuclei.** Confocal microscope immunofluorescence images of un-transfected NIH3T3 nuclei. Antibodies directed against H3K9me3 were used as well as DAPI to stain the DNA. H3K9me3 is shown in green and DAPI cyan. The scale bar is 5 μm.

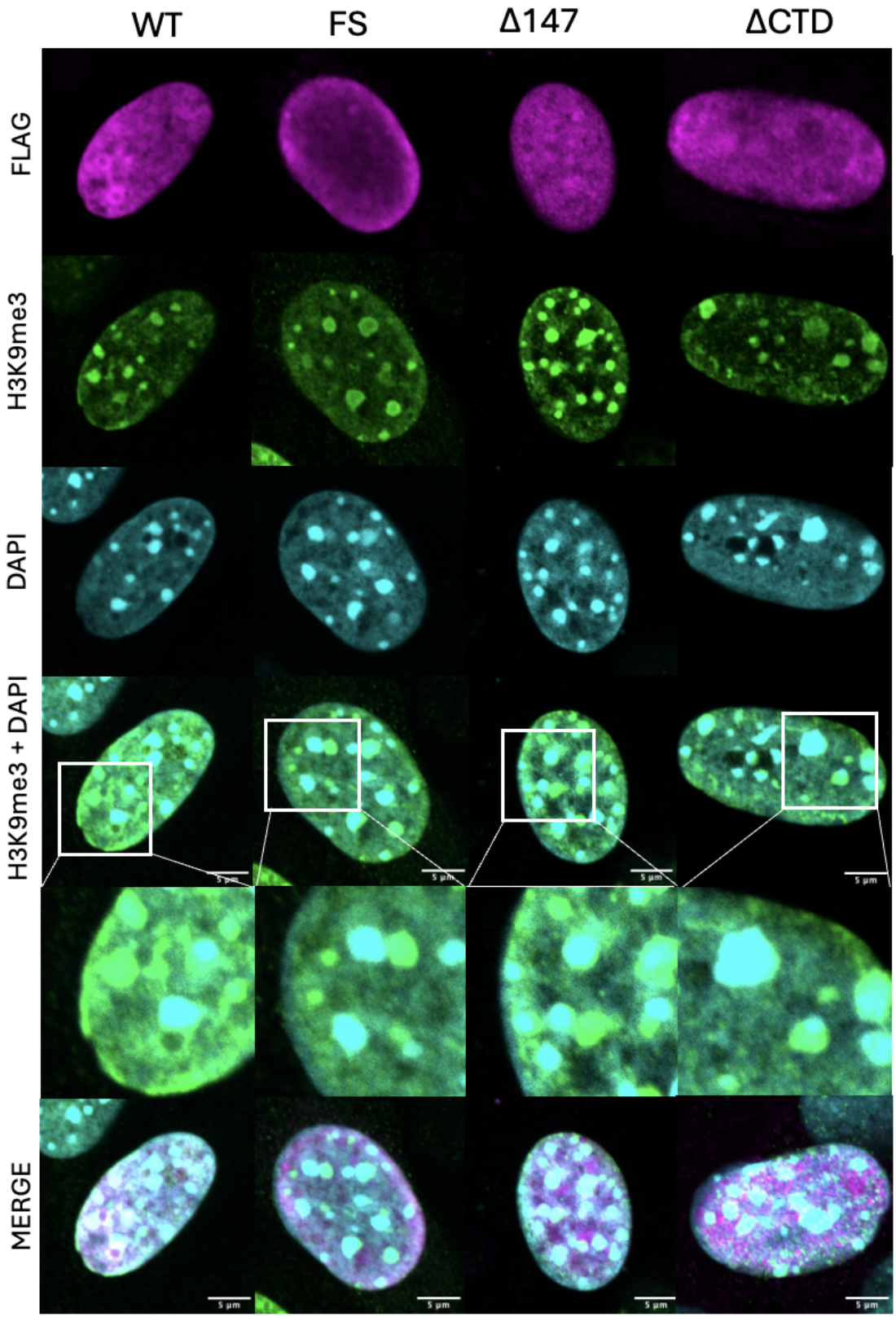

Figure 4.12: **Co-localisation of H3K9me3 foci and DAPI foci in NIH3T3 nuclei.** Confocal microscope immunofluorescence images of transiently transfected NIH3T3 nuclei. The NIH3T3 cells were transiently transfected with H1.4 and H1.4 CTD mutants contructs with c-terminal FLAG tags. Antibodies directed against the FLAG tag and H3K9me3 were used as well as DAPI to stain the DNA in order to compare the co-localisation of H3K9me3 foci and DAPI foci in NIH3T3 cells transiently transfected with H1.4-FLAG, H1.4-FS-FLAG, H1.4-Δ147-FLAG, and H1.4-ΔCTD-FLAG. FLAG channel is shown in magenta, H3K9me3 in green, and DAPI in cyan. The scale bar is 5 μm.

4.5 Impact of H1.4 CTD on H1.4K26 Methylation Patterning

Since the N-terminal domain of H1.4 contains a methylation site that has been demonstrated to interact with HP1α the impact of the expression of H1.4-FS on the patterning of H1.4K26me in NIH3T3 cells was investigated. To do this NIH3T3 cells were transiently transfected with either H1.4-FLAG or H1.4-FS-FLAG and then processed for immunofluorescence with the use of an anti-FLAG antibody, an anti-H1.4K26me antibody, and DAPI to stain the DNA (see Section 2.9.2).

NIH3T3 cells expressing WT H1.4 showed more diffuse H1.4K26me patterning compared to those expressing H1.4-FS (Figure 4.7 & 4.8). This suggests that there may be more methylated H1.4K26 present in the cells expressing WT H1.4 than in the cells expressing H1.4-FS. To determine if this more diffuse patterning was due to the over-expression of a functional protein, the H1.4K26me patterning of un-transfected NIH3T3 cells was also observed (Figure 4.11). These un-transfected cells displayed a more discrete H1.4K26me patterning that appeared more similar to the patterning observed with the expression of H1.4-FS (Figure 4.8 & 4.12). This result suggests that the overexpression of functional H1.4 in the NIH3T3 cells results in increased amounts of methylated H1.4K26, likely due to the expression of both endogenous and exogenous H1.4. However, the expression of H1.4-FS results in a similar level of H1.4K26me as un-transfected cells. This may suggest that H1.4-FS is not getting methylated on lysine 26 as readily as WT H1.4

As lysine 26 is located on the N-termial domain of H1.4 it remains unaffected by the p.Lys148Glnfs*48 frameshift mutation that causes Rahman syndrome. However, it has been previously demonstrated that the length of the CTD of linker histones affects the affinity of linker histones to chromatin. While only the globular domain is required for binding, H1.1 without a CTD has a lower affinity for chromatin than H1.1 with a CTD *in vivo* (Hendzel et al., 2004). Truncations to the CTD, such as the frameshift mutation found in H1.4-FS may disrupt the affinity for H1.4-FS to bind to chromatin and impact how readily the protein gets methylated on lysine 26 and be a reason behind the differences in H1.4K26me patterning. However, it is not possible to determine if this is occurring from these images and further investigation would need to be done.

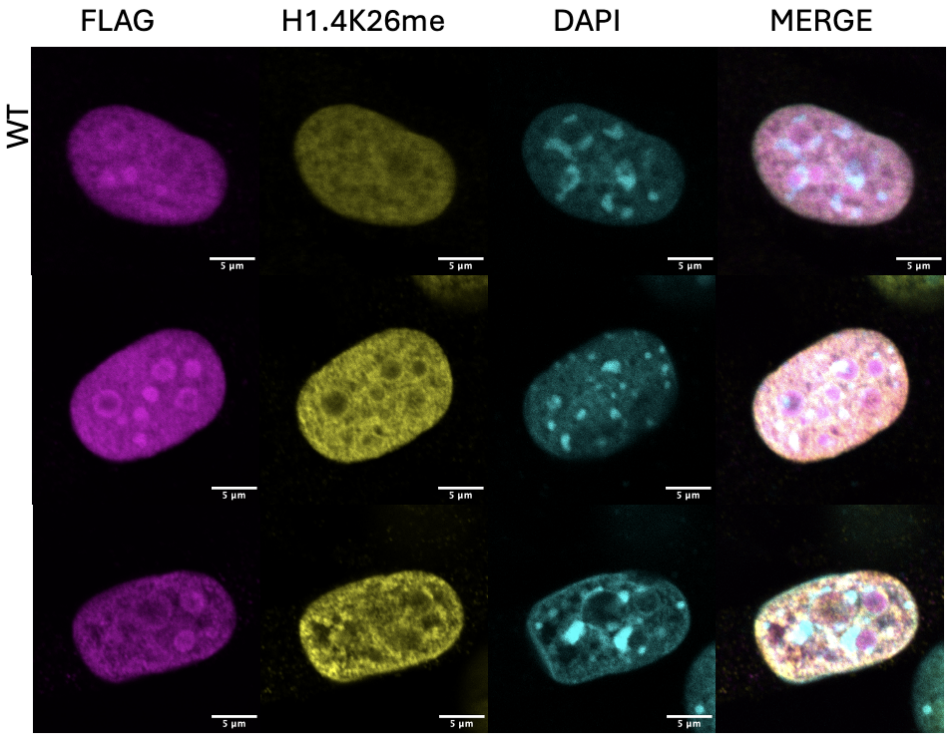

Figure 4.13: **H1.4-FLAG (WT) localisation and H1.4K26me patterning in NIH3T3 nuclei** Confocal microscope immunofluorescence images of transiently transfected NIH3T3 nuclei with a pcDNA3.1 plasmid expressing WT H1.4 with a c-terminal FLAG tag. Antibodies directed against the FLAG tag and H1.4K26me were used as well as DAPI to stain the DNA. H1.4 (WT) is shown in magenta, H1.4K26me in yellow, and DAPI cyan. The scale bar is 5 μm.

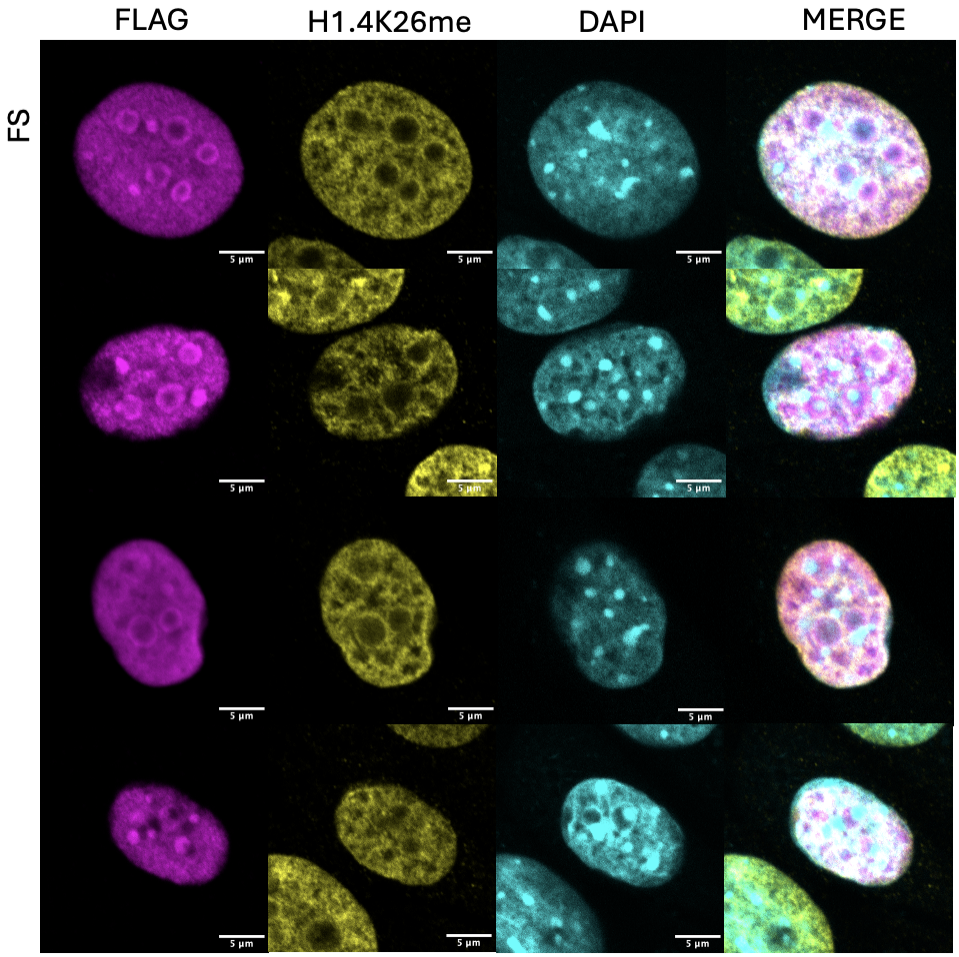

Figure 4.14: **H1.4-FS-FLAG (FS) localisation and H1.4K26me patterning in NIH3T3 nuclei** Confocal microscope immunofluorescence images of transiently transfected NIH3T3 nuclei with a pcDNA3.1 plasmid expressing H1.4-FS-FLAG with a c-terminal FLAG tag. Antibodies directed against the FLAG tag and H1.4K26me were used as well as DAPI to stain the DNA. H1.4-FS-FLAG is shown in magenta, H1.4K26me in yellow, and DAPI cyan. The scale bar is 5 μm.

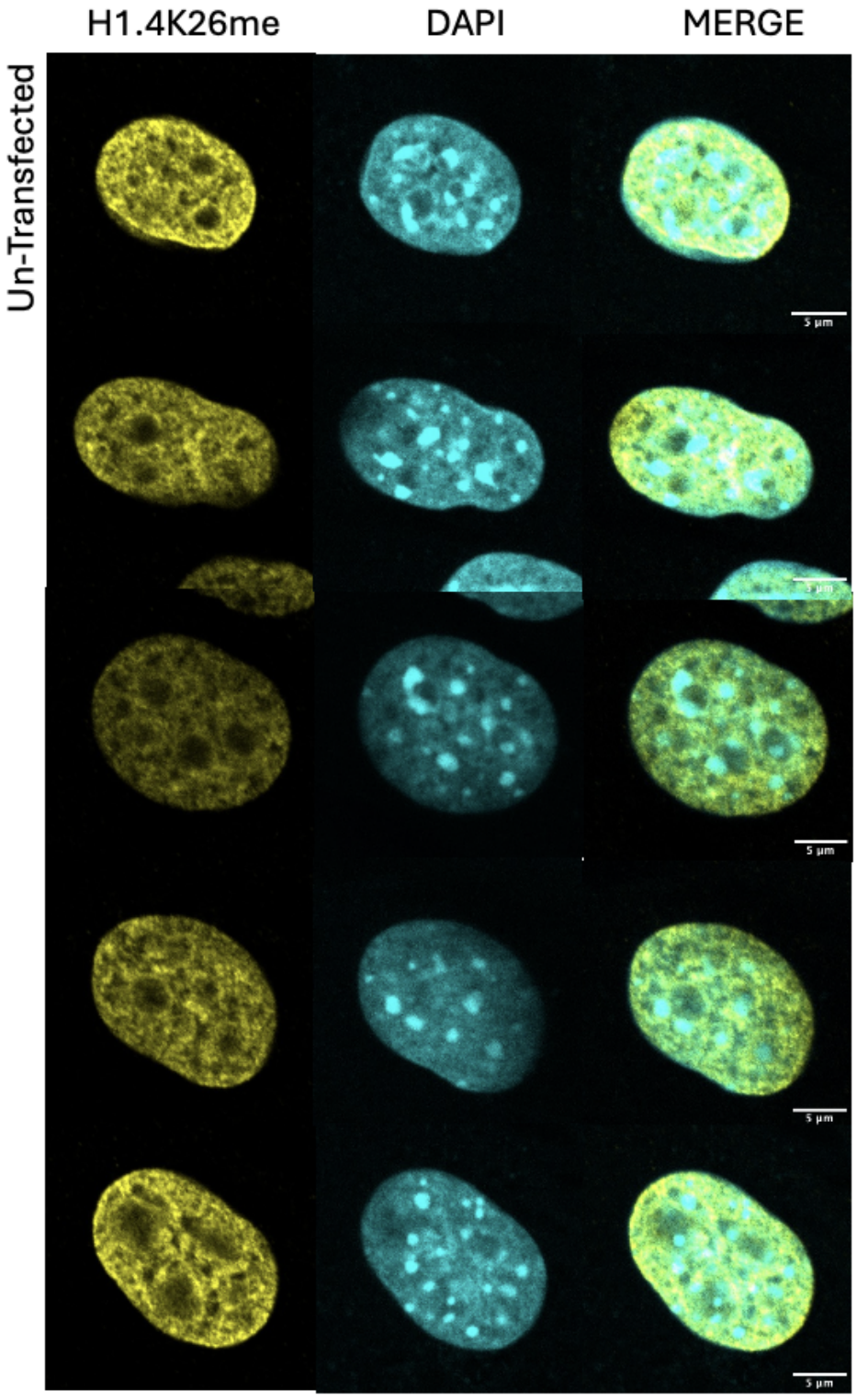

Figure 4.15: **H1.4K26me patterning in NIH3T3 nuclei** Confocal microscope immunofluorescence images of un-transfected NIH3T3 nuclei. Antibodies directed against H1.4K26me were used as well as DAPI to stain the DNA. H1.4K26me is shown in yellow, and DAPI cyan. The scale bar is 5 μm

4.6 H1.4 Overexpression Does Not Alter PIN1 Localisation

Pin1 is a peptidyl-prolyl isomerase (PPIase) that catalyses cis-trans prolyl isomerisation in proteins containing pSer/pThr-Pro motifs (Jinasena et al., 2019). Four of these motifs are found in the CTD

of histone H1.4 (Figure 4.14). However, only one Thr-Pro phosphorylation site is found in the CTD of H1.4-FS (Figure 4.14). As Pin1 has been shown to stabilise the chromatin-H1 interaction, loss of these Pin1 recognition sites may result in the H1.4-FS having an altered localisation with chromatin (Jinasena et al., 2019).

Figure 4.16: **Pin1 recognition site locations in H1.4 and H1.4-FS (p.Lys148Glnfs*48).** Amino acid sequences of H1.4 and the Rahman Syndrome varient p.Lys148Glnfs*48 (H1.4-FS). The globular domain is highlighted yellow and the Ser/Thr-Pro phosphorylation sites on the CTD that are recognised by Pin1 are highlighted blue. The change in the reading frame due to the frameshift mutation in H1.4-FS is highlighted in green.

To investigate if expression of the Rahman syndrome p.Lys148Glnfs*48 variant resulted in changes to the patterning of Pin1 *in vivo* NIH3T3 cells were transiently transfected with H1.4-FLAG or H1.4-FS-FLAG and then processed for immunofluorescence with the use of an anti-FLAG antibody, an anti-PIN1 antibody, and DAPI to stain the DNA (see Section 2.9.2). Expression of both H1.4-FLAG (Figure 4.15) and H1.4-FS-FLAG (Figure 4.16) resulted in a diffuse PIN1 pattern across the nucleus. PIN1 was also observed in the cytoplasm with expression of both H1.4-FLAG and H1.4-FS-FLAG. No differences in the patterning of Pin1 were observed between the NIH3T3 cells expressing either H1.4-FLAG or H1.4-FS-FLAG. Overall this indicates that the expression of H1.4-FS-FLAG does not impact the patterning of Pin1.

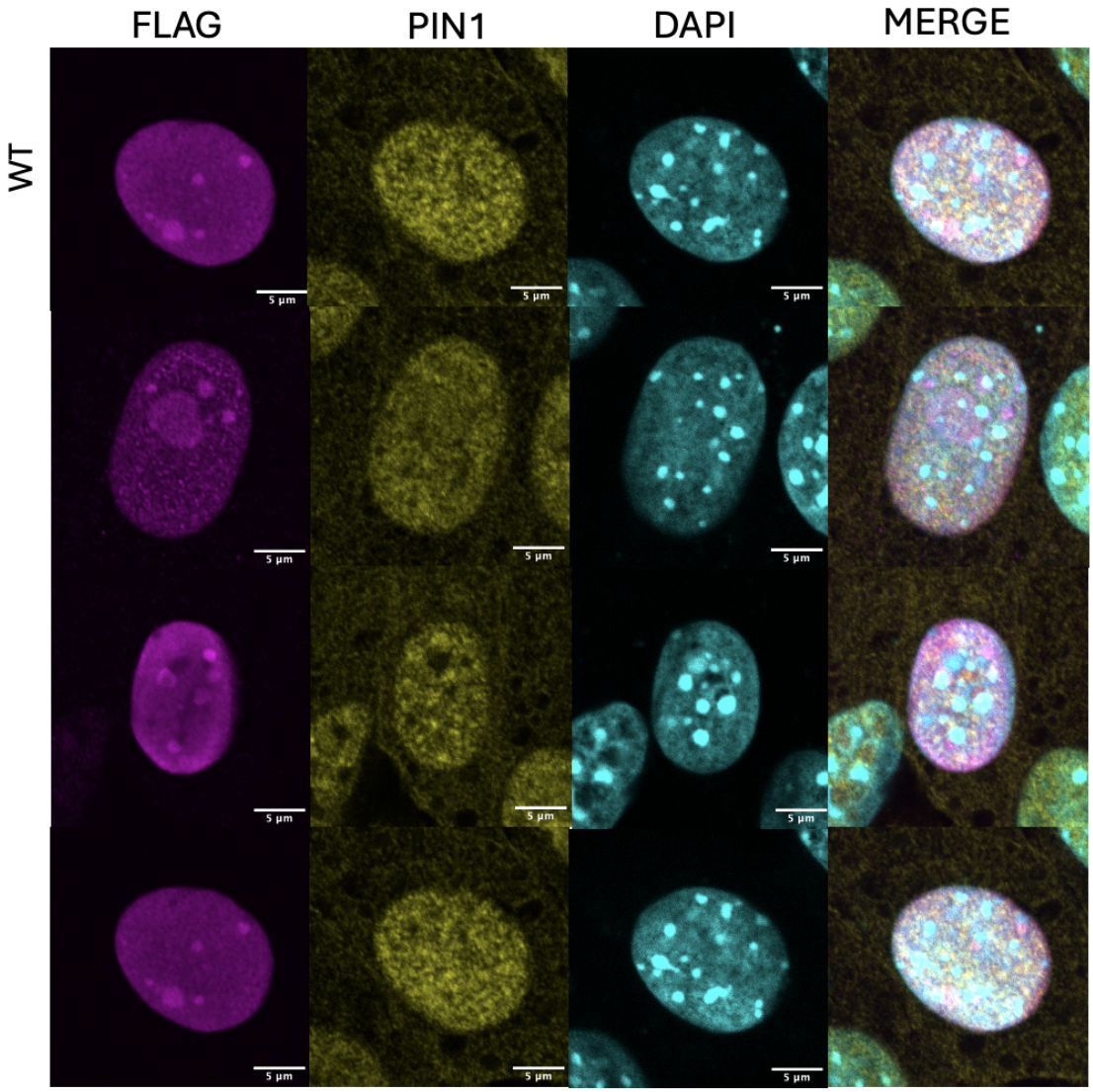

Figure 4.17: **H1.4-WT-FLAG (WT) localisation and Pin1 patterning in NIH3T3 nuclei** Confocal microscope immunofluorescence images of transiently transfected NIH3T3 nuclei with a pcDNA3.1 plasmid expressing WT H1.4 with a c-terminal FLAG tag. Antibodies directed against the FLAG tag and PIN1 were used as well as DAPI to stain the DNA. H1.4 (WT) is shown in magenta, PIN1 in yellow, and DAPI cyan. The scale bar is 5 μm.

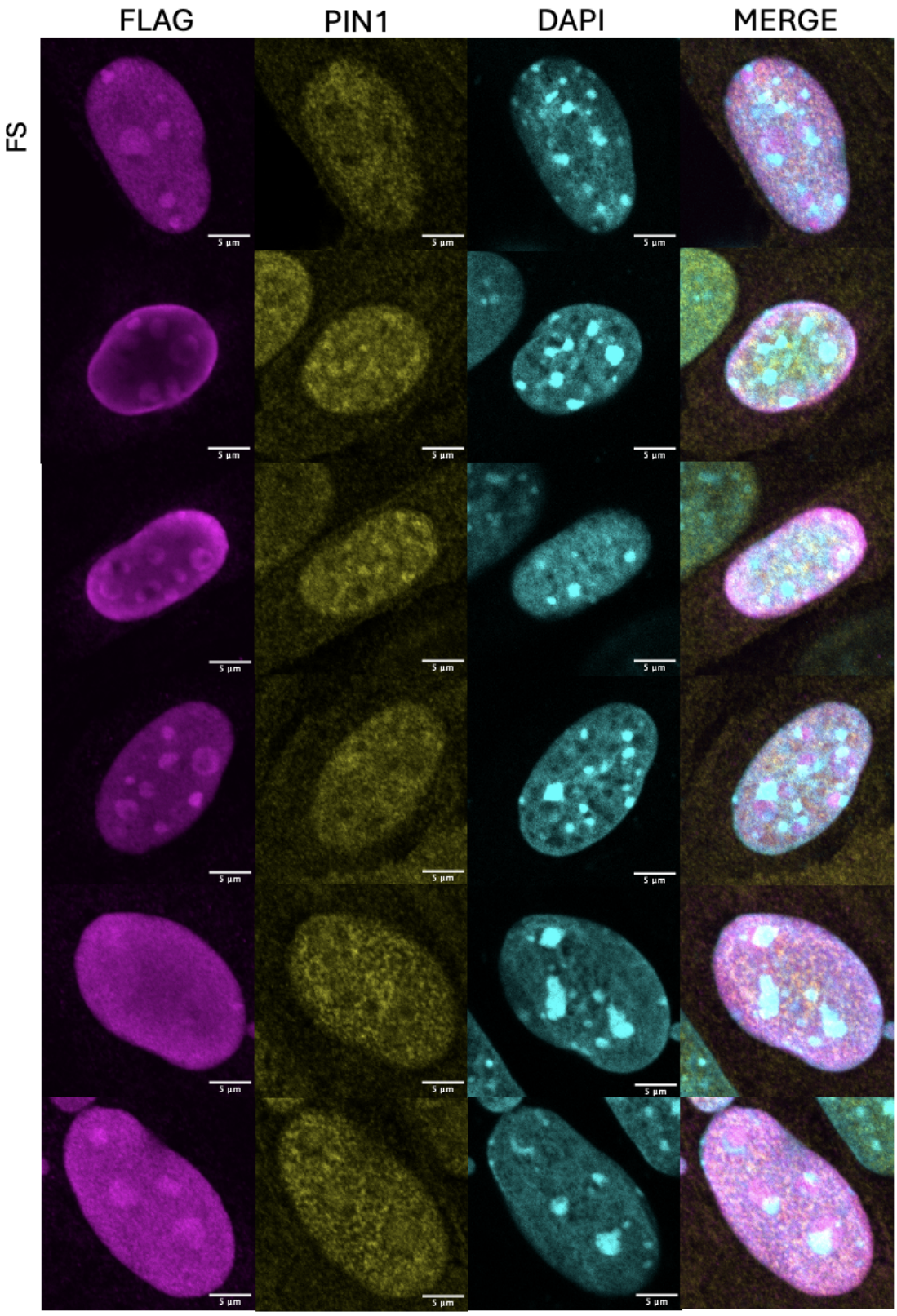

Figure 4.18: **H1.4-FS-FLAG (FS) localisation and Pin1 patterning in NIH3T3 nuclei** Confocal microscope immunofluorescence images of transiently transfected NIH3T3 nuclei with a pcDNA3.1 plasmid expressing H1.4-FS with a c-terminal FLAG tag. Antibodies directed against the FLAG tag and PIN1 were used as well as DAPI to stain the DNA. H1.4-FS-FLAG (FS) is shown in magenta, PIN1 in yellow, and DAPI cyan. The scale bar is 5 μm.

4.7 Exploring if Alterations to H1.4 CTD Effect Lamin A/C Network

Fibroblasts from an individual with Rahman syndrome who displayed a premature ageing phenotype were shown to have abnormal lamin A/C patterning (Flex et al., 2019). These aberrations to the nuclear lamina were found to be progressive over cell culture passages (Flex et al., 2019). Lamin A/C proteins at the nuclear periphery are important for the structural stability of the nuclear membrane. Disruptions to heterochromatin associated with the nuclear lamina from knockdown of HP1α have also been shown to disturb the organisation of nuclear lamina (Pradhan et al., 2021).

To investigate the importance of the H1.4 CTD in the formation of normal nuclear morphology, as suggested by Rahman Syndrome findings, NIH3T3 mouse fibroblast cells were transiently transfected with either H1.4-FLAG, H1.4-FS-FLAG or H1.4-Δ147-FLAG (see Section 2.9.2). An anti-lamin A/C antibody was used to visualize the Lamin A/C inside the nucleus.

NIH3T3 cells expressing H1.4-FLAG (Figure 4.18) and H1.4-Δ147-FLAG (Figure 4.20) had a well-defined layer of peripherally associated Lamin A/C giving a 'ring' like appearance around the nucleus. No breaks in the peripheral lamina, blebs, or invaginations were observed indicating that it is functioning normally. Some abnormalities to the nuclear lamina were observed in NIH3T3 cells expressing H1.4-FS-FLAG as indicated by Figure 4.18. A nucleus with a break to the peripheral lamina was observed as well as what may be an invagination of the lamina. However, due to the limited sample size, the frequency at which these abnormalities occur is unable to be determined and therefore further investigation is required.

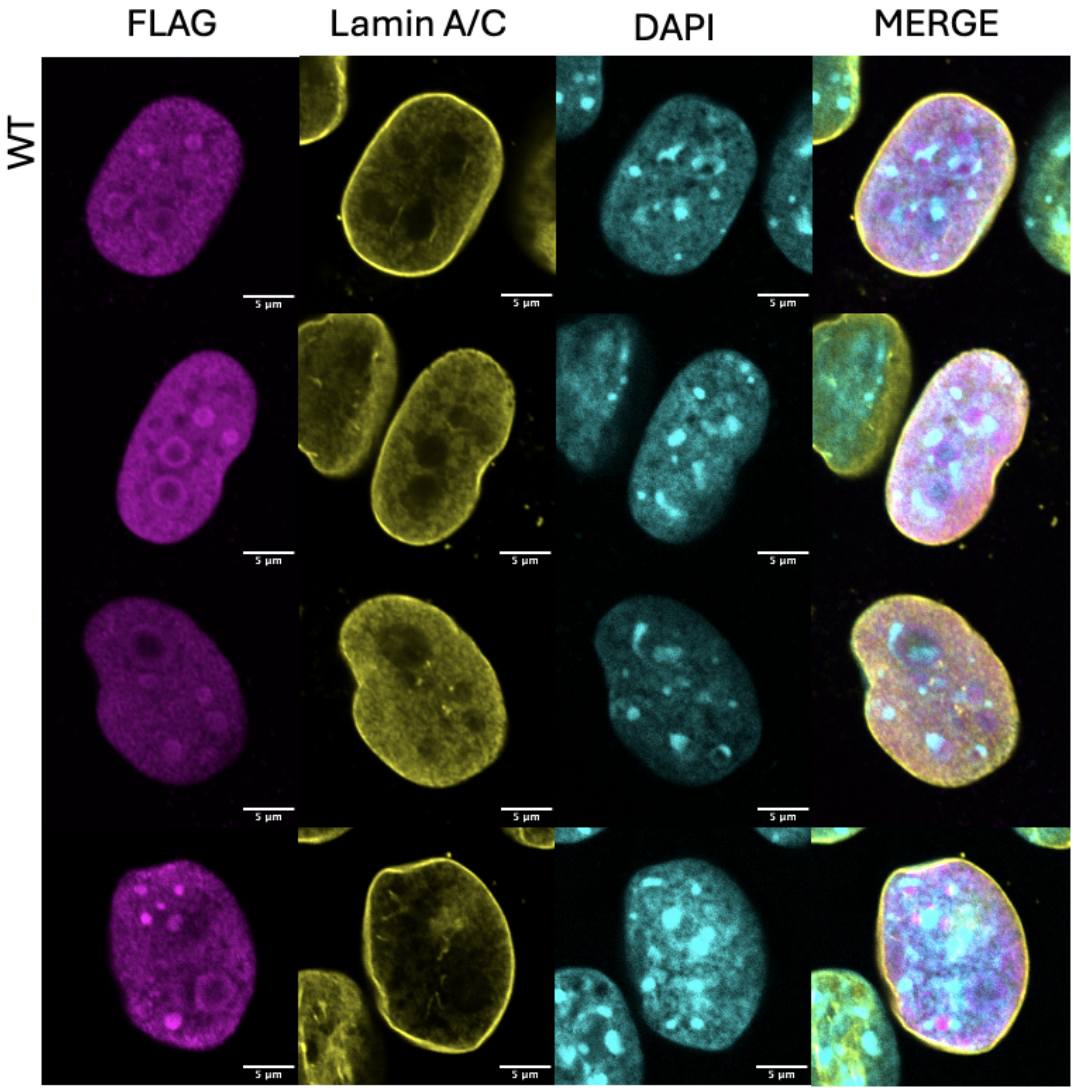

Figure 4.19: **H1.4-FLAG and Lamin A/C localisation in NIH3T3 nuclei** Confocal microscope immunofluorescence images of transiently transfected NIH3T3 nuclei with a pcDNA3.1 plasmid expressing H1.4 with a c-terminal FLAG tag. Antibodies directed against the FLAG tag and PIN1 were used as well as DAPI to stain the DNA. H1.4-FLAG (WT) is shown in magenta, Lamin A/C in yellow, and DAPI cyan. The scale bar is 5 μm.

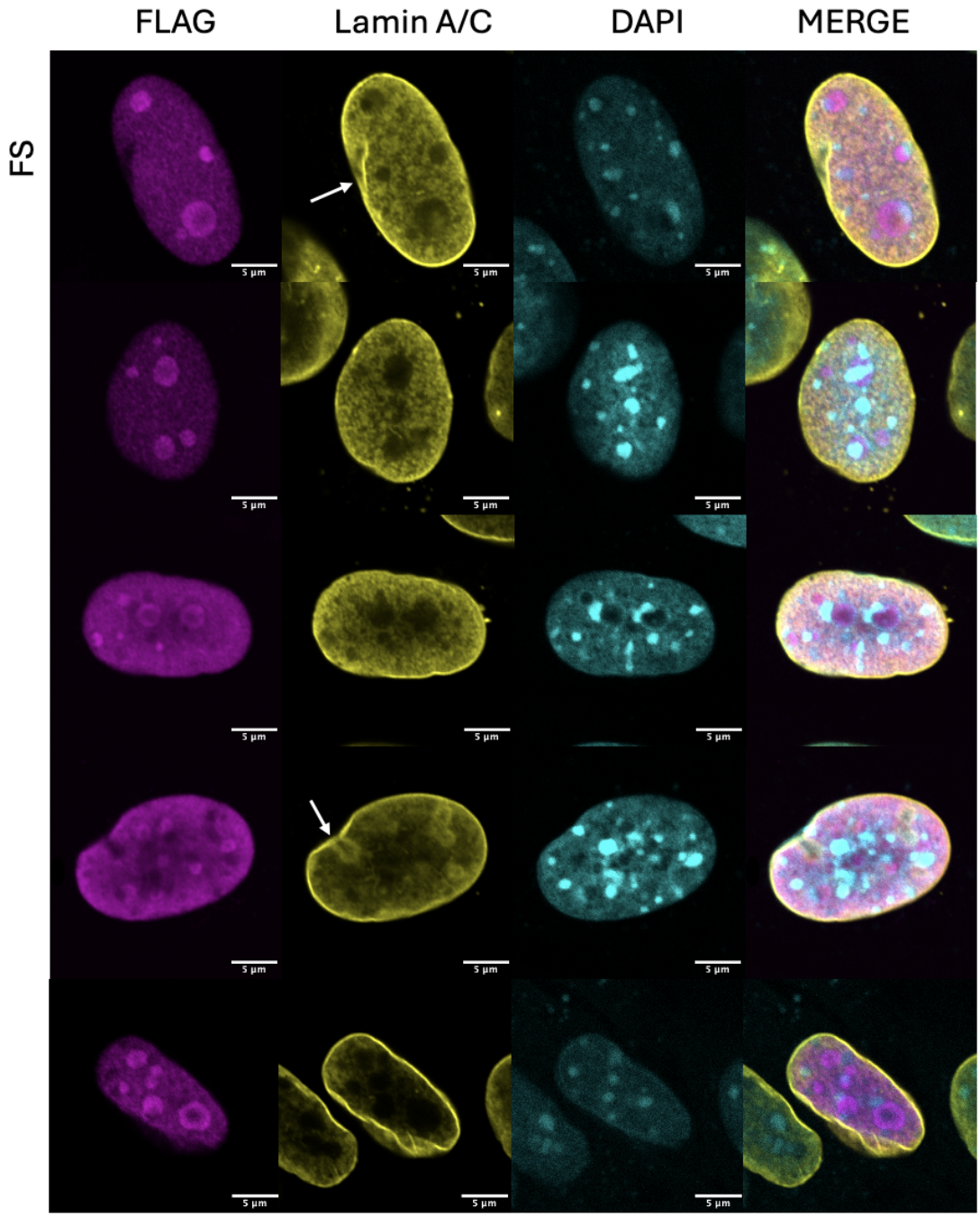

Figure 4.20: **H1.4-FS-FLAG localisation in NIH3T3 nuclei** Confocal microscope immunofluorescence images of transiently transfected NIH3T3 nuclei with a pcDNA3.1 plasmid expressing H1.4-FS with a c-terminal FLAG tag. Antibodies directed against the FLAG tag and PIN1 were used as well as DAPI to stain the DNA. H1.4-FS-FLAG (FS) is shown in magenta, Lamin A/C in yellow, and DAPI cyan. The scale bar is 5 μm.

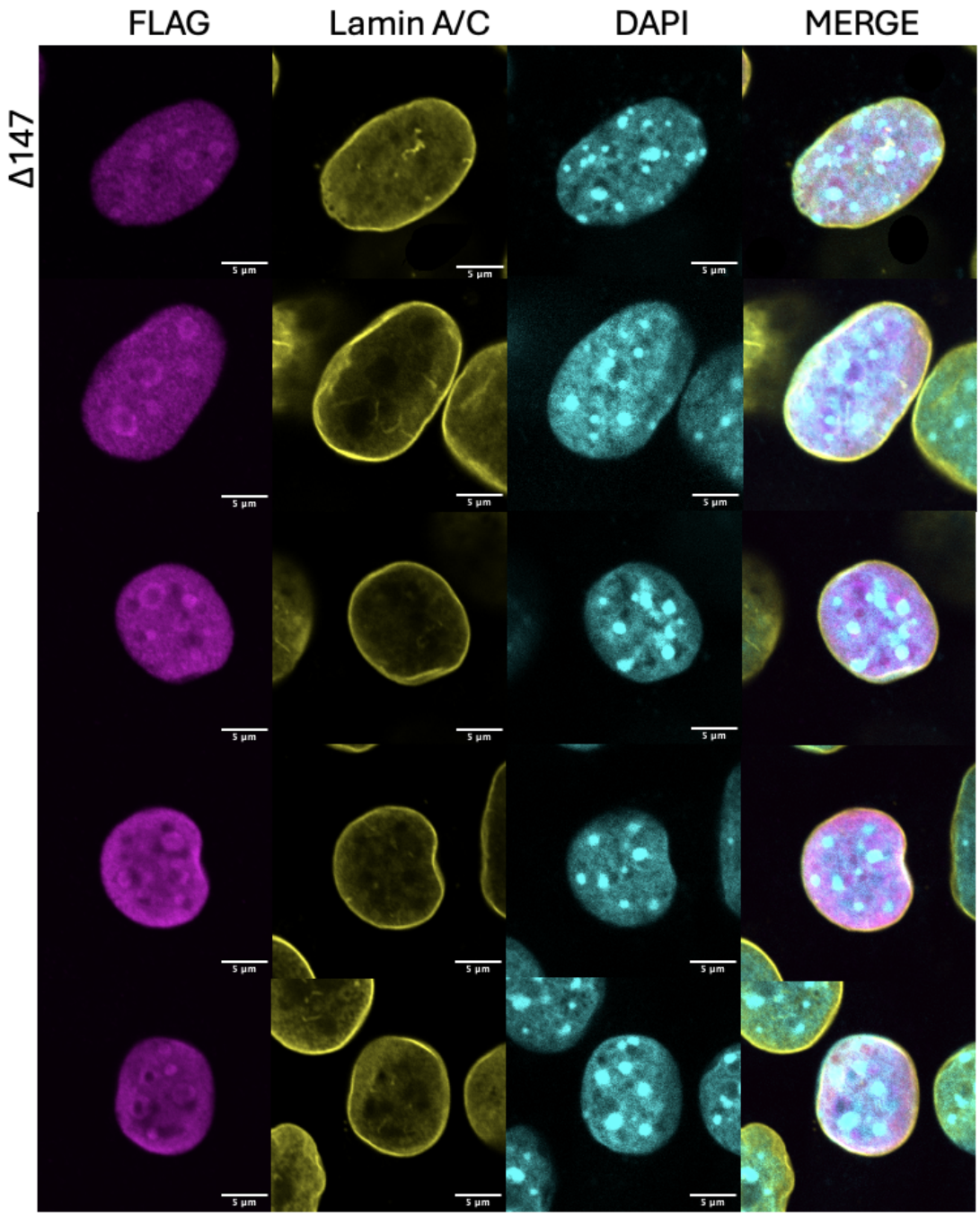

Figure 4.21: **H1.4 Δ147-FLAG and Lamin A/C localisation in NIH3T3 nuclei.** Confocal microscope immunofluorescence images of transiently transfected NIH3T3 nuclei with a pcDNA3.1 plasmid expressing H1.4 Δ147 with a c-terminal FLAG tag. Antibodies directed against the FLAG tag and PIN1 were used as well as DAPI to stain the DNA. H1.4 Δ147-FLAG (Δ147) is shown in magenta, Lamin A/C in yellow, and DAPI cyan. The scale bar is 5 μm.

4.8 Rahman H1.4-FS Increases Nucleus Size

It was noticed that the nucleus of cells in immunofluorescence studies appeared larger when expressing the Rahman syndrome H1.4 (Tremblay et al., 2021). To determine if this result also occurred with the expression of H1.4-FS-FLAG and with the CTD deletion mutants, H1.4Δ147-FLAG and H1.4

ΔCTD-FLAG, the size of transfected nuclei were measured (Figure 4.21).

A sample of 20 nuclei, from across all of the immunofluorescence experiments in this study, was used to determine the average nuclear area. The nuclear area was determined from confocal microscopy images, where a medial slice of the nucleus was viewed and then measured using Image J. The nuclear area of NIH3T3 cells expressing H1.4-FLAG, H1.4-FS-FLAG, H1.4Δ147-FLAG, and H1.4ΔCTD-FLAG were compared. The results determined that the NIH3T3 cells expressing H1.4-FS-FLAG tended to have a larger nucleus than those expressing H1.4-FLAG (Figure 4.21). NIH3T3 cells expressing H1.4Δ147-FLAG or H1.4ΔCTD-FLAG had no significant difference in nucleus size compared to H1.4-FLAG (Figure 4.21).

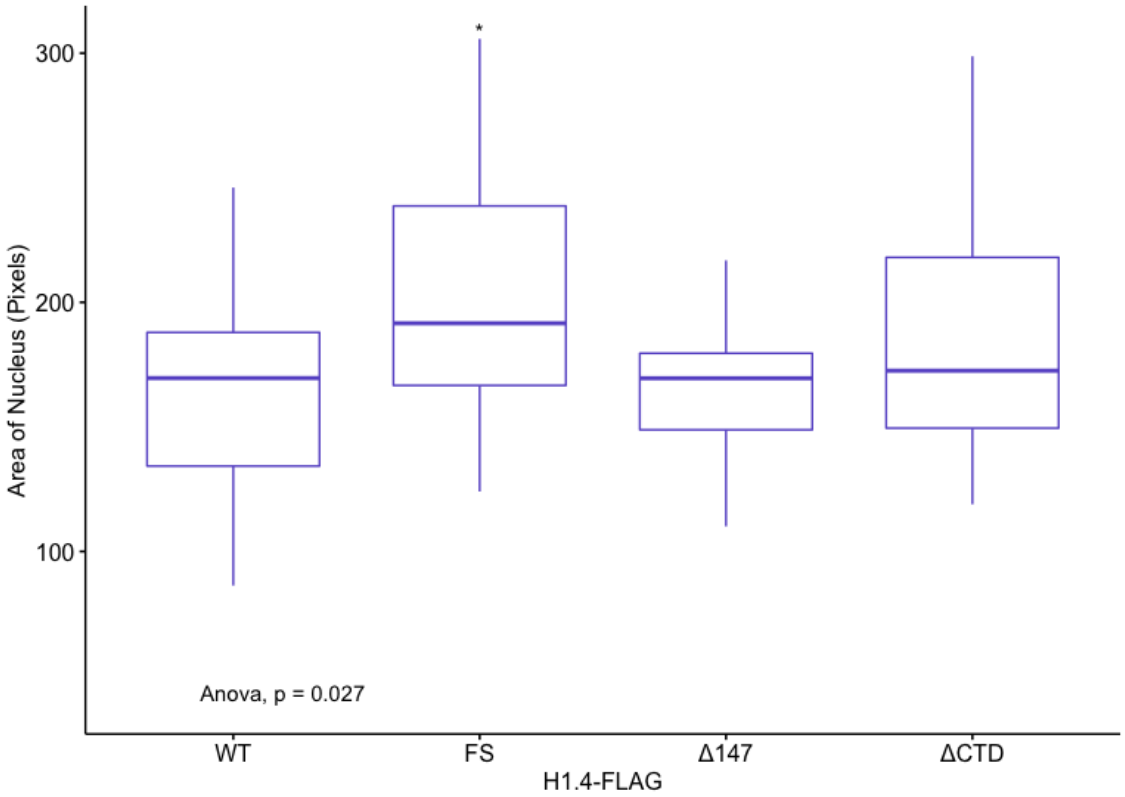

Figure 4.22: **Box plot of nucleus area.** The nucleus area of NIH3T3 cells transfected with either H1.4-FLAG (WT), H1.4-FS-FLAG(FS), H1.4Δ147-FLAG (Δ147) or H1.4ΔCTD-FLAG (ΔCTD) was measured and the average area was compared to WT. The nucleus area was measured using Image J software. Each Image was imported into Image J, the perimeter of the nucleus was selected and the area in pixels was measured. Statistical significance was initially determined using an ANOVA test. Post-hoc t-tests comparing the median area (pixels) of H1.4-FS-FLAG(FS), H1.4Δ147-FLAG (Δ147) and, H1.4ΔCTD-FLAG (ΔCTD) to the median area (pixels) of H1.4-FLAG (WT) were then used. *$p<0.05$.

4.9 Summary

These findings demonstrate that the CTD of H1.4 is important for HP1α nuclear localisation as the expression of H1.4 proteins that have a truncated or frameshift altered CTD interfere with HP1α localisation and with heterochromatin foci as indicated by alterations to H3K9me and DAPI. H1.4Δ147, H1.4ΔCTD, and H1.4-FS had reduced co-localisation with HP1α indicating that they are no longer

able to interact with HP1α *in vivo* (see Section 4.3). However, as complete co-localisation between H3K9me3 foci and DAPI foci were not observed in NIH3T3 cells expressing H1.4-FLAG, it was not able to be determined if this result in the H1.4 CTD mutants was due to the over-expression of exogenous protein or due to an effect of the H1.4 CTD mutants.

The expression of H1.4-FS resulted in a larger nucleus size, however, this was not observed in the expression of H1.4Δ147 and H1.4ΔCTD. This indicates that the new altered CTD may have an effect on the cell as this was not observed with expression of H1.4Δ147-FLAG (Figure 4.21). The shape of the nucleus is supported through the combination of lamin, chromatin, and the cytoskeleton (Stephens et al., 2019). Lamin and lamin associated heterochromatin both provide a resistive force to the nucleus and disruption to either result in changes to the mechanical strength of the nucleus (Pradhan et al., 2021; Stephens et al., 2019). Atomic force microscopy (AFM) and micropipette aspiration studies have shown that alterations to heterochromatin result in a weaker nucleus, despite no alterations to lamin occurring (Pradhan et al., 2021; Stephens et al., 2019; Stephens et al., 2018). The role of HP1α in the maintenance of this peripheral heterochromatin had also been displayed with HP1α knockdown (KD) MCF7 cells (Pradhan et al., 2021). HP1α KD results in disruptions to heterochromatin organisation and the association of heterochromatin to the nuclear lamina (Pradhan et al., 2021).

As it has been indicated that the expression of H1.4-FS may result in disrupted heterochromatin, this may be the reason for the change in nucleus size. A nucleus with less resistive force due to disrupted heterochromatin may have a flatter shape due to the lack of structural support (Figure 4.22.B). When imaged this may result in the nucleus appearing larger despite the overall volume of the nucleus not changing (Figure 4.22).

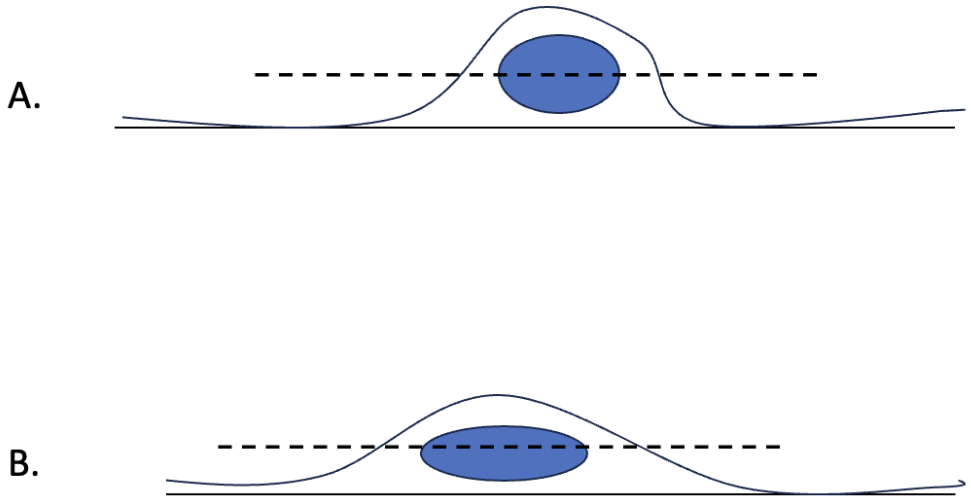

Figure 4.23: **Changes to heterochromatin may result in a flatter nucleus shape.** (A) A normal cell with the nucleus shown in blue. The dotted line represents the focal plane when imaging using a confocal microscope. (B) An example of how changes to the structural stability of the nucleus (blue) may result in it appearing flatter. The dotted line shows the focal plane when imaging using a confocal microscope. The flatter shape makes the nucleus longer and therefore appear larger when looking at just one focal plane.

The differences in expression of the H1.4-FLAG proteins are visualised during immunofluorescence by the signal intensity of FLAG. The higher the signal intensity of the FLAG channel the higher the expression levels. While only nuclei that have a similar low-level intensity are selected, there can still be variation in expression levels. Differences in the level of expression of the H1.4-FLAG proteins investigated may also impact the results. For example, abnormal DAPI patterning was more frequently observed with the expression of H1.4ΔCTD-FLAG and H1.4-FS-FLAG however some cells did still show normal DAPI patterning. To address this a stable cell line expressing the H1.4 CTD mutant proteins could be used.

Chapter 5

Discussion and Future Directions

5.1 The H1.4-HP1α Interaction

It has been previously established that the presence of H3K9me3 alone is insufficient for targeting HP1α to chromatin (Daujat et al., 2005; Hale et al., 2006; Kumar & Kono, 2020). The interaction between H1 and HP1 has been suggested to function as an additional mechanism to bring HP1 to chromatin (Daujat et al., 2005; Hale et al., 2006; Kumar & Kono, 2020). Histone H1.4 and HP1α are both important for heterochromatin homeostasis and have been demonstrated to interact both *in vitro* and *in vivo* (Daujat et al., 2005; Hale et al., 2006; Kumar & Kono, 2020). Loss of HP1α is associated with disruptions to heterochromatin and changes to the mechanical properties of the nucleus (Pradhan et al., 2021). Disruptions to H1.4, such as the frameshift mutations associated with Rahman Syndrome, are also associated with loss of heterochromatin homeostasis (Flex et al., 2019). While the interaction between H1.4 and HP1α has been demonstrated, the mode of interaction and the exact function are still debated in the literature (Kumar & Kono, 2020).

Two potential modes of the H1.4-HP1α interaction have been suggested. Daujat et al. (2005) demonstrated that HP1α specifically binds to H1.4 methylated on lysine 26 (H1.4K26me). This interaction was lost when H1.4K26me was not present. HP1α without a chromodomain was no longer able to bind to H1.4K26me, demonstrating that this interaction was mediated through the chromodomain (Daujat et al., 2005). It has also been demonstrated that H1.4 binds to HP1α through an interaction between the CTD of H1.4 and the hinge region of HP1α (Hale et al., 2006). Loss of the CTD disrupted the binding of H1.4 to the hinge region of HP1α (Hale et al., 2006). This model of the H1.4-HP1α interaction was suggested to allow for HP1α to simultaneously bind to methylated H3K9 through the chromodomain and to H1.4 through the hinge region (Hale et al., 2006). Conversely, Ryan and Tremethick (2018) put forward their findings that the presence of H1.4 impeded the binding of HP1α to nucleosomal arrays. Suggesting that H1.4 was not an additional method for targeting HP1α to chromatin (Ryan & Tremethick, 2018). These studies highlight that a further understanding of the mechanism and purpose of the H1.4-HP1α interaction is required.

5.2 H1.4 CTD Truncation's Disrupt H1.4-HP1α Co-Localisation

This research investigated the minimal length of the H1.4 CTD needed for its interaction with HP1α. Along with investigating if the H1.4-FS mutant found in individuals with Rahman Syndrome could still interact with HP1α. While it has been previously demonstrated that H1.4 without a CTD no

longer interacts with HP1α, the exact regions of the CTD required for this interaction to occur have not been established. It has also not been previously investigated if H1.4-FS can interact with HP1α.

As expected from previously published research by Hale et al., (2006), H1.4 lacking the entire CTD was observed to have reduced co-localisation with endogenous HP1α when expressed in NIH3T3 cells. This reduction in co-localisation with HP1α was also observed with the expression of H1.4 with a loss of 72 terminal amino acids and the H1.4 frameshift mutant. These results demonstrate that expression of the H1.4 CTD mutants impacts the behavior of endogenous HP1α. This provides more evidence of the link between H1.4 and HP1α in heterochromatin domains and suggests that a loss of interaction between the H1.4 CTD and HP1α hinge region could be disrupting the co-localisation of H1.4 to HP1α.

In vitro protein binding assays were performed to directly investigate the binding of the H1.4 CTD mutants with HP1α. H1.4 proteins with a terminal deletion of either 59 or 70 amino acids were used along with the H1.4 frameshift mutant. However, due to time constraints and technical issues with background binding, the *in vitro* binding assays were not achieved. Therefore it is unknown if H1.4 with partial loss of the CTD or the H1.4 frameshift mutant can bind to HP1α *in vitro* .

Therefore further work is required to identify if the H1.4 CTD mutants investigated in this study disrupt the interaction with HP1α. A loss of the H1.4-HP1α interaction may be a potential mechanism to explain why heterochromatin is disrupted in individuals with Rahman Syndrome and provide further insights into the role of this interaction in heterochromatin homeostasis.

5.3 Expression of H1.4-FS Affects Heterochromatin and Nuclear Morphology

Rahman Syndrome has been associated with a loss of heterochromatin homeostasis (Flex et al., 2019). This research aimed to investigate if a loss of HP1α could be a potential mechanism behind this previously observed phenotype due to a disruption to HP1α from a loss of interaction with H1.4.

The findings from this investigation indicate that expression of the H1.4 frameshift mutant in NIH3T3 cells results in disruptions to heterochromatin. Abnormal DAPI foci were observed indicating there was a disruption to chromatin organisation and heterochromatin homeostasis. Typical DAPI patterning has multiple round discrete foci throughout the nucleus, however, nuclei with larger and more diffuse DAPI foci were observed with expression of the H1.4-FS mutant. Co-localisation with HP1α was also found to be reduced. However, the *in vitro* protein binding assays performed to confirm this were not optimised in time, and therefore it is unknown if there is a true loss of interaction. Changes to the nuclear morphology were also observed, with a larger nucleus size occurring in NIH3T3 cells expressing the H1.4 frameshift mutant. Flex et al.(2019) also demonstrated that disruptions to Lamin A/C were more prevalent with increased cell passages. As the H1.4 frameshift mutant was only transiently transfected into NIH3T3 cells this would need to be repeated with stable expression of the H1.4 frameshift mutant to better determine its effect on Lamin A/C.

A larger nucleus area was been previously observed in primary rat embryonic neurons exogenously expressing a different Rahman syndrome variant, c.430dupG (Tremblay et al., 2021). This variant is

caused by a frameshift mutation at amino acid 144 that changes an alanine to a glycine. The nucleus area was measured from an optical section through the center of the nucleus. Only the NIH3T3 cells exogenously expressing the H1.4 frameshift protein were observed to have significantly larger nuclei compared to the NIH3T3 cells expressing exogenous wild-type H1.4. However, as both these observations were from measuring the area of optical slices of the nuclei it is not determined if there is an increase in nuclear volume or if, the nucleus has changed in shape due to disruptions to the lamina and/or mechanical properties of the nucleus. A flatter shape may cause the appearance of a larger nucleus without an increase in total volume. A similar change in area was observed in HP1α knockdown (KD) MCF7 cells (Pradhan et al., 2021). This was determined to be a result of the HP1α KD cells having a flatter shape than the control cells due to disruptions to heterochromatin and Lamin A/C which resulted in softer MCF7 nuclei (Pradhan et al., 2021). This resulted in the flatter nuclei having the appearance of a larger nucleus size when viewed as an optical slice (Pradhan et al., 2021). Potentially this finding of larger nuclei could suggest that expression of the H1.4 Rahman syndrome frameshift mutant is affecting the mechanical properties of the nucleus as a result of loss of chromatin condensation and HP1α function.

Overall, this research suggests that expression of the H1.4-FS mutant results in changes to heterochromatin patterning and a change in nuclear morphology. However, due to the small sample size, the significance of changes observed in DAPI and Lamin A/C patterning can't be determined and therefore further investigation is required to confirm these findings.

5.4 H1.4 Frameshift Mutation is More Disruptive Than H1.4-Δ147

The mutation in the Rahman syndrome H1.4 variant p.Lys148Glnfs*48 (H1.4-FS) starts at amino acid 148 causing a change in the reading frame and an early stop codon. This results in the expression of an H1.4 protein with a wild-type sequence up to amino acid 148 and a 46 amino acid long frameshift region. The behavior of this H1.4 mutant was compared to that of an H1.4 CTD truncation mutant that ends at amino acid 147 (Δ147). This was designed to determine if the frameshift region was causing a different phenotype to Δ147 as this would suggest that the additional 46 amino acids have an additional influence on H1.4 function. If the frameshift region had no function it would be expected to behave similarly to the Δ147 H1.4 mutant.

The transient transfection of the H1.4-Δ147 and H1.4-frameshift mutants resulted in observed differences in nuclear phenotypes. Nuclei with larger and more aggregated DAPI foci were more prevalent with expression of the frameshift mutant than Δ147. This suggests that expression of the H1.4 frameshift mutant may be more disruptive to heterochromatin organisation than H1.4 Δ147. It was also noted that the DAPI patterning of NIH3T3 cells expressing the H1.4 frameshift mutant was more similar to the DAPI patterning of NIH3T3 cells expressing H1.4 missing the entire CTD. This suggests that the additional frameshift region may be preventing the remaining CTD from having any functionality and therefore causing it to behave more like an H1.4 protein missing its entire CTD.

Interestingly, the expression of H1.4 Δ147 resulted in no significant difference in nucleus size when compared to NIH3T3 cells expressing exogenous wild-type H1.4. This finding suggests that the first 147 amino acids of the H1.4 CTD may be enough to ensure nuclear function. However to confirm this

further investigation would be required.

5.5 Future Directions

5.5.1 Mapping the Region of the H1.4 CTD Required to Interact With the HP1α Hinge

To better understand the mechanism behind the interaction between the H1.4 CTD and the hinge region (HR) of HP1α, the region of the H1.4 CTD required for this interaction will be investigated in future research. While *in vitro* binding assays were attempted in this research to address this question they were not optimised. Therefore completion of the GST-pulldown assay along with the addition of an *In vivo* technique such as a fluorescence resonance energy transfer (FRET) assay will be performed to detect the H1.4 and HP1α interaction.

These techniques will be used to determine what truncations of the H1.4 result in the loss of the H1.4-HP1α interaction both *in vitro* and *in vivo*. The interaction of H1.4-FS with HP1α will also be investigated using these techniques to determine if it can interact with HP1α. The same H1.4 CTD deletion mutants designed for this research (Figure 3.1) will initially be used for future research, however, additional H1.4 CTD deletion mutants may need to be designed to further tweeze apart the specific regions of the CTD required.

As previously discussed, unpublished results investigating the H1.4-HP1α imply that an additional component, such as RNA, is required for this reaction to occur. As both the HR of HP1α and the CTD of H1.4 are highly basic domains, the presence of RNA to mediate their interaction likely contributes to the stabilisation of the interaction *in vivo* . Truncations to the H1.4 CTD and the associated loss of positively charged lysine residues may reduce its affinity with negatively charged nucleic acids, such as RNA. The frameshift mutation associated with Rahman syndrome also results in a more negatively charged CTD. Therefore this future research would contribute to identifying if the loss of interaction is based on the overall loss of charge of the H1.4 CTD due to truncation or if there are perhaps specific charge patches on the H1.4 CTD that need to be present for binding to HP1α.

5.5.2 Investigating if expression of Frameshift H1.4 Changes Chromatin Dynamics

Reduction of heterochromatin markers, Lamin A/C abnormalities, and increased nuclear size have all been observed in association with the Rahman syndrome H1.4 frameshift mutants (Flex et al., 2019; Tremblay et al., 2021). Similar findings were also observed here such as abnormal DAPI foci and larger nuclei with the expression of the H1.4 frameshift mutant in NIH3T3 cells. This suggests that there may be changes in chromatin dynamics with the expression of the H1.4 frameshift mutants and therefore further research would be done to examine this.

The lamin abnormalities observed in Rahman syndrome patient fibroblasts and the increase in nucleus size observed previously in primary rat neurons and in this study suggest that there may be changes to the mechanical properties of the nucleus (Flex et al., 2019; Tremblay et al., 2021). Changes to chromatin dynamics in the nucleus have been previously observed to impact the resistive force of the nucleus and this may also be occurring in Rahman Syndrome (Pradhan et al., 2021; Stephens et al.,

2019; Stephens et al., 2018).

To investigate this techniques such as atomic force microscopy (AFM) and micropipette aspiration will be used. These techniques allow for the analysis of the mechanical properties of a nucleus and can give an insight into how the expression of the H1.4 frameshift mutant affects the chromatin dynamics. Chromatin is a key structural support to the nucleus shape and loss of heterochromatin specifically has been shown to disrupt Lamin A/C at the nuclear periphery. Therefore if expression of the H1.4 frameshift mutant results in a weaker nuclear membrane this would suggest that it is disrupting normal chromatin dynamics and chromatin condensation. It would also potentially explain the observed change in nucleus size as a weaker nuclear membrane would result in a flatter shape that may appear larger when viewed as an optical slice.

The use of these methods would allow for a more complete understanding of the mechanical properties of the nuclei expressing exogenous frameshift H1.4. This is to investigate both changes to the nuclear membrane stiffness and the overall integrity of the nucleus (Pradhan et al., 2021). The use of ATM allows for testing of any local deformities at specific regions of the nuclear membrane (Narasimhan et al., 2020; Pradhan et al., 2021; Thomas et al., 2013). Micropipette aspiration tests the stiffness of the entire nucleus (Narasimhan et al., 2020; Pradhan et al., 2021; Thomas et al., 2013).

Overall, this should contribute to an explanation for the observed increase in nucleus size. Results from AFM would give more information regarding what is occurring at the nuclear periphery after the expression of exogenous frameshift H1.4 (Narasimhan et al., 2020; Pradhan et al., 2021; Thomas et al., 2013). This is due to the probe used in ATM only indenting a local region of the nuclear membrane, where mainly lamin proteins and lamin-associated heterochromatin contribute to the nuclear stiffness (Pradhan et al., 2021). While micropipette aspiration would provide more information about how the expression of exogenous frameshift H1.4 affects chromatin dynamics throughout the nucleus (Pradhan et al., 2021; Thomas et al., 2013). As bulk chromatin throughout the nucleus is a key contributor to global nuclear stiffness (Pradhan et al., 2021).

Overall these future investigations would allow for further understanding of how this rare genetic disorder is functioning and potentially contribute to a better understanding of the role of H1.4 in chromatin dynamics.

Appendix A

Appendix

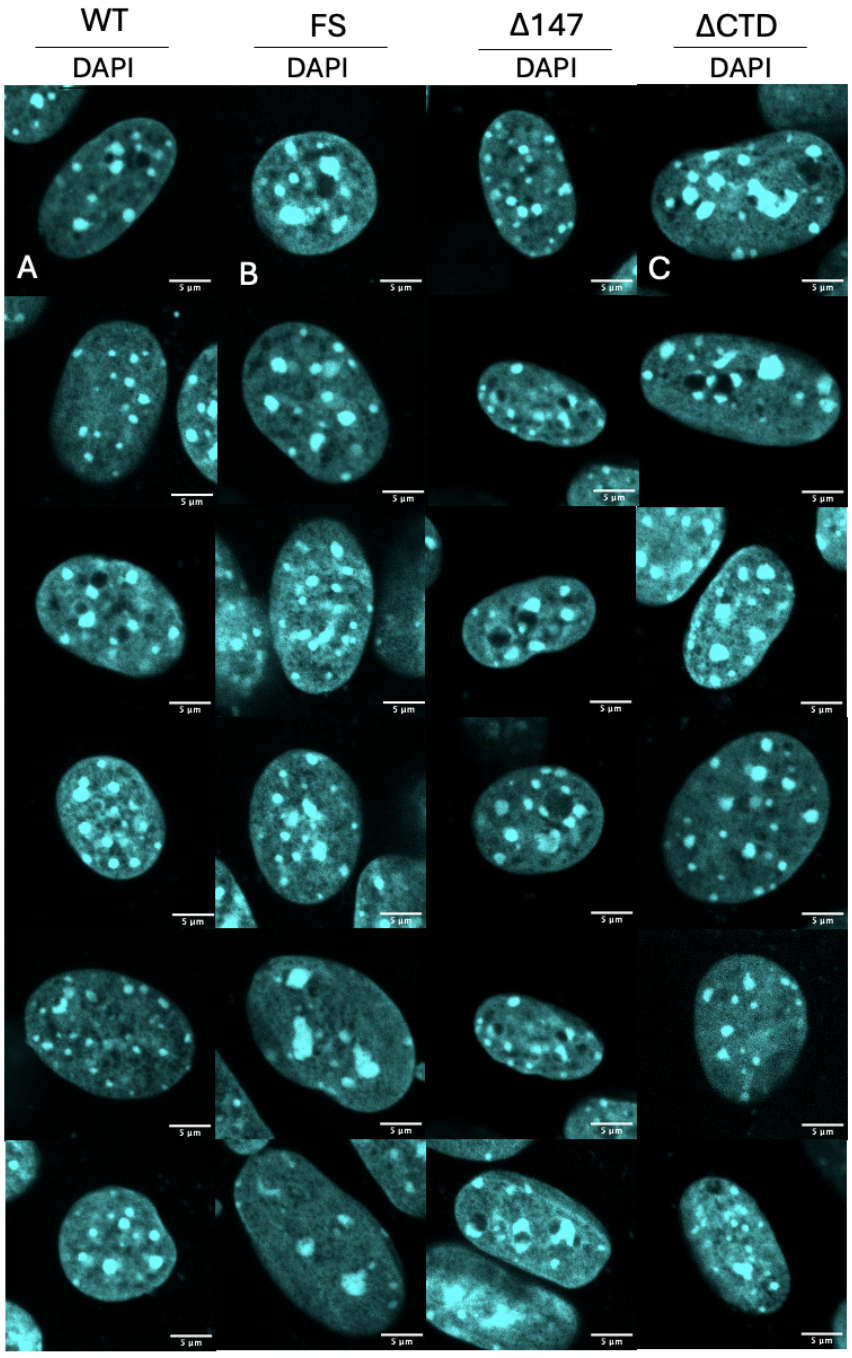

Figure A.1: **DAPI foci patterning in NIH3T3 cells.** Confocal microscope immunofluorescence images of NIH3T3 cells. Comparison of Co-localisation of DAPI foci in NIH3T3 cells transiently transfected with H1.4-FLAG, H1.4-FS-FLAG, H1.4-Δ147-FLAG, and H1.4-ΔCTD-FLAG. DAPI is shown in cyan. (A) Normal DAPI foci patterning is shown as round discrete foci. (B) An example of abnormal DAPI foci patterning in NIH3T3 cells expressing H1.4-FS-FLAG. DAPI foci are larger and misshapen. (C) An example of abnormal DAPI foci patterning in NIH3T3 cells expressing H1.4-ΔCTD-FLAG. DAPI foci are larger, misshapen, and not evenly dispersed across the nucleus. The scale bar is 5 μm.

Bibliography

Allan, J., Hartman, P. G., Crane-Robinson, C., & Aviles, F. X. (1980). The structure of histone H1 and its location in chromatin. *Nature*, *288*(5792), 675–679. https://doi.org/10.1038/288675a0

Azzaz, A. M., Vitalini, M. W., Thomas, A. S., Price, J. P., Blacketer, M. J., Cryderman, D. E., Zirbel, L. N., Woodcock, C. L., Elcock, A. H., Wallrath, L. L., & Shogren-Knaak, M. A. (2014). Human Heterochromatin Protein 1α Promotes Nucleosome Associations That Drive Chromatin Condensation. *Journal of Biological Chemistry*, *289*(10), 6850–6861. https://doi.org/10.1074/jbc.m113.512137

Beacon, T. H., Delcuve, G. P., López, C., Nardocci, G., Kovalchuk, I., van Wijnen, A. J., & Davie, J. R. (2021). The dynamic broad epigenetic (H3K4me3, H3K27ac) domain as a mark of essential genes. *Clinical Epigenetics*, *13*(1). https://doi.org/10.1186/s13148-021-01126-1

Bednar, J., Garcia-Saez, I., Boopathi, R., Cutter, A. R., Papai, G., Reymer, A., Syed, S. H., Lone, I. N., Tonchev, O., Crucifix, C., Menoni, H., Papin, C., Skoufias, D. A., Kurumizaka, H., Lavery, R., Hamiche, A., Hayes, J. J., Schultz, P., Angelov, D., & Petosa, C. (2017). Structure and Dynamics of a 197 bp Nucleosome in Complex with Linker Histone H1. *Molecular Cell*, *66*(3), 384-397.e8. https://doi.org/10.1016/j.molcel.2017.04.012

Burkardt, D., & Tatton-Brown, K. (2020, December 3). *HIST1H1E Syndrome* (M. P. Adam, G. M. Mirzaa, R. A. Pagon, S. E. Wallace, L. J. Bean, K. W. Gripp, & A. Amemiya, Eds.). PubMed; University of Washington, Seattle. https://www.ncbi.nlm.nih.gov/books/NBK564966/

Caputi, F. F., Candeletti, S., & Romualdi, P. (2017). Epigenetic Approaches in Neuroblastoma Disease Pathogenesis. *Neuroblastoma - Current State and Recent Updates*. https://doi.org/10.5772/intechopen.69566

Clausell, J., Happel, N., Hale, T. K., Doenecke, D., & Beato, M. (2009). Histone H1 Subtypes Differentially Modulate Chromatin Condensation without Preventing ATP-Dependent

Remodeling by SWI/SNF or NURF. *PLoS ONE*, *4*(10), e0007243. https://doi.org/10.1371/journal.pone.0007243

Cutter, A. R., & Hayes, J. J. (2015). A brief review of nucleosome structure. *FEBS Letters*, *589*(20PartA), 2914–2922. https://doi.org/10.1016/j.febslet.2015.05.016

da Costa-Nunes, J. A., & Noordermeer, D. (2023). TADs: Dynamic structures to create stable regulatory functions. *Current Opinion in Structural Biology*, *81*, 102622. https://doi.org/10.1016/j.sbi.2023.102622

Daujat, S., Zeissler, U., Waldmann, T., Happel, N., & Schneider, R. (2005). HP1 Binds Specifically to Lys26-methylated Histone H1.4, whereas Simultaneous Ser27 Phosphorylation Blocks HP1 Binding. *Journal of Biological Chemistry*, *280*(45), 38090–38095. https://doi.org/10.1074/jbc.c500229200

de Wit, E., Vos, Erica S. M., Holwerda, Sjoerd J. B., Valdes-Quezada, C., Verstegen, Marjon J. A. M., Teunissen, H., Splinter, E., Wijchers, Patrick J., Krijger, Peter H. L., & de Laat, W. (2015). CTCF Binding Polarity Determines Chromatin Looping. *Molecular Cell*, *60*(4), 676–684. https://doi.org/10.1016/j.molcel.2015.09.023

Finch, J. T., & Klug, A. (1976). Solenoidal model for superstructure in chromatin. *Proceedings of the National Academy of Sciences*, *73*(6), 1897–1901. https://doi.org/10.1073/pnas.73.6.1897

Flex, E., Martinelli, S., Van Dijck, A., Ciolfi, A., Cecchetti, S., Coluzzi, E., Pannone, L., Andreoli, C., Radio, F. C., Pizzi, S., Carpentieri, G., Bruselles, A., Catanzaro, G., Pedace, L., Miele, E., Carcarino, E., Ge, X., Chijiwa, C., Lewis, M. E. S., & Meuwissen, M. (2019). Aberrant Function of the C-Terminal Tail of HIST1H1E Accelerates Cellular Senescence and Causes Premature Aging. *The American Journal of Human Genetics*, *105*(3), 493–508. https://doi.org/10.1016/j.ajhg.2019.07.007

Fyodorov, D. V., Zhou, B.-R., Skoultchi, A. I., & Bai, Y. (2017). Emerging roles of linker histones in regulating chromatin structure and function. *Nature Reviews Molecular Cell Biology*, *19*(3), 192–206. https://doi.org/10.1038/nrm.2017.94

Ghosh, R. P., & Meyer, B. J. (2021). Spatial Organization of Chromatin: Emergence of Chromatin Structure During Development. *Annual Review of Cell and Developmental Biology*, *37*(1), 199–232. https://doi.org/10.1146/annurev-cellbio-032321-035734

Hale, T. K., Contreras, A., Morrison, A. J., & Herrera, R. E. (2006). Phosphorylation of the Linker Histone H1 by CDK Regulates Its Binding to HP1α. *Molecular Cell*, *22*(5), 693–699. https://doi.org/10.1016/j.molcel.2006.04.016

Hansen, A. S., Cattoglio, C., Darzacq, X., & Tjian, R. (2017). Recent evidence that TADs and chromatin loops are dynamic structures. *Nucleus*, *9*(1), 20–32. https://doi.org/10.1080/19491034.2017.1389365

Hansen, A. S., Pustova, I., Cattoglio, C., Tjian, R., & Darzacq, X. (2017). CTCF and cohesin regulate chromatin loop stability with distinct dynamics. *ELife*, *6*, e25776. https://doi.org/10.7554/eLife.25776

Hendzel, M. J., Lever, M. A., Crawford, E., & Th'ng, J. P. H. (2004). The C-terminal domain is the primary determinant of histone H1 binding to chromatin in vivo. *The Journal of Biological Chemistry*, *279*(19), 20028–20034. https://doi.org/10.1074/jbc.M400070200

Hildebrand, E. M., & Dekker, J. (2020). Mechanisms and Functions of Chromosome Compartmentalization. *Trends in Biochemical Sciences*, *45*(5), 385–396. https://doi.org/10.1016/j.tibs.2020.01.002

Janssen, A., Colmenares, S. U., & Karpen, G. H. (2018). Heterochromatin: Guardian of the Genome. *Annual Review of Cell and Developmental Biology*, *34*(1), 265–288. https://doi.org/10.1146/annurev-cellbio-100617-062653

Jinasena, D., Simmons, R., Gyamfi, H., & Fitzkee, N. C. (2019). Molecular Mechanism of the Pin1–Histone H1 Interaction. *Biochemistry*, *58*(6), 788–798. https://doi.org/10.1021/acs.biochem.8b01036

Kim, S., & Shendure, J. (2019). Mechanisms of Interplay between Transcription Factors and the 3D Genome. *Molecular Cell*, *76*(2), 306–319. https://doi.org/10.1016/j.molcel.2019.08.010

Knapp, K., Naik, N., Ray, S., van Haaften, G., & Bicknell, L. S. (2023). Histones: coming of age in Mendelian genetic disorders. *Journal of Medical Genetics*, *60*(3), 213–222. https://doi.org/10.1136/jmg-2022-109085

Kornberg, R. D., & Lorch, Y. (1999). Twenty-Five Years of the Nucleosome, Fundamental Particle of the Eukaryote Chromosome. *Cell*, *98*(3), 285–294. https://doi.org/10.1016/s0092-8674(00)81958-3

Kumar, A., & Kono, H. (2020). Heterochromatin protein 1 (HP1): interactions with itself and chromatin components. *Biophysical Reviews*, *12*(2), 387–400. https://doi.org/10.1007/s12551-020-00663-y

Kuzmichev, A., Jenuwein, T., Tempst, P., & Reinberg, D. (2004). Different Ezh2-Containing Complexes Target Methylation of Histone H1 or Nucleosomal Histone H3. *Molecular Cell*, *14*(2), 183–193. https://doi.org/10.1016/s1097-2765(04)00185-6

Lammerding, J. (2011). Mechanics of the Nucleus. *Comprehensive Physiology*, *1*(2). https://doi.org/10.1002/cphy.c100038

Lu, X., & Hansen, J. C. (2004). Identification of Specific Functional Subdomains within the Linker Histone H10 C-terminal Domain. *Journal of Biological Chemistry*, *279*(10), 8701–8707. https://doi.org/10.1074/jbc.m311348200

Luger, K., Dechassa, M. L., & Tremethick, D. J. (2012). New insights into nucleosome and chromatin structure: an ordered state or a disordered affair? *Nature Reviews Molecular Cell Biology*, *13*(7), 436–447. https://doi.org/10.1038/nrm3382

Maeshima, K., Imai, R., Tamura, S., & Nozaki, T. (2014). Chromatin as dynamic 10-nm fibers. *Chromosoma*, *123*(3), 225–237. https://doi.org/10.1007/s00412-014-0460-2

Martins, F., Sousa, J., Pereira, C. D., Cruz e Silva, O. A. B., & Rebelo, S. (2020). Nuclear envelope dysfunction and its contribution to the aging process. *Aging Cell*, *19*(5). https://doi.org/10.1111/acel.13143

Marzluff, W. F., & Koreski, K. P. (2017). *Birth and Death of Histone mRNAs*. *33*(10), 745–759. https://doi.org/10.1016/j.tig.2017.07.014

Missag Hagop Parseghian. (2015). What is the role of histone H1 heterogeneity? A functional model emerges from a 50 year mystery. *AIMS Biophysics*, *2*(4), 724–772. https://doi.org/10.3934/biophy.2015.4.724

Morrison, O., & Thakur, J. (2021). Molecular Complexes at Euchromatin, Heterochromatin and Centromeric Chromatin. *International Journal of Molecular Sciences*, *22*(13), 6922. https://doi.org/10.3390/ijms22136922

Narasimhan, B. N., Ting, M. S., Kollmetz, T., Horrocks, M. S., Chalard, A. E., & Malmström, J. (2020). Mechanical Characterization for Cellular Mechanobiology: Current Trends and Future Prospects. *Frontiers in Bioengineering and Biotechnology*, *8*. https://doi.org/10.3389/fbioe.2020.595978

Nielsen, A. L., Oulad-Abdelghani, M., Ortiz, J. A., Remboutsika, E., Chambon, P., & Losson, R. (2001). Heterochromatin Formation in Mammalian Cells. *Molecular Cell*, *7*(4), 729–739. https://doi.org/10.1016/s1097-2765(01)00218-0

Nishino, Y., Eltsov, M., Joti, Y., Ito, K., Takata, H., Takahashi, Y., Hihara, S., Frangakis, A. S., Imamoto, N., Ishikawa, T., & Maeshima, K. (2012). Human mitotic chromosomes consist predominantly of irregularly folded nucleosome fibres without a 30-nm chromatin structure. *The EMBO Journal*, *31*(7), 1644–1653. https://doi.org/10.1038/emboj.2012.35

Olins, A. L., & Olins, D. E. (1974). Spheroid Chromatin Units (ngr Bodies). *Science*, *183*(4122), 330–332. https://doi.org/10.1126/science.183.4122.330

Padeken, J., Methot, S. P., & Gasser, S. M. (2022). Establishment of H3K9-methylated heterochromatin and its functions in tissue differentiation and maintenance. *Nature Reviews Molecular Cell Biology*. https://doi.org/10.1038/s41580-022-00483-w

Parmar, J. J., & Padinhateeri, R. (2020). Nucleosome positioning and chromatin organization. *Current Opinion in Structural Biology*, *64*, 111–118. https://doi.org/10.1016/j.sbi.2020.06.021

Perišić, O., Collepardo-Guevara, R., & Schlick, T. (2010). Modeling studies of chromatin fiber structure as a function of DNA linker length. *Journal of Molecular Biology*, *403*(5), 777–802. https://doi.org/10.1016/j.jmb.2010.07.057

Pradhan, S., Solomon, R., Gangotra, A., Yakubov, G. E., Willmott, G. R., Whitby, C. P., Hale, T. K., & Williams, M. A. K. (2021). Depletion of HP1α alters the mechanical properties of MCF7 nuclei. *Biophysical Journal*, *120*(13), 2631–2643. https://doi.org/10.1016/j.bpj.2021.05.017

Prendergast, L., & Reinberg, D. (2021). The missing link*er*: emerging trends for H1 variant-specific functions. *Genes & Development*, *35*(1-2), 40–58. https://doi.org/10.1101/gad.344531.120

Rada-Iglesias, A., Grosveld, F. G., & Papantonis, A. (2018). Forces driving the three-dimensional folding of eukaryotic genomes. *Molecular Systems Biology*, *14*(6). https://doi.org/10.15252/msb.20188214

Rajderkar, S., Barozzi, I., Zhu, Y., Hu, R., Zhang, Y., Li, B., Alcaina Caro, A., Fukuda-Yuzawa, Y., Kelman, G., Akeza, A., Blow, M. J., Pham, Q., Harrington, A. N., Godoy, J., Meky, E. M., von Maydell, K., Hunter, R. D., Akiyama, J. A., Novak, C. S., & Plajzer-Frick, I. (2023). Topologically associating domain boundaries are required for normal genome function. *Communications Biology*, *6*(1), 1–10. https://doi.org/10.1038/s42003-023-04819-w

Roque, A., Ponte, I., & Suau, P. (2016). Post-translational modifications of the intrinsically disordered terminal domains of histone H1: effects on secondary structure and chromatin dynamics. *Chromosoma*, *126*(1), 83–91. https://doi.org/10.1007/s00412-016-0591-8

Routh, A., Sandin, S., & Rhodes, D. (2008). Nucleosome repeat length and linker histone stoichiometry determine chromatin fiber structure. *Proceedings of the National Academy of Sciences*, *105*(26), 8872–8877. https://doi.org/10.1073/pnas.0802336105

Ryan, D. P., & Tremethick, D. J. (2018). The interplay between H2A.Z and H3K9 methylation in regulating HP1α binding to linker histone-containing chromatin. *Nucleic Acids Research*, *46*(18), 9353–9366. https://doi.org/10.1093/nar/gky632

Salinas-Pena, M., Rebollo, E., & Jordan, A. (2024). Imaging analysis of six human histone H1 variants reveals universal enrichment of H1.2, H1.3, and H1.5 at the nuclear periphery and nucleolar H1X presence. *ELife*, *12*. https://doi.org/10.7554/elife.91306

Sancho, M., Diani, E., Beato, M., & Jordan, A. (2008). Depletion of Human Histone H1 Variants Uncovers Specific Roles in Gene Expression and Cell Growth. *PLoS Genetics*, *4*(10), e1000227. https://doi.org/10.1371/journal.pgen.1000227

Sequeira-Mendes, J., & Gutierrez, C. (2015). Genome architecture: from linear organisation of chromatin to the 3D assembly in the nucleus. *Chromosoma*, *125*(3), 455–469. https://doi.org/10.1007/s00412-015-0538-5

Stephens, A. D., Banigan, E. J., & Marko, J. F. (2019). Chromatin's physical properties shape the nucleus and its functions. *Current Opinion in Cell Biology*, *58*, 76–84. https://doi.org/10.1016/j.ceb.2019.02.006

Stephens, A. D., Liu, P. Z., Banigan, E. J., Almassalha, L. M., Backman, V., Adam, S. A., Goldman, R. D., & Marko, J. F. (2018). Chromatin histone modifications and rigidity affect nuclear morphology independent of lamins. *Molecular Biology of the Cell*, *29*(2), 220–233. https://doi.org/10.1091/mbc.e17-06-0410

Sterner, D. E., & Berger, S. L. (2000). Acetylation of Histones and Transcription-Related Factors. *Microbiology and Molecular Biology Reviews*, *64*(2), 435–459. https://doi.org/10.1128/mmbr.64.2.435-459.2000

Szerlong, H. J., & Hansen, J. C. (2011). Nucleosome distribution and linker DNA: connecting nuclear function to dynamic chromatin structure. *Biochemistry and Cell Biology*, *89*(1), 24–34. https://doi.org/10.1139/o10-139

Th'ng, J. P. H., Sung, R., Ye, M., & Hendzel, M. J. (2005). H1 Family Histones in the Nucleus. *Journal of Biological Chemistry*, *280*(30), 27809–27814. https://doi.org/10.1074/jbc.m501627200

Thomas, G., Burnham, N. A., Camesano, T. A., & Wen, Q. (2013). Measuring the Mechanical Properties of Living Cells Using Atomic Force Microscopy. *Journal of Visualized Experiments*, *76*. https://doi.org/10.3791/50497

Tremblay, M. W., Green, M. V., Goldstein, B. M., Aldridge, A. I., Rosenfeld, J. A., Streff, H., Tan, W. D., Craigen, W., Bekheirnia, N., Al Tala, S., West, A. E., & Jiang, Y. (2021). Mutations of the histone linker *H1–4* in neurodevelopmental disorders and functional characterization of neurons expressing C-terminus frameshift mutant H1.4. *Human Molecular Genetics*, *31*(9), 1430–1442. https://doi.org/10.1093/hmg/ddab321

Woodcock, C. L., L. L. Y. Frado, & Rattner, J. B. (1984). The higher-order structure of chromatin: evidence for a helical ribbon arrangement. *Journal of Cell Biology*, *99*(1), 42–52. https://doi.org/10.1083/jcb.99.1.42

Worcel, A., Strogatz, S., & Riley, D. (1981). Structure of chromatin and the linking number of DNA. *Proceedings of the National Academy of Sciences*, *78*(3), 1461–1465. https://doi.org/10.1073/pnas.78.3.1461

Zhou, B.-R., & Bai, Y. (2019). Chromatin structures condensed by linker histones. *Essays in Biochemistry*, *63*(1), 75–87. https://doi.org/10.1042/ebc20180056